THE ROLE OF THE MNPO IN BODY FLUID BALANCE AND BLOOD PRESSURE REGULATION

Alexandria B. Marciante, B.S.

DISSERTATION

Presented to the Graduate Council of the
Graduate School of Biomedical Sciences
University of North Texas
Health Science Center at Fort Worth
in Partial Fulfillment of the Requirements

For the Degree of

DOCTOR OF PHILOSOPHY

By

Alexandria B. Marciante, B.S.
Fort Worth, Texas
April 2019

Copyright by
Alexandria B. Marciante
2019

ACKNOWLEDGEMENTS

I would like thank Dr. J. Thomas Cunningham for his outstanding mentorship over the past four years. He has provided invaluable opportunities to increase my professional skills and has always encouraged me to challenge myself in research, academics and life. I truly could not have imagined a better or more fulfilling experience for myself than these past four years working for him. His insight and advice is deeply appreciated and always valued.

I would like to acknowledge my advisory committee members Drs. Steve Mifflin, Ann Schreihofer, Styliani Goulopoulou, Rong Ma, Nicoleta Bugnariu, and John Planz. Your guidance and commitment to my success has been an invaluable experience and aided in my growth as a graduate student. To Dr. Rebecca L. Cunningham, thank you for being a wonderful academic advisor and providing humor to my day.

I would also like to thank my lab colleagues, especially Kirthikaa Balipattabi, Joel Little, Dr. Gef Farmer, Martha Bachelor and Dr. Lei Wang for your endless support, friendship and guidance from my first year. To my friends outside of the lab, your constant support along this journey has made my time at UNTHSC a fulfilled and wonderful chapter of my life. I would also like to thank Carla Johnson for all her help and support through these last four years.

Finally, to my loving parents Al and Sara Marciante, to my sister Cassie Marciante, and my wonderful husband Adam—thank you for always believing in me and your endless support, for encouraging me to follow my dreams, and being in my corner, by my side for it all.

TABLE OF CONTENTS

TABLE OF CONTENTS (cont.)

Page

LIST OF TABLES

Page

LIST OF ILLUSTRATIONS

Page

CHAPTER 1

CHAPTER 2

LIST OF ILLUSTRATIONS (cont.)

Page

CHAPTER 3

CHAPTER 4

CHAPTER 5

LIST OF ILLUSTRATIONS (cont.)

Page

SPECIFIC AIMS

The median preoptic nucleus (MnPO) is a midline nucleus located along the anterior wall of the third ventricle between two circumventricular organs, the subfornical organ (SFO) and the organum vasculosum of the lamina terminalis (OVLT). The SFO and OVLT project to the MnPO to regulates neuroendocrine, autonomic, arousal, and fluid balance. The MnPO and other regions in the anterior ventral region of the third ventricle contribute to several forms of neurogenic hypertension. Recent studies from our laboratory have shown that the MnPO is necessary for hypertension produced by chronic intermittent hypoxia (CIH). Chronic intermittent hypoxia (CIH) is a rodent model designed to mimic the intermittent hypoxemia experienced in obstructive sleep apnea (OSA). Exposure to CIH leads to hypertension and other cardiovascular comorbidities consistent with patients suffering from OSA. In OSA patients, the hypertension and increased sympathetic nerve activity can persist into the waking periods in the absence of hypoxia as the disease progresses eventually resulting in cardiovascular morbidities including heart disease. This is also a feature of the CIH model.

These studies indicate that the MnPO contributes to the sustained component of CIH hypertension. Hypertension due to CIH initially develops during hypoxia from signaling through the hindbrain and may be sustained for the entire diurnal cycle through multiple mechanisms that include activity of the forebrain, specifically through modulation by the MnPO. The MnPO is an integrating center in the hypothalamus that has projections to the paraventricular nucleus (PVN), which is involved in blood pressure regulation and the hypothalamic-pituitary-adrenal axis. Many studies have shown that the MnPO is necessary for CIH hypertension. However, the phenotypes of

the MnPO neurons responsible for CIH hypertension have not yet been fully elucidated. By identifying the neurons involved in signaling to the PVN and selectively inhibiting their activity through regulating MnPO activity, it may be possible to interrupt and attenuate the sustained hypertension that develops during CIH.

The goal of these studies is to determine which neurons in the MnPO contribute to CIH hypertension based on their projections, and, if by blunting their activity, it may attenuate the CIH-induced sustained hypertension. **The working hypothesis** is that pathway-specific MnPO neurons mediate stimulus-dependent drinking behavior and neuroendocrine function, and MnPO neurons projecting to the PVN mediate the sustained hypertension during normoxia that is associated with CIH.

Specific Aim 1. Acute inhibition of MnPO neurons will decrease Fos expression, neuronal firing rate, and drinking behavior. These studies use Cre-independent G_i designer receptors exclusively activated by designer drugs (DREADDs) that chemogenetically induce inhibition of transduced neurons in response to the exogenous ligand, clozapine-*N*-oxide (CNO). The G_i DREADDs utilized in these experiments contain a CaMKIIa promotor packaged in an adeno-associated virus (AAV) vector and microinjected into the MnPO. These experiments evaluate MnPO individual responses to CNO-induced inhibition at the neuronal level using loose cell and whole cell recordings. Additonally, these experiments also define at the physiological level how the MnPO regulates drinking behavior with and without neuronal inhibition.

Specific Aim 2. Lesions of MnPO neurons projecting to the PVN will attenuate chronic increases in blood pressure. These studies use retrograde transport of Cre with AAV9 from the PVN to the MnPO in combination with caspase-3 flex virus dependent on Cre to selectively induce apoptosis in PVN-projecting MnPO neurons. These studies are performed to measure chronic changes in blood pressure during a 7-day CIH protocol and to assess functional neuroanatomy related to MnPO signaling due to CIH.

CHAPTER I: INTRODUCTION

THE ROLE OF THE MnPO IN THE REGULATION OF DRINKING BEHAVIOR, NEUROENDOCRINE AND AUTONOMIC FUNCTION

The median preoptic nucleus (MnPO) is a region in the forebrain that lies on the anteroventral wall of the 3rd ventricle (AV3V) [1]. Neurons in the MnPO are involved in thermoregulation, osmoregulation, sleep, body fluid balance and cardiovascular and autonomic function [1-4]. For the purpose of this dissertation, the focus will be primarily on the role of the MnPO in regulating body fluid homeostasis and cardiovascular responses as it relates to blood pressure regulation.

Many studies have assessed the importance of the MnPO in the development of hypertension, maintenance of body fluid homeostasis, and regulation of neurohumoral function [1, 2, 4-10]. The MnPO receives afferent signals from circumventricular organs (CVOs) the organum vasculosum of the lamina terminalis (OVLT) and the subfornical organ (SFO) that lie just dorsal and ventral to the MnPO on the AV3V, respectively, responding to fluctuations in plasma osmolality, or other humoral factors [1, 3, 4, 9]. One of the humoral factors the CVOs and MnPO respond to is angiotensin II (ANG II) through angiotensin type 1a receptors (AT1aRs) [11]. When there is an increase in plasma osmolality or certain humoral factors, like ANG II, the SFO and OVLT stimulate the MnPO to increase thirst, cardiovascular responses, and efferent signaling to the supraoptic nucleus (SON) and paraventricular nucleus (PVN), as well as other downstream nuclei to influence neuroendocrine and autonomic function [1, 12]. The AV3V is has been shown to control both drinking and blood pressure [13]. However, studies have not yet been conducted to study the role of pathway-specific MnPO neurons in regulation with body fluid homeostasis associated with water consumption or autonomic function. The current studies test the role of the MnPO in regulating body fluid

homeostasis and stimuli dependence, as well as blood pressure regulation in a well-defined hypertension model.

The MnPO and Drinking Responses

Thirst is a complex and necessary process that is vital to maintaining body fluid homeostasis. Varying concentrations of circulating factors, such as ANG II, and changes in plasma osmolality are stimuli important for influencing centrally-mediated physiological outcomes, including drinking behavior. Small increases of < 2% in the effective osmotic pressure of plasma can induce thirst in mammals [14]. Circulating factors like ANG II and hypertonicity are sensed by ANG II-sensitive and osmosensitive neurons of circumventricular organs (CVOs), the subfornical organ (SFO) and organum vasculosum of the lamina terminalis (OVLT) located on the anteroventral wall of the 3rd ventricle (AV3V in the forebrain to drive thirst-related neural pathway. The area postrema (AP), a CVO in the hindbrain, is more involved in inhibiting food intake in response to circulating hormones signaling satiety (i.e. amylin and leptin) [15]. The SFO and OVLT perceive plasma volume and vascular perfusion pressure and have projections that terminate in the median preoptic nucleus (MnPO, Figure 1) [1]. The MnPO regulates many homeostatic functions, including drinking responses related to thirst [1, 4, 5, 13, 16, 17].

Cellular vs Extracellular Dehydration

Cellular and extracellular dehydration increase water consumption to overcome physiological insults like hyperosmolality and hypovolemia. During chronic dehydration,

such as in a 48 hour water deprivation model, cellular (hyperosmolality) and extracellular (hypovolemia) dehydration are both driving factors for water consumption [18]; however, it is important to assess both forms of dehydration independently of the other to understand how they may mechanistically differ. Cellular dehydration associated with hypertonicity of body fluids, is detected by osmoreceptors in the SFO and OVLT and is a major physiological stimulus of thirst and vasopressin secretion [15, 19]. Extracellular dehydration associated with hypovolemia is mediated by ANG II binding to angiotensin type 1a receptors (AT1aRs) in the SFO and OVLT, with the SFO acting as the main site of the dipsogenic action of circulating ANG II [15, 20].

Early studies in rats used neuroanatomical tracing to determine efferent pathways emanating from the SFO and OVLT [21, 22]. From these studies, many efferent downstream nuclei were identified, including the supraoptic nucleus (SON), paraventricular nucleus (PVN), lateral hypothalamus (LH), paraventricular nucleus of the thalamus (PVT), and the MnPO. However, the MnPO also has connections that are consistent with a role in drinking behavior such as receiving glutamatergic (GLUT) projections from the SFO and OVLT and sending axons to the hypothalamic and thalamic nuclei involved in thirst-related signaling [1, 5, 15, 16]. A potential role for the MnPO in thirst were from experiments initially conducted in goats, and later confirmed in rats, indicating that adipsia could result from AV3V lesions [23-25]. Additionally, early electrophysiology experiments in sheep and rats indicated increases in MnPO neuron firing rate as a result of systemic doses of hypertonic saline or direct microinjection of ANG II in the SFO [26-28]. The hypothesis that the MnPO acts as the major relay site for thirst-signaling originated in studies conducted by Mangiapane, et al. [29], where total

electrolytic ablation of MnPO neurons attenuated ANG II and osmotic-induced drinking. Deficits in drinking to various concentrations of ANG II (1 and 2 mg/kg sc) and hypertonic saline (3 and 6% w/v sc) stimuli was further supported in studies conducted by Cunningham, et al. using ibotenic acid to destroy MnPO neurons, while maintaining integrity of fibres of passage [2].

More recently, studies have demonstrated that the MnPO neurons likely involved in regulating thirst are excitatory. Studies by Leib, et al. used channel-rhodopsin2 (ChR2)-expressing SFO^{GLUT} neurons and photostimulation of axons innervating the MnPO, as well as fibers of passage targeting the OVLT, drives robust and specific water consumption [13]. When either the SFO^{GLUT} along with or separately from the $OVLT^{GLUT}$ neurons are ablated, photostimulation-induced drinking is not completely blocked as long as the MnPO is intact [26]. Additionally, photostimulation of neuronal nitric oxide synthase (NOS1)-positive MnPO neurons ($MnPO^{NOS1}$) and $OVLT^{NOS1}$ with direct connections to SFO^{NOS1} neurons selectively induced water drinking in satiated mice [16].

Studies have indicated that excitatory neuronal phenotypes of the MnPO relaying thirst-signaling from the SFO and OVLT to downstream areas of the brain, and eventually cortical regions to induce water consumption. However, these studies do not address whether or not signaling from the MnPO to downstream thirst-regulating regions is stimulus-dependent. Although cellular and extracellular dehydration may have different centrally mediated mechanisms, both result in a similar behavioral outcome: thirst. To model the physiological mechanisms associated, studies have used hyperosmotic saline and angiotensin II (ANG II) to mimic thirst associated with cellular and extracellular dehydration, respectively [30-32]. The first aim of these dissertation works

directly addresses how thirst-induced signaling from the MnPO causes differential signaling in a stimulus-dependent manner to downstream thirst-regulating nuclei.

Signaling Mechanisms: Cellular Dehydration

Early studies have provided clear evidence that cellular dehydration is necessary for thirst and arginine vasopressin (AVP) release during hyperosmotic challenges [18, 33, 34]. Hyperosmotic extracellular fluid causes cells to shrink, postulating the idea that osmoreceptors are sensory receptors that are intrinsically sensitive to osmotic stimuli [33]. A review by Bourque posits that the osmotic set-point is encoded by the resting electrical potential of osmosensitive cells and that the magnitude and polarity of basal osmotic perturbations can cause proportions changes in action potential firing rate of downstream neurons [35]. It is important to note that osmoreceptors involved in contributing to the homeostasis of body fluid are located both centrally and in the periphery.

In the periphery, osmoreceptors have been found to be located in the blood vessels that collect absorbed solutes from the intestines, thereby allowing afferent connections to the CNS to induce anticipatory responses to ingested materials that may cause systemic osmotic perturbations in rats and man [36-38]. The molecular and cellular structure of peripheral osmoreceptors remains unknown; however, there is evidence for afferent neural connections through the vagus [39, 40] and splanchnic nerve [41] from osmoreceptors in the periphery. In the present studies, we focus on central osmoreceptor activity.

Many studies have shown that lesioning or ablating the SFO and OVLT attenuates thirst and cardiovascular responses to osmotic and ANG II challenges [42-44]. Early studies in sheep and dogs demonstrated that lesioning the OVLT, OVLT and SFO, but not the SFO alone significantly attenuated water consumption in response to systemic infusion of hypertonic saline [45, 46]. Electrophysiological studies have also demonstrated that in a specific population of OVLT neurons, there is a positive correlation between action potential discharge and hyperosmolality [45, 47]. Based on these studies and others, the OVLT has been proposed to be the primary site for osmosensing in the mammalian brain. In addition to the OVLT, the SFO [48], MnPO [49] and magnocellular neurosecretory cells (MNCs) of the SON [50] and PVN [51] have all been shown to have intrinsic osmosensitivity, where these neurons are excitable to a hyperosmotic stimulus or inhibited by a hypo-osmotic stimulus. The SON largely functions to regulate body fluid homeostasis by influencing sodium excretion, and blood volume through the magnocellular neurosecretory system and the release of oxytocin in rats to mediate natriuresis and decrease salt-appetite in part in rats and sheep. [35, 52], and vasopressin in rats and man to promote thirst and water reabsorption [35, 53].

Experiments in MNCs have been shown to be osmotically stimulated through a mechanical process. Opening of nonselective cation channels causes a decrease in cell volume, resulting in depolarization of the cell, whereas closing a basal cation current can increase cell volume and concomitant hyperpolarization of the cell [54]. The identity of the osmosensory transduction has been shown to be encoded by a member of the transient receptor potential (TRP) channels, which are permeable to Ca^{2+} and is consistent with what is seen in MNCs where the osmosensory transduction current is

mediated by a non-selective cation channel that has a high degree of permeability to Ca^{2+} [55]. Other ion channels have been suggested to be involved in osmoreception as well. In theory, the inward current that mediates depolarizing responses to hypertonic fluid could be assisted by the activation of other Na^{+} or Ca^{2+} channels, by the inhibition of K^{+} conductance or by the modulation of an electrogenic transporter [35]. Studies have indicated that a MnPO neuronal population displays intrinsic osmosensitivity through specific Na^{+} sensors that could also contribute to differential stimuli-based signaling [49].It has been suggested that in MNCs hypertonicity causes upregulation of a slow voltage-gated K^{+} current that may play an important role in inducing phasic bursting activity to cause AVP secretion [56, 57].

The MnPO has projections that terminate in the SON and PVN. Studies conducted by Honda, et al. in an anesthetized rat preparation, was able to show that hyperosmotic stimulation of MnPO neurons activates MNCs in both the SON and PVN, indicating that the MnPO is one of the osmosensitive sites controlling electrical activity of SON and PVN MNCs [58, 59]. Lesioning or ablating the MnPO inhibits water consumption in dehydrated rats [2]. Optogenetic approaches have demonstrated that activation of glutamatergic neurons in the MnPO causes robust increases in water consumption, while the opposite is true for activation of GABAergic neurons in the same region [5].

Recent studies conducted by Leib, et al. suggest that along with the PVN, LH, and PVT also receive signaling from the MnPO related to water intake [13]. Consistent with these results, there have been multiple studies indicating hyperosmotically-induced increases in Fos expression, a marker used to identify acute activation of the activator

protein-1 (AP-1) complex in neurons through MAPK and ERK signaling, in the MnPO and connected pathways [13, 17, 60].

Signaling Mechanisms: Extracellular Dehydration

When peripherally or centrally injected, ANG II can increase in water intake in 15 minutes that are beyond what an animal would spontaneously drink daily [30]. Studies have been conducted indicating that the AV3V region is necessary to adequately sense and integrate peripherally generated ANG II-induced thirst [14]. The AV3V region is well populated with angiotensinergic nerve endings and AT1aRs that generate vigorous drinking to the dipsogenic action of ANG II [30]. The SFO has been shown to have highly dense connectivity to the MnPO [61]. It has been proposed that the SFO and OVLT are directly stimulated by circulating ANG II, which then in turn stimulates the MnPO [1, 30]. While this may be true, the MnPO has also been shown to be ANG II-sensitive and respond to centrally-derived ANG II [62, 63].

Fos-immunoreactivity has been a common method to map neuronal activation to acute responses in affected regions of the brain to a specific stimulus. In one study, ANG II was administered to rats intracerebroventricularly (icv) and induced significant increases in Fos expression in the SFO, MnPO, SON, and the posterior magnocellular neurons (PM) of the PVN. However, the ANG II-induced Fos was blocked by concomitant administration of losartan, a commonly used antihypertensive that antagonizes AT1aRs [64]. These results indicate a role of ANG II and its direct effects on the MnPO within the blood brain barrier. Additionally, studies have been conducted using AT1aR knockdown in the MnPO and tested responses to subcutaneously (sc,

peripheral) and icv (central) administration of ANG II [62]. In these studies, Shell, et al. found that drinking response was significantly reduced to centrally administered ANG II, but not to peripheral ANG II. The authors suggest that peripherally administered ANG II may involve glutamate that produces drinking in the absence of AT1aRs or the possibility of a different type of ANG II receptor that mediates thirst. Glutamatergic neural pathways likely play an important role in mediating thirst [65]. ICV injection of NMDA receptor antagonist, MK801, has been shown to block drinking responses stimulated by ANG II, intragastric hypertonic saline or water deprivation for 22 hours, as well as suppressed ANG II and water deprivation induced increase in fos expression in the MnPO. Thus, suggesting a glutamatergic input to the MnPO mediates both osmoregulatory and ANG II-stimulated thirst [66, 67]. Studies have shown that in addition to the MnPO, the OVLT and magnocellular neurons of the SON and PVN also receive projections from the SFO [61, 68, 69]. Therefore, the observed effects may be due to other connections from the SFO to the SON or PVN that induce AVP release and mediate thirst in that manner [30, 70].

Although ANG II is a potent peptide hormone that is effective at inducing thirst, it has been shown that it can also increase blood pressure and in turn may affect thirst and drinking responses [71]. Studies previously conducted by Evered, et al. (1988) have shown that ANG II induces thirst in rats that are hypovolemic and hypotensive. In normotensive rats given ANG II, thirst was still induced but to a lesser degree than the hypotensive rats and in hypertensive rats, ANG II was ineffective at inducing thirst due to immobilizing deficits from the high blood pressure [71]. Therefore, the association of

ANG II-induced thirst and its effects on blood pressure must be considered while studying one or the other.

Arginine Vasopressin

AVP is a peptide hormone that works to increase water retention by reabsorbing water from the collecting duct of the kidneys, and increase sodium excretion [19]. Thirst and AVP release act to maintain homeostasis in response to cellular and extracellular dehydration: plasma osmolality, blood pressure or volume [19]. Under normal conditions, the SFO and OVLT signal to both the PVN and, to a larger degree, the SON magnocellular neurons to release AVP in response to increased plasma osmolality and elevated ANG II concentrations [53]. Anticipatory signals for thirst and AVP release have been shown to converge on the same homeostatic neurons of the SFO, which monitor the tonicity of blood [19].

Studies have shown that SFO^{NOS1} neurons are activated by water restriction and rapidly return to baseline after water access before plasma osmolality returns to normal [17, 72]. In studies conducted in rodents, there appears to be an approximate 10 min delay between water consumption and its absorption into the bloodstream [19, 73]. The time discrepancy that mediates this delay has been thought to be attributed to water taste receptor cells, potentially acid-sensing receptors on the tongue, that could track fluid ingestion immediately, while fluid tonicity and blood volume and pressure is more delayed [17, 19, 74]. This delayed signal may originate from the osmosensitive esophageal and gastric cells through the sensory vagus nerve, which then acts in a feedback loop to signal water satiety [75]. In contrast, anticipatory, feedforward control of the hypothalamus

signals for thirst and AVP release to regulate water absorption and prevent homeostatic perturbations [76]. These feedforward signals for thirst and AVP release converge on the same homeostatic neurons detecting the feedback signals of osmolality and circulating ANG II [19].

The MnPO plays a particularly important role in regulating AVP release. Fos immunohistochemistry and electrophysiology experiments have shown the MnPO relays signals related to plasma osmolality and ANG II from the SFO and OVLT to the vasopressin-secreting SON and PVN magnocellular neurons, as well [1, 59, 77, 78]. The MnPO was first identified in studies in rats and sheep to play particularly important role in osmoregulation and AVP secretion. Lesioning the MnPO alone or in conjunction with the OVLT, resulted in systemic hypertonicity from the resulting dysregulation of AVP secretion [29, 79]. The importance of the MnPO in AVP regulation is exemplified when GABA agonists muscimol or baclofen are directly injected into the MnPO, osmotically stimulated vasopressin secretion is inhibited [80]. Additionally, AVP release is stimulated when direct injection of glutamatergic agonist n-methyl d-aspartate (NMDA) is directly injected into the MnPO [81].

In addition to the excitatory effects the MnPO has on magnocellular, vasopressin-containing neurons during hyperosmotic or ANG II stimulation, the MnPO has also been shown to elicit an inhibitory input to AVP neurons in the SON during water loading and plasma hypotonicity. Electrophysiology experiments indicated that during hypotonic bath application, some MnPO neurons increased activity [82]. Experiments conducted by Nissen and Renaud indicated that hypotonically-sensitive MnPO neurons may be GABAergic and involved in inhibiting SON AVP secretion [83]. Additionally, studies have

demonstrated that animals with periventricular lesions damaging the MnPO prevented AVP secretion from falling in response to water loading and plasma hypotonicity [23, 84]. Thus, preventing GABAergic-mediated inhibition from the MnPO on the SON and allowing AVP secretion to be unaffected and dysregulating water loading.

The MnPO and Autonomic Function

ANG II is thought to have multiple functions depending on its cellular localization. ANG II is able to function both as a hormone in the periphery as well as a peptide neurotransmitter in the brain. As a neurotransmitter, it can regulate neurons projecting into nuclei responsible for water and electrolyte homeostasis and those projecting to preganglionic nerves controlling SNA [85]. However, ANG II can also be augmented during hypoxic insults, such as those associated with Obstructive Sleep Apnea (OSA), resulting in chronic hypertension [86-88]. Recent studies have found that an intact MnPO is necessary for the development of chronic intermittent hypoxia (CIH)-induced hypertension [7, 89], as well as ANG II-induced hypertension [9, 10]. The role of the MnPO in the development of hypertension in CIH associated with OSA is the focus of the second aim.

Obstructive Sleep Apnea

OSA is a disease that has been prominent throughout the past few hundred years, but has only recently gained attention for research within the last 40 to 50 years [90]. According to the American Sleep Apnea Association, an estimated 22% of Americans suffer from sleep apnea, with 80% of those having undiagnosed moderate to

severe obstructive sleep apnea [88]. In OSA repeated momentary interruptions of respiration during all stages of sleep causes a lack of oxygen in the blood to different regions of the body [91]. OSA can be defined as the periodic cessation in breathing rhythm (apnea) or periodic sustained reduction in breath amplitude (hypopneas), causing significant arterial deficits in blood oxygen concentration (hypoxemia) and increases in blood carbon dioxide (hypercapnia) [90]. This lack of circulating oxygen and increased circulating carbon dioxide leads to hypertension, which can persist from sleep to waking hours through elevated sympathetic nerve activity [90].

The hypoxia associated with OSA has been proposed to lead to advanced cardiovascular diseases, such as stroke, hypertension, and myocardial ischemia, if not treated [92]. Obstruction of the extrathoracic upper airway, seen in OSA, in conjunction with the cessation of brain stem respiratory motor output produces stress on the vasculature leading to over compensation by the autonomic nervous system (ANS) [90]. Sympathetic nerve activity is increased due to chemoreflex activation from the hindbrain and angiotensinergic pathway stimulation from the forebrain. It is proposed that activation of the renin-angiotensin system (RAS) contributes to the sustained component of hypertension. This can be better understood by studying the mechanisms underlying its initiation and maintenance.

Chronic Intermittent Hypoxia

Chronic intermittent hypoxia (CIH) is a model using rodents, first described by Fletcher, et al. [93], designed to mimic the intermittent hypoxemia experienced in OSA and central sleep apnea. CIH mimics the intermittent hypoxemia using a hypoxic

environment in a controlled chamber. This causes many of the characteristic pathophysiological symptoms in rats as those associated with OSA in humans, including increased blood pressure [94]. The autonomic nervous system is particularly important in the study of CIH, as it encompasses both the sympathetic nervous system (SNS) and the parasympathetic nervous system (PNS). Hypoxia is responsible for increasing activity of the SNS and diminishing activity of the PNS, causing the body to be in a sympathetic-driven state, rather than in the homeostatic regulation state when at rest [95]. Hypoxia also causes local vascular effects that lead to increased cardiac output and peripheral vasoconstriction that contribute elevated blood pressure [94].

CIH results in periods of hypoxemia that stimulate peripheral carotid body chemoreceptors, ventilatory hypoxic reflexes, and a decrease in baroreflex efficiency, leading to increased arterial blood pressure due to elevated sympathetic nerve activity [96, 97]. Studies have shown CIH induces a simultaneous decrease in baroreceptor sensitivity with an increase in hypoxic ventilatory gain, and that CIH induced persistent hypertension, preceded by early changes in carotid body chemosensory control of cardiorespiratory and autonomic function [98].

The Renin-Angiotensin System

The RAS plays an important, systemic role in blood pressure and volume regulation. In instances of hypovolemia or hypotension, peripheral ANG II concentration is increased (Figure 2) to induce vasoconstriction, stimulate AVP secretion, and induce thirst to raise blood volume and pressure back to homeostasis [99]. Dysregulation (i.e. episodic hypoxia) of the RAS can contribute to the pathogenesis and development of

hypertension [93]. The peripheral RAS has been heavily studied and characterized, however, although still somewhat controversial, there is also convincing evidence for a brain RAS as well [63, 100].

Through autocrine and paracrine signaling, the brain RAS functions as a neurotransmitter to regulate blood pressure [100]. Angiotensinogen, a precursor required to generate all ANG II peptides (Figure 2) has been shown to be produced in astrocytes and neurons in brain regions including the SFO [63, 101], MNCs of the PVN [102], and hindbrain ventrolateral medulla and nucleus tractus solitarus (NTS) [103]. ANG II nerve fibers have been identified in the SFO, MnPO, SON, PVN and posterior pituitary [104], as well as in secretory vesicles [105] that are proposed to be synaptic vesicles [106]. The synthesis and modulation of renin centrally has been less clear. Studies in dog and rat brain indicated the presence of renin-like enzymatic activity [107], while others have shown renin protein and mRNA are present in astrocytes and neurons in rat, mouse, and human [108]. Additionally, studies by Lavoie, et al. using transgenes in a mouse model demonstrated that renin- and angiotensinogen-expressing cells are similarly distributed within the SFO, PVN and RVLM [106, 109].

The presence of renin alone does not lead to increases in ANG II but also requires angiotensinogen to be present as well [110]. Angiotensinogen is converted by renin to angiotensin I (ANG I), and angiotensin converting enzyme (ACE) can then convert ANG I to ANG II, as in the periphery (Figure 2). ANG II then binds to AT1aRs, promoting kinase activation to increase neuronal firing, norepinephrine release and sympathetic outflow, as well as oxidative stress by allowing for synthesis of superoxide through activation of nicotinamide adenine dinucleotide phosphate (NADPH) oxidase.

ACE has been found to be upregulated during CIH exposure in the MnPO and is a common therapeutic target for patients with hypertension (i.e. ACE inhibitors) [6, 8]. In rodents AT1 receptors can be separated into AT1a and AT1b receptors, with AT1aRs suggested to play a role in the blood pressure regulation, AVP release and thirst while AT1bRs mainly regulate water intake [111]. ANG II has also been shown with a similar affinity to bind to AT2 receptors, which are mainly involved in regulating compensatory mechanisms in rats [112]. Additionally, AT4 receptors, sensitive to ANG IV, have also been shown to be present in the brain and involved in memory and Alzheimer's disease [113].

More recently discovered was a new arm of the RAS that functions opposite of the ACE/ANG II/AT1aR axis. The other axis of the RAS involves a second ACE (ACE2) that is able to convert ANG II to a vasodilatory metabolite, ANG-(1-7). ANG-(1-7) can bind to Mas receptors in the brain, resulting in the attenuation of effects induced by ANG II and promote production of nitric oxide (NO), as well as augment the metabolic actions of bradykinin via inhibition of ACE activity [114, 115]. ANG-(1-7) was shown to be present as an endogenous constituent of the brain including the hypothalamus, medulla oblangata, and amygdala, adrenal glands and plasma of normal rats [114, 116]. ACE2 in the brain has been shown to be widely distributed in the cytoplasmic space of neuronal cell bodies in rodents [117].

Studies in humans have shown that ACE2 shedding, a process by a member of the 'A Disintegrin and Metalloproteases' family (ADAM17), cleaves ACE2 from the plasma membrane and contributes to the loss of the enzyme's compensatory actions in the CNS during the development of neurogenic hypertension [114, 118, 119]. Upon brain RAS

over-activation, AT1aRs become significantly upregulated in neurons, microglia and astrocytes which further potentiates the development of hypertension [62, 120]. Studies conducted by Xu, et al. have shown that neuronal AT1aRs are essential for driving ADAM17-mediated ACE2 shedding in neurogenic hypertension [119]. These studies also indicated that reactive oxygen species (ROS) generation and extracellular signal-regulated kinase (ERK), downstream AT1aR-mediated mechanisms, also play a critical role in mediating the AT1aR-driven increase of ADAM17 in neurons [119]

Hypertension Pathogenesis and Angiotensin II

Peripheral chemoreceptors in the carotid bodies sense circulating oxygen and central chemoreceptors provide feedback for carbon dioxide levels [121]. Due to the hypoxemic effect of decreased oxygenation in hypoxic conditions, the brain releases signaling molecules to increase sympathetic nerve activity, in an effort to increase circulating oxygen to vital organs—like the brain and heart. The hypoxemic environment enhances carotid body sensory activity and the ROS generated from the hypoxia-reoxygenation cycles causes carotid reflex sensitization [90]. The source of ROS appears to be mitochondrial, however, plasma membrane NADPH oxidase may also contribute to ROS production that then mediates the effects of ANG II [63, 90]. Patients with OSA have an increased plasma concentration of ANG II [90], which is derived from the prohormone angiotensinogen that is released by the liver and may stimulate angiotensin production in the brain [106]. The high circulating concentration of plasma ANG II is thought to increase NADPH oxidase levels leading to further ROS production in the carotid body [90]. This process causes a viscous feed-forward redox stimulation of the

NADPH oxidase enzymes that contributes to hypertension and other cardiovascular diseases [90, 122, 123]. Generation of ROS activates the sympathetic nervous system through the central nervous system [124]. The increased level of ROS from the hypoxic environment leads to carotid body responses from the decreased levels of oxygen [125].

Hypertension is a chronic elevation of the 24-hour average blood pressure and can be a neurogenic disease if its pathogenesis includes the afferent arm of baroreceptors, chemoreceptors, and renal afferents, or the central circuitry [126]. ANG II is an effector of the brain's RAS, which enhances sympathetic nerve activity and contributes to hypertension induced by CIH through its effects on sympathetic outflow [11, 127]. ANG II can act directly on the central nervous system, leading to sympathetic activation [106]. Sympathetic outflow normally leads to increased ANG II, but during dysregulation the SNS leads to increased ANG II during sleep and ANG II leads to increased sympathetic nerve activity in the waking period; which may contribute to the tonic activation of the peripheral chemoreceptors [94]. When arterial oxygen is low and arterial carbon dioxide is high, the activation of central and peripheral chemoreceptors on the carotid bodies leads to increased receptor firing to the hindbrain [128]. Carotid chemoreceptor afferents terminate in the dorsomedial and medial subnuclei of the NTS in the hindbrain and the carotid baroreceptor afferents project to the dorsal and lateral divisions of the NTS in the hindbrain [129]. The NTS signals the rostral ventrolateral medulla (RVLM) directly or indirectly via the caudal ventrolateral medulla (CVLM) [129, 130]. RVLM neurons receive excitatory (glutamatergic) inputs from the forebrain, commissural NTS, and the area postrema (AP) and receive inhibitory (GABAergic) inputs from the

CVLM; the more excitatory inputs or diminished inhibitory inputs can result increased RVLM activity leading to hypertension [131].

Baroreceptor reflex control can by reduced by diminished inhibition of the RVLM by the CVLM, while the abnormal discharge of chemoreceptor afferents is increased via NTS excitatory inputs to the RVLM by the ensuing hypoxia [129, 131]. Therefore, increased RVLM activity increases sympathetic output via the sympathetic preganglionic neurons in the intermediolateral nucleus (IML) of the spinal cord, leading to an increase in sympathetic outflow to the vasculature and heart, inducing a hypertensive state [128, 129].

The CVOs are stimulated by ANG II which decreases baroreflex sensitivity and increases sympathetic activity, making the CVOs critical for the development and sustainability of hypertension in blunting the inhibitory effects of the NTS and CVLM signaling to the RVLM in high renin models [132]. The production of cytosolic or mitochondrial ROS in the SFO is a primary product of the central actions of circulating ANG II and mediates its physiological effects, which is then potentially relayed through the AT1aR target [11, 85]. The SFO projects to the other nuclei in the AV3V region of the brain including the MnPO and the OVLT; both of which are rich in angiotensin receptors [11]. The MnPO projects to the PVN in the hypothalamus and is a major component in regulation of sympathetic outflow [1].

The NTS also has afferents that stimulate the PVN, causing the hypothalamic region to then project its signal to the RVLM to contribute sympathetic outflow [133]. The AV3V region, PVN, SON, and the RVLM compose the main ANG II-sensitive pathways stimulated by the circulating ANG II, aldosterone, and sodium concentration [134] and can be viewed in Figure 3.

Elevated activity of the angiotensinergic pathways can promote sympathoexcitation although the mechanisms responsible for sustained sympathetic activation are unknown [134]. One experiment demonstrated that hypothalamic stimulation hyperpolarizes baroreceptor-sensitive NTS cells, making them less excitable and this is mediated by $GABA_A$ receptors in the NTS [129]. Inhibition of baroreflex and pressor response evoked during the defense response was in part due to activity of the arterial chemoreflex [129]. Electrical or chemical stimulation of the RVLM increases sympathetic nerve activity and arterial pressure as can disinhibition of the RVLM with the $GABA_A$ antagonist bicuculline [135].

Sustained Hypertension

Several mechanisms have been proposed to contribute to sustained hypertension associated with CIH including changes in chemoreceptor reflex sensitivity [136], baroreceptor flex function [97, 137], and catecholamine neurons in the NTS in the hindbrain [138]. Another contributing mechanism may be through increased sympathetic tone to the kidneys causing increased plasma renin-angiotensin (PRA) concentrations (Figure 3) [93]. This could result in ANG II-induced CVO activation and lead to MnPO stimulation of the PVN. Activation of MnPO neurons that project to the PVN would stimulate preautonomic neurons in the PVN, creating a vicious cycle increasing sympathetic tone (Figure 3) [139, 140]. We have previously shown that the MnPO is necessary for CIH hypertension and the MnPO neurons that project to the PVN have an excitatory effect on PVN activity [7, 89]. Studies have also shown that CIH hypertension relies on elevated sympathetic tone and ongoing PVN neuronal activity [12, 89]. However,

the role and phenotype of the neurons involved in the MnPO—PVN pathway during CIH-induced hypertension has not yet been studied but is important in order to fully understand the neural mechanism of how CIH-induced hypertension is maintained even during a normoxic setting.

The Role of the MnPO in CIH Hypertension

In many animal models, electrolytic lesions of the AV3V region reverse or inhibit many forms of hypertension. The nuclei that compose the AV3V regions all increase expression of the FosB transcription factor after 7 days of CIH and serves as a marker of neuronal activity [141]. FosB is a transcription factor mediated by the activator protein-1 (AP-1) complex. ΔFosB is a splice variant of FosB and is involved in chronic transcriptional activation relating to neural adaptations related to chronic behavioral changes, like CIH hypertension [142]. Knockdown of transcription factor ΔFosB, using a virally induced dominant negative inhibitor (ΔJunD) in the MnPO that antagonizes ΔFosB and other AP-1 mediated transcription factors significantly attenuated the sustained component of CIH-induced hypertension [7, 140].

Studies have shown knockdown of AT1ARs in the SFO decreases CIH hypertension and FosB in the PVN and MnPO [11]. This is consistent with the hypothesis that increased activation of the peripheral renin-angiotensin system can contribute to CIH hypertension through the SFO. Our lab has also successfully performed experiments demonstrating the importance of a fully functioning MnPO in the development of CIH-induced hypertension. Chronic ICV infusion of losartan attenuated hypertension in animals exposed to CIH compared to controls, as well as inhibited

increases in FosB expression of downstream targets including the PVN and RVLM [87, 140]. Additionally, knockdown of ACE in the MnPO also resulted in data consistent with these studies [8]. The knockdown of AT_1aRs in the MnPO using a complimentary short hairpin RNA blocked the sustained component of CIH-induced hypertension [62]. In these studies, FosB staining in MnPO, PVN, and the RVLM is attenuated, as well, suggesting that these regions are involved in CIH hypertension.

The Role of the PVN in CIH Hypertension

The hypothalamic region of the central nervous system—specifically the paraventricular nucleus (PVN)—has been implicated as a major site in the pathogenesis and maintenance of hypertension, as it is a key area for integrating central and peripheral stimuli to regulate blood pressure [143, 144]. The PVN is an important regulator of autonomic and neuroendocrine function that is still not yet fully understood [143]. The PVN contains two distinct neuronal phenotypes the magnocellular and parvocellular cells [53]. The parvocellular cells can then be further subdivided into dorsal, ventral, lateral, medial, and periventricular subregions (Figure 4), with each region influencing unique functions [7, 53, 89]. Studies have shown that the PVN nuclei contain many pre-autonomic neurons that are sensitive to changes in osmolality and influence autonomic function [143, 145, 146]. Many studies have also shown that an increase in excitability and synaptic plasticity in the neuronal activity of PVN neurons leads to an elevated sympathetic outflow [12, 140, 144, 147].

The PVN can influence activity in autonomic premotor regions of the hindbrain, specifically the RVLM that regulates sympathetic outflow. Menani et al. noted that ‘an

important direct connection of the AV3V with the hindbrain is made through the PVN, which mono-or polysynaptically connects with sympathetic neurons in the IML (intermedial lateral column of the spinal cord) or indirectly affects sympathetic activity through connections with the RVLM' [148]. Studies also show that the MnPO influences sympathetic responses through a glutamatergic input to parvocellular neurons of the PVN that connect to sympathetic vasoconstrictor pathways [1, 149]. These observations are consistent with our working hypothesis that the MnPO influences CIH hypertension through its projections to the PVN.

The Working Hypothesis

When the MnPO receives signals related to changes in osmolality, ANG II, or other stimuli affecting cardiovascular, autonomic, or fluid homeostasis, the PVN is stimulated connecting the AV3V to the hindbrain. Together, the MnPO and PVN influence sympathetic outflow through monosynaptic and polysynaptic connections with the RVML and the IML effecting autonomic function [140, 148]. Studies have shown that during the initiation of CIH, chemoreceptors become sensitized and increase afferent stimulation of regions in the hindbrain that increase sympathetic outflow and plasma renin angiotensin [88, 140]. As the disease progresses, peripheral ANG II becomes inappropriately elevated and is sensed by the CVO's (SFO and OVLT—as mentioned above and shown in Figure 2), sensitizing the MnPO [140]. The MnPO projects to and stimulates pre-sympathetic neurons in the PVN that then mono- or polysynaptically 'closes the loop' by projecting signals to the IML and RVLM, and along with long-term facilitation, chemoreflex sensitivity, and eventual baroreflex desensitization, continues

and maintains increased sympathetic outflow, resulting in sustained hypertension [12, 90, 126, 139, 148]. Sustained hypertension and chronic increases in sympathetic outflow as a result of CIH associated with OSA leads to many end organ damages, such as heart disease, stroke, and mortality [90].

Conclusion

The MnPO is an integrative nucleus that plays an extremely important role in the maintenance of body fluid homeostasis and blood pressure regulation. Many studies have outlined the importance and necessity for the MnPO in homeostatic function; however, -specific MnPO neurons involved in regulating body fluid homeostasis and blood pressure regulation remain to be determined, as well as if MnPO neurons regulated in a stimulus-dependent manner.

The studies in this project directly address these discrepancies and demonstrate how selectively activating or inhibiting excitatory neurons acutely or chronically in the MnPO regulates activity at the protein, neuronal behavioral and physiological level. These studies are an important step in answering questions involving intracellular communication within the MnPO, how MnPO activation or inhibition can affect neuronal properties, and how this produces changes in projection terminals involved regulating neuroendocrine and autonomic function. These studies also test the efficacy of induced inhibition of pathway-specific MnPO neurons in acute as well as chronic studies, while addressing the mechanisms underlying the early development of sustained hypertension in CIH associated with OSA, a growing disease affecting the aging population. The results of these experiments provide new information about how

dysregulation of the MnPO—PVN pathway heavily contributes to CIH-induced hypertension, possibly providing a potential therapeutic target for those suffering from OSA that may be resistant to the benefits of continuous positive airway pressure (CPAP) or other pharmacological treatments. These studies provide relevance to studying the early pathogenesis of ANG II-induced disease states and associated dysregulation of centrally-mediated mechanisms.

Figure 1. *Sagittal section of the AV3V region and hypothalamic projections from the MnPO.* Depicted summary of hyperosmotic and ANG II-induced neural signaling in drinking behavior and AVP release. ANG II, angiotensin II; AV3V, anteroventral 3rd ventricle; MnPO, median preoptic nucleus; SFO, subfornical organ; SON, supraoptic nucleus; PP, posterior pituitary; PVN, paraventricular nucleus.

Figure 1.

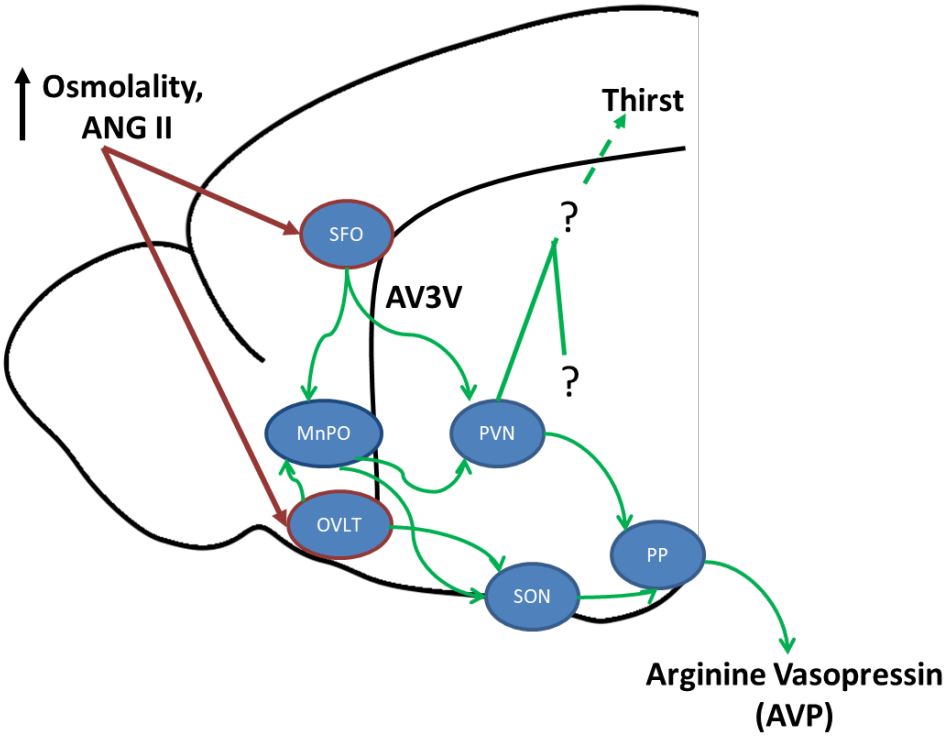
Osmolality,
ANG II
Thirst
SFO
AV3V
?
?
MnPO
PVN
OVLT
PP
SON
Arginine Vasopressin
(AVP)

Figure 2. *Diagram showing activation of the peripheral RAS and its systemic effects.* Upon increases in sympathetic activation, decreases in blood pressure and decreases in sodium delivery to the distal tubule, the kidney releases renin into the bloodstream and cleaves the angiotensin (ANG) precursor, angiotensinogen, released from the liver to form ANG I. The lungs release angiotensin converting enzyme (ACE) to then cleave ANG I into the active neuropeptide, ANG II. ANG II then binds to angiotensin type 1a receptors (AT1aRs) in peripheral organs and in the central nervous system to increase blood pressure and blood volume (adapted from Bader and Ganten [99]).

Figure 2.

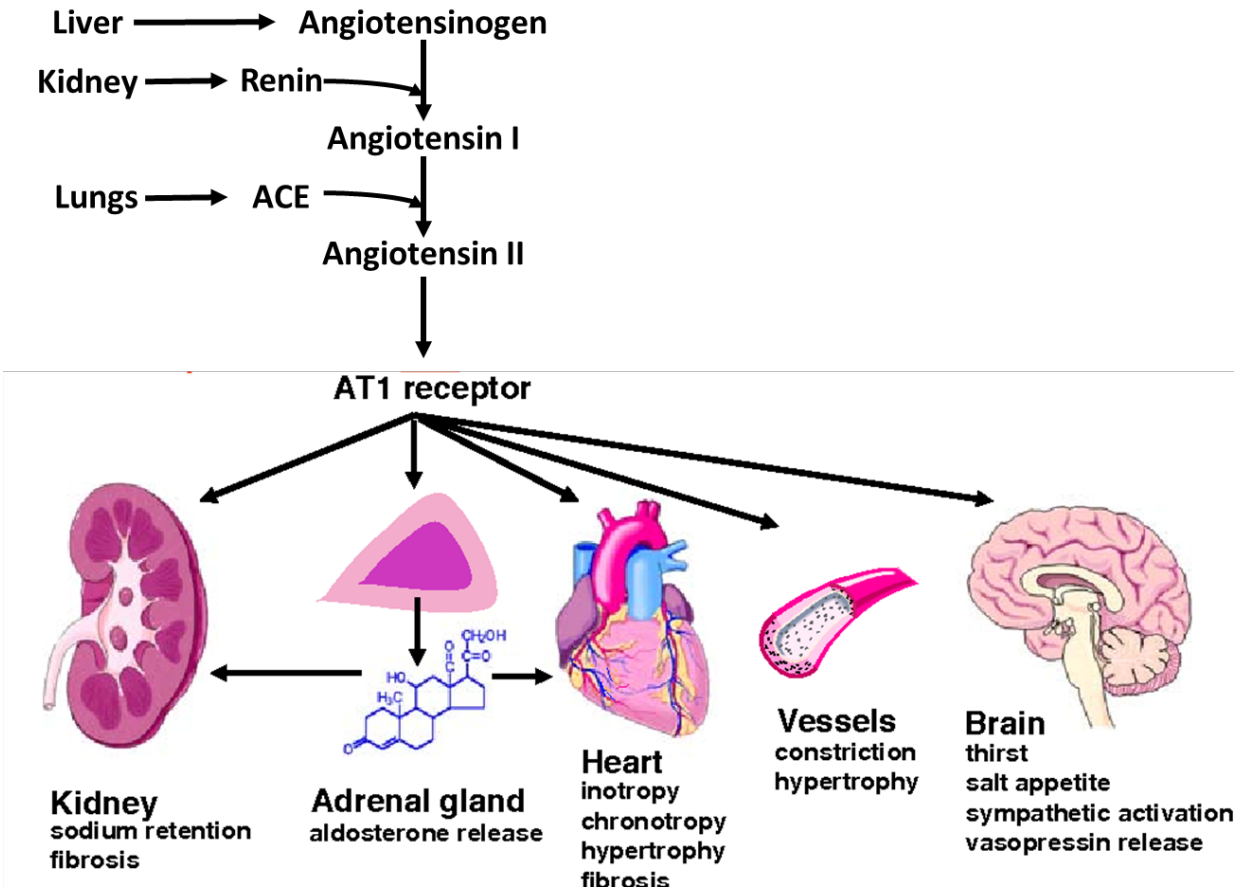
Liver
Angiotensinogen
Kidney
Renin
Angiotensin I
Lungs
ACE
Angiotensin II
AT1 receptor
Kidney
sodium retention
fibrosis
Adrenal gland
aldosterone release
Heart
inotropy
chronotropy
hypertrophy
fibrosis
Vessels
constriction
hypertrophy
Brain
thirst
salt appetite
sympathetic activation
vasopressin release

Figure 3. *Schematic diagraming the proposed mechanism of how CIH initiates hypertension.* CIH causes upregulation through the hindbrain to increase sympathetic nerve activity (SNA). This can lead to upregulated plasma renin activity (PRA) and activation of the renin-angiotensin system, which results in a concomitant increase in Angiotensin II and stimulates the sensory circumventricular organs—subfornical organ (SFO) and organum vasculosum of the lamina terminalis (OVLT)—that project to the median preoptic nucleus (MnPO) [86, 140, 150]. The MnPO has direct downstream effects that terminate in the supraoptic nucleus (SON) and paraventricular nucleus (PVN). Excitatory neurons in the PVN, particularly those in the parvocellular region, can excite neurons of the nucleus tract solitarius (NTS) and rostral ventrolateral medulla (RVLM), resulting in a vicious cycle from continuous elevated sympathetic outflow. This is a proposed pathway for the initiation of hypertension and how elevated blood pressure is sustained. Abbreviation: AP, area postrema; CVLM, caudal ventrolateral medulla; IML, intermediolateral nucleus of the spinal cord (adapted from Shell, et. al. [140]).

Figure 3.

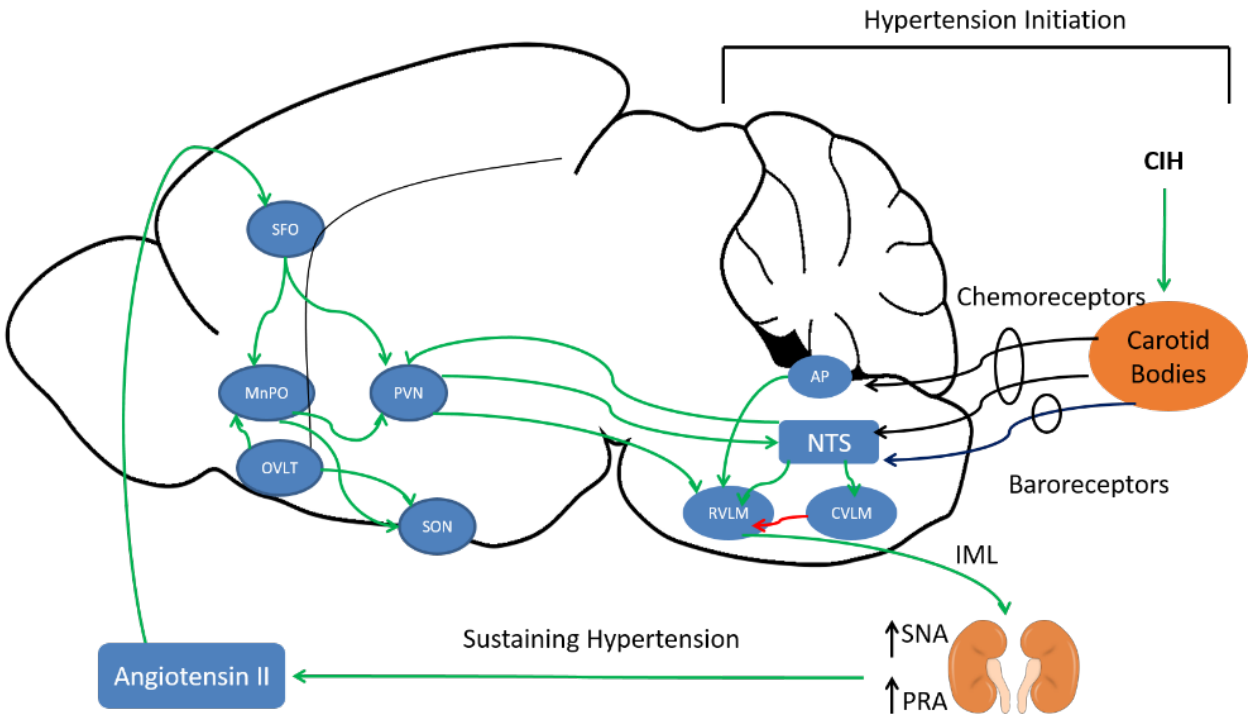
Hypertension Initiation
CIH
Chemoreceptors
Carotid Bodies
SFO
MnPO
PVN
OVLT
SON
AP
NTS
RVLM
CVLM
Baroreceptors
IML
Sustaining Hypertension
↑SNA
↑PRA
Angiotensin II

Figure 4. *Diagram of the PVN of the hypothalamus morphological divisions and their major functions.* 3V, 3rd ventricle; dp, dorsal; lp, lateral; mpd, medial dorsal; mpv, medial ventral (parvocellular); pm, posterior (magnocellular); adapted from Mack, et al. [151].

Figure 4.

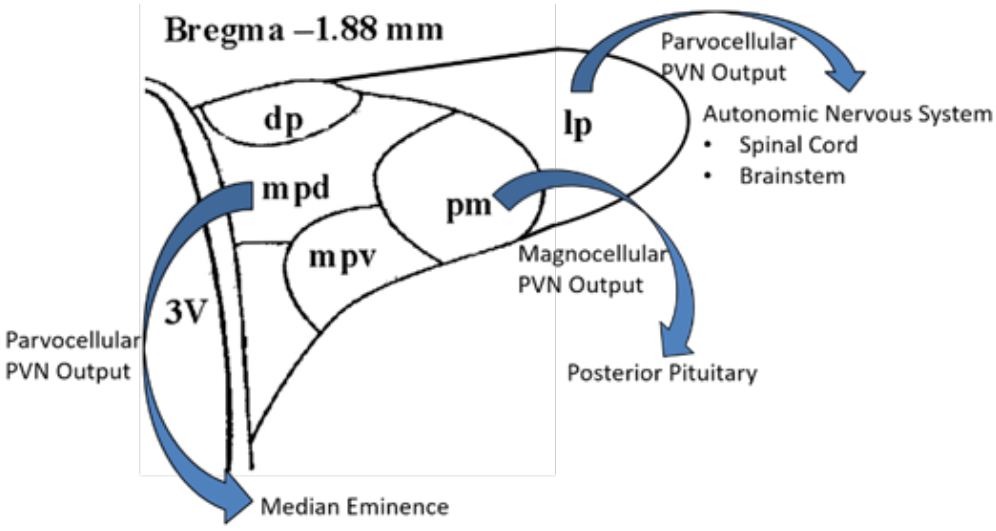
Bregma –1.88 mm
dp
mpd
pm
mpv
3V
lp
Parvocellular
PVN Output
Autonomic Nervous System
• Spinal Cord
• Brainstem
Magnocellular
PVN Output
Posterior Pituitary
Parvocellular
PVN Output
Median Eminence

References

1. McKinley MJ, Yao ST, Uschakov A, McAllen RM, Rundgren M, Martelli D. The median preoptic nucleus: front and centre for the regulation of body fluid, sodium, temperature, sleep and cardiovascular homeostasis. Acta Physiol (Oxf) 2015;214:8-32. doi: 10.1111/apha.12487. Epub 12015 Apr 12481.

2. Cunningham JT, Beltz T, Johnson RF, Johnson AK. The effects of ibotenate lesions of the median preoptic nucleus on experimentally-induced and circadian drinking behavior in rats. Brain Res 1992;580:325-330.

3. Johnson AK, Cunningham JT, Thunhorst RL. Integrative role of the lamina terminalis in the regulation of cardiovascular and body fluid homeostasis. Clin Exp Pharmacol Physiol 1996;23:183-191.

4. Allen WE, DeNardo LA, Chen MZ, et al. Thirst-associated preoptic neurons encode an aversive motivational drive. Science 2017;357:1149-1155.

5. Abbott SB, Machado NL, Geerling JC, Saper CB. Reciprocal Control of Drinking Behavior by Median Preoptic Neurons in Mice. J Neurosci 2016;36:8228-8237.

6. Cunningham JT, Knight WD, Mifflin SW, Nestler EJ. An essential role for ΔFosB in the median preoptic nucleus in the sustained hypertensive effects of chronic intermittent hypoxia. Hypertension 2012;60:179-187.

7. Cunningham JT, Knight WD, Mifflin SW, Nestler EJ. An Essential role for DeltaFosB in the median preoptic nucleus in the sustained hypertensive effects of chronic intermittent hypoxia. Hypertension 2012;60:179-187.

8. Faulk KE, Nedungadi TP, Cunningham JT. Angiotensin converting enzyme 1 in the median preoptic nucleus contributes to chronic intermittent hypoxia hypertension. Physiol Rep 2017;5.

9. Ployngam T, Collister JP. Role of the median preoptic nucleus in chronic angiotensin II-induced hypertension. Brain Res 2008;1238:75-84.

10. Ployngam T, Collister JP. An intact median preoptic nucleus is necessary for chronic angiotensin II-induced hypertension. Brain Res 2007;1162:69-75.

11. Saxena A, Little JT, Nedungadi TP, Cunningham JT. Angiotensin II type 1a receptors in subfornical organ contribute towards chronic intermittent hypoxia-associated sustained increase in mean arterial pressure. Am J Physiol Heart Circ Physiol 2015;308:H435-446.

12. Mifflin S, Cunningham JT, Toney GM. Neurogenic mechanisms underlying the rapid onset of sympathetic responses to intermittent hypoxia. J Appl Physiol (1985) 2015;119:1441-1448.

13. Leib DE, Zimmerman CA, Poormoghaddam A, et al. The Forebrain Thirst Circuit Drives Drinking through Negative Reinforcement. Neuron 2017;96:1272-1281 e1274.

14. McKinley MJaAKJ. The Physiological Regulation of Thirst and Fluid Intake. News Physiol Sci 2004;19:1-6.

15. McKinley MJ, Denton DA, Ryan PJ, Yao ST, Stefanidis A, Oldfield BJ. From sensory circumventricular organs to cerebral cortex: neural pathways controlling thirst and hunger. J Neuroendocrinol 2019:e12689.

16. Augustine V, Gokce SK, Lee S, et al. Hierarchical neural architecture underlying thirst regulation. Nature 2018;555:204-209.

17. Oka Y, Ye M, Zuker CS. Thirst driving and suppressing signals encoded by distinct neural populations in the brain. Nature 2015;520:349-352.

18. Kaufman JTFaS. Cellular and extracellular dehydration, and angiotensin as stimuli to drinking in the common iguana *Iguana iguana*. J Physiol 1976;265:21.

19. Bichet DG. Vasopressin and the Regulation of Thirst. Ann Nutr Metab 2018;72 Suppl 2:3-7.

20. Fitzsimons JT. Angiotensin, thirst, and sodium appetite: retrospect and prospect. Fed Proc 1978;37:2669-2675.

21. Gu GB, Simerly RB. Projections of the sexually dimorphic anteroventral periventricular nucleus in the female rat. J Comp Neurol 1997;384:142-164.

22. Miselis RR. The efferent projections of the subfornical organ of the rat: a circumventricular organ within a neural network subserving water balance. Brain Res 1981;230:1-23.

23. Andersson B, Leksell LG, Lishajko F. Perturbations in fluid balance induced by medially placed forebrain lesions. Brain Res 1975;99:261-275.

24. Buggy J, Fink GD, Johnson AK, Brody MJ. Prevention of the development of renal hypertension by anteroventral third ventricular tissue lesions. Circ Res 1977;40:I110-117.

25. Black SL. Preoptic hypernatremic syndrome and the regulation of water balance in the rat. Physiol Behav 1976;17:473-482.

26. McAllen RM, Pennington GL, McKinley MJ. Osmoresponsive units in sheep median preoptic nucleus. Am J Physiol 1990;259:R593-600.

27. Tanaka J, Kaba H, Saito H, Seto K. Subfornical organ efferents influence the activity of median preoptic neurons projecting to the hypothalamic paraventricular nucleus in the rat. Exp Neurol 1986;93:647-651.

28. Tanaka J, Nomura M, Kariya K, Nishimura J, Kimura F. Median preoptic neurons projecting to the hypothalamic paraventricular nucleus are sensitive to blood pressure changes. Brain Res 1993;605:338-341.

29. Mangiapane ML, Thrasher TN, Keil LC, Simpson JB, Ganong WF. Deficits in drinking and vasopressin secretion after lesions of the nucleus medianus. Neuroendocrinology 1983;37:73-77.

30. Fitzsimons JT. Angiotensin, thirst, and sodium appetite. Physiol Rev 1998;78:583-686.

31. Goldstein R, Beideman LR, Stern JA. Effect of water deprivation and saline-induced thirst on the conditioned heart rate response of the rat. Physiol Behav 1970;5:583-587.

32. Johnson AK, Cunningham JT. Brain mechanisms and drinking: the role of lamina terminalis-associated systems in extracellular thirst. Kidney Int Suppl 1987;21:S35-42.

33. Verney EB. The antidiuretic hormone and the factors which determine its release. Proc R Soc Lond B Biol Sci 1947;135:25-106.

34. McKinley MJ, Blaine EH, Denton DA. Brain osmoreceptors, cerebrospinal fluid electrolyte composition and thirst. Brain Res 1974;70:532-537.

35. Bourque CW. Central mechanisms of osmosensation and systemic osmoregulation. Nat Rev Neurosci 2008;9:519-531.

36. Andersen LJ, Jensen TU, Bestle MH, Bie P. Gastrointestinal osmoreceptors and renal sodium excretion in humans. Am J Physiol Regul Integr Comp Physiol 2000;278:R287-294.

37. Carlson SH, Beitz A, Osborn JW. Intragastric hypertonic saline increases vasopressin and central Fos immunoreactivity in conscious rats. Am J Physiol 1997;272:R750-758.

38. Choi-Kwon S, Baertschi AJ. Splanchnic osmosensation and vasopressin: mechanisms and neural pathways. Am J Physiol 1991;261:E18-25.

39. Baertschi AJ, Pence RA. Gut-brain signaling of water absorption inhibits vasopressin in rats. Am J Physiol 1995;268:R236-247.

40. Osaka T, Kobayashi A, Inoue S. Vago-sympathoadrenal reflex in thermogenesis induced by osmotic stimulation of the intestines in the rat. J Physiol 2002;540:665-671.

41. Vallet PG, Baertschi AJ. Spinal afferents for peripheral osmoreceptors in the rat. Brain Res 1982;239:271-274.

42. Collister JP, Olson MK, Nahey DB, Vieira AA, Osborn JW. OVLT lesion decreases basal arterial pressure and the chronic hypertensive response to AngII in rats on a high-salt diet. Physiol Rep 2013;1:e00128.

43. Meehan J, Collister JP. Lesion of the Subfornical Organ attenuates Neuronal Activation of the Paraventricular Nucleus in response to Angiotensin II in normal rats. Open J Neurosci 2011;1:1.

44. Vieira AA, Nahey DB, Collister JP. Role of the organum vasculosum of the lamina terminalis for the chronic cardiovascular effects produced by endogenous and exogenous ANG II in conscious rats. Am J Physiol Regul Integr Comp Physiol 2010;299:R1564-1571.

45. Thrasher TN, Keil LC, Ramsay DJ. Lesions of the organum vasculosum of the lamina terminalis (OVLT) attenuate osmotically-induced drinking and vasopressin secretion in the dog. Endocrinology 1982;110:1837-1839.

46. McKinley M. J. DDA, Leksell L. G., Mouw D. R., Scoggins B. A., Smith M. H., Weisinger R. S., Wright R. D. Osmoregulatory thirst in sheep is disrupted by ablation of the anterior wall of the optic recess. Brain Res 1982;236:5.

47. Vivas L, Chiaraviglio E, Carrer HF. Rat organum vasculosum laminae terminalis in vitro: responses to changes in sodium concentration. Brain Res 1990;519:294-300.

48. Andersen JW WD, Ferguson AV. Instrinsic osmosensitivity of subfornical organ neurons. Neuroscience 2000;100:537-547.

49. Grob M, Drolet G, Mouginot D. Specific Na+ sensors are functionally expressed in a neuronal population of the median preoptic nucleus of the rat. J Neurosci 2004;24:3974-3984.

50. Oliet SH, Bourque CW. Properties of supraoptic magnocellular neurones isolated from the adult rat. J Physiol 1992;455:291-306.

51. Qiu DL, Shirasaka T, Chu CP, et al. Effect of hypertonic saline on rat hypothalamic paraventricular nucleus magnocellular neurons in vitro. Neurosci Lett 2004;355:117-120.

52. Weisinger RS, Denton DA, McKinley MJ. Self-administered intravenous infusion of hypertonic solutions and sodium appetite of sheep. Behav Neurosci 1983;97:433-444.

53. Swanson LW, Sawchenko PE. Hypothalamic integration: organization of the paraventricular and supraoptic nuclei. Annu Rev Neurosci 1983;6:269-324.

54. Oliet SH, Bourque CW. Mechanosensitive channels transduce osmosensitivity in supraoptic neurons. Nature 1993;364:341-343.

55. Zhang Z, Bourque CW. Calcium permeability and flux through osmosensory transduction channels of isolated rat supraoptic nucleus neurons. Eur J Neurosci 2006;23:1491-1500.

56. Roper P, Callaway J, Armstrong W. Burst initiation and termination in phasic vasopressin cells of the rat supraoptic nucleus: a combined mathematical, electrical, and calcium fluorescence study. J Neurosci 2004;24:4818-4831.

57. Roper P, Callaway J, Shevchenko T, Teruyama R, Armstrong W. AHP's, HAP's and DAP's: how potassium currents regulate the excitability of rat supraoptic neurones. J Comput Neurosci 2003;15:367-389.

58. Honda K, Negoro H., Higuchi T., Takano S. Activation of supraoptic neurosecretory cells by local osmotic stimulation of the median preoptic nucleus. Neurosci Lett 1990;119:167-170.

59. Honda K, Aradachi H, Higuchi T, Takano S, Negoro H. Activation of paraventricular neurosecretory cells by local osmotic stimulation of the median preoptic nucleus. Brain Res 1992;594:335-338.

60. Gvilia I, Angara C, McGinty D, Szymusiak R. Different neuronal populations of the rat median preoptic nucleus express c-fos during sleep and in response to hypertonic saline or angiotensin-II. J Physiol 2005;569:587-599.

61. Duan PG, Kawano H, Masuko S. Collateral projections from the subfornical organ to the median preoptic nucleus and paraventricular hypothalamic nucleus in the rat. Brain Res 2008;1198:68-72.

62. Brent Shell GF, T. Nedungadi, Lei Wang, Alexandria Marciante, Brina Snyder, Rebecca Cunningham, and J. Cunningham. Angiotensin Type 1a Receptors in the Median Preoptic Nucleus Support Intermittent Hypoxia-Induced Hypertension. American Journal of Physiology - Regulatory, Integrative and Comparative Physiology 2019.

63. Coble JP, Grobe JL, Johnson AK, Sigmund CD. Mechanisms of brain renin angiotensin system-induced drinking and blood pressure: importance of the subfornical organ. Am J Physiol Regul Integr Comp Physiol 2015;308:R238-249.

64. Rowland NE, Li BH, Rozelle AK, Smith GC. Comparison of fos-like immunoreactivity induced in rat brain by central injection of angiotensin II and carbachol. Am J Physiol 1994;267:R792-798.

65. Berntson G.G. CJT. Handbook of Neuroscience for the Behavioral Sciences. Hoboken, New Jersey: John Wiley & Sons, Inc., 2009.

66. Xu Z, Herbert J. Effects of intracerebroventricular dizocilpine (MK801) on dehydration-induced dipsogenic responses, plasma vasopressin and c-fos expression in the rat forebrain. Brain Res 1998;784:91-99.

67. Xu Z, Lane JM, Zhu B, Herbert J. Dizocilpine maleate, an N-methyl-D-aspartate antagonist, inhibits dipsogenic responses and C-Fos expression induced by intracerebral infusion of angiotensin II. Neuroscience 1997;78:203-214.

68. Kawano H, Masuko S. Region-specific projections from the subfornical organ to the paraventricular hypothalamic nucleus in the rat. Neuroscience 2010;169:1227-1234.

69. Miselis RR. The subfornical organ's neural connections and their role in water balance. Peptides 1982;3:501-502.

70. Mahon JM, Allen M, Herbert J, Fitzsimons JT. The association of thirst, sodium appetite and vasopressin release with c-fos expression in the forebrain of the rat after intracerebroventricular injection of angiotensin II, angiotensin-(1-7) or carbachol. Neuroscience 1995;69:199-208.

71. Evered MD, Robinson MM, Rose PA. Effect of arterial pressure on drinking and urinary responses to angiotensin II. Am J Physiol 1988;254:R69-74.

72. Zimmerman CA, Lin YC, Leib DE, et al. Thirst neurons anticipate the homeostatic consequences of eating and drinking. Nature 2016;537:680-684.

73. Hiyama TY, Noda M. Sodium sensing in the subfornical organ and body-fluid homeostasis. Neurosci Res 2016;113:1-11.

74. Zocchi D, Wennemuth G, Oka Y. The cellular mechanism for water detection in the mammalian taste system. Nat Neurosci 2017;20:927-933.

75. Williams E.K. CRB, Strochlic D.E., Umans B.D., Lowell B.B., Liberles S.D. Sensory neurons that detect stretch and nutrients in the digestive system. Cell 2016:12.

76. Andermann M.L. LBB. Toward a wiring diagram understanding of appetitie control. Neuron 2017;95:22.

77. Tanaka J, Ushigome A, Matsuda M, Saito H. Responses of median preoptic neurons projecting to the hypothalamic paraventricular nucleus to osmotic stimulation in Wistar-Kyoto and spontaneously hypertensive rats. Neurosci Lett 1995;191:47-50.

78. Stocker SD, Toney GM. Vagal afferent input alters the discharge of osmotic and ANG II-responsive median preoptic neurons projecting to the hypothalamic paraventricular nucleus. Brain Res 2007;1131:118-128.

79. Gardiner TW, Verbalis JG, Stricker EM. Impaired secretion of vasopressin and oxytocin in rats after lesions of nucleus medianus. Am J Physiol 1985;249:R681-688.

80. Yamaguchi K, Yamada T. Roles of forebrain GABA receptors in controlling vasopressin secretion and related phenomena under basal and hyperosmotic circumstances in conscious rats. Brain Res Bull 2008;77:61-69.

81. Yamaguchi KaW, K. . Contribution of N-methyl-aspartate receptors in the anteroventral third ventricular region to vasopressin secretion, but not to cardiovascular responses provoked by hyperosmolality and protaglandin E2 in concious rats. Brain Res 2002;58:9.

82. Travis KA, Johnson AK. In vitro sensitivity of median preoptic neurons to angiotensin II, osmotic pressure, and temperature. Am J Physiol 1993;264:R1200-1205.

83. Nissen R, Renaud LP. GABA receptor mediation of median preoptic nucleus-evoked inhibition of supraoptic neurosecretory neurones in rat. J Physiol 1994;479 (Pt 2):207-216.

84. Johnson AK, Hoffman WE, Buggy J. Attenuated pressor responses to intracranially injected stimuli and altered antidiuretic activity following preoptic-hypothalamic periventricular ablation. Brain Res 1978;157:161-166.

85. Han SY, Bouwer GT, Seymour AJ, Korpal AK, Schwenke DO, Brown CH. Induction of hypertension blunts baroreflex inhibition of vasopressin neurons in the rat. Eur J Neurosci 2015;42:2690-2698.

86. Foster GE, Hanly PJ, Ahmed SB, Beaudin AE, Pialoux V, Poulin MJ. Intermittent hypoxia increases arterial blood pressure in humans through a Renin-Angiotensin system-dependent mechanism. Hypertension 2010;56:369-377.

87. Knight WD, Saxena A, Shell B, Nedungadi TP, Mifflin SW, Cunningham JT. Central losartan attenuates increases in arterial pressure and expression of FosB/DeltaFosB along the autonomic axis associated with chronic intermittent hypoxia. Am J Physiol Regul Integr Comp Physiol 2013;305:R1051-1058.

88. Marcus NJ, Li YL, Bird CE, Schultz HD, Morgan BJ. Chronic intermittent hypoxia augments chemoreflex control of sympathetic activity: role of the angiotensin II type 1 receptor. Respir Physiol Neurobiol 2010;171:36-45.

89. Sharpe AL, Calderon AS, Andrade MA, Cunningham JT, Mifflin SW, Toney GM. Chronic intermittent hypoxia increases sympathetic control of blood pressure: role of neuronal activity in the hypothalamic paraventricular nucleus. Am J Physiol Heart Circ Physiol 2013;305:H1772-1780.

90. Dempsey JA, Veasey SC, Morgan BJ, O'Donnell CP. Pathophysiology of sleep apnea. Physiol Rev 2010;90:47-112.

91. Patil SP, Schneider H, Schwartz AR, Smith PL. Adult obstructive sleep apnea: pathophysiology and diagnosis. Chest 2007;132:325-337.

92. Greenberg HE, Sica A, Batson D, Scharf SM. Chronic intermittent hypoxia increases sympathetic responsiveness to hypoxia and hypercapnia. J Appl Physiol (1985) 1999;86:298-305.

93. Fletcher EC, Orolinova N, Bader M. Blood pressure response to chronic episodic hypoxia: the renin-angiotensin system. J Appl Physiol 2002;92:627-633.

94. Al-Hashmi MAA-AaKM. Obstructive Sleep Apnoea/Hypopnoea Syndrome and Hypertension. Sultan Qaboos University Medical Journal 2008;8:266-274.

95. Dergacheva O, Dyavanapalli J, Pinol RA, Mendelowitz D. Chronic intermittent hypoxia and hypercapnia inhibit the hypothalamic paraventricular nucleus neurotransmission to parasympathetic cardiac neurons in the brain stem. Hypertension 2014;64:597-603.

96. Iturriaga R, Andrade DC, Del Rio R. Crucial Role of the Carotid Body Chemoreceptors on the Development of High Arterial Blood Pressure During Chronic Intermittent Hypoxia. Adv Exp Med Biol 2015;860:255-260.

97. Silva AQ, Schreihofer AM. Altered sympathetic reflexes and vascular reactivity in rats after exposure to chronic intermittent hypoxia. J Physiol 2011;589:1463-1476.

98. Del Rio R, Moya EA, Iturriaga R. Carotid body potentiation during chronic intermittent hypoxia: implication for hypertension. Front Physiol 2014;5:434.

99. Bader M, Ganten D. Update on tissue renin-angiotensin systems. J Mol Med (Berl) 2008;86:615-621.

100. Grobe JL, Grobe CL, Beltz TG, et al. The brain Renin-angiotensin system controls divergent efferent mechanisms to regulate fluid and energy balance. Cell Metab 2010;12:431-442.

101. Sinnayah P, Lazartigues E, Sakai K, Sharma RV, Sigmund CD, Davisson RL. Genetic ablation of angiotensinogen in the subfornical organ of the brain prevents the central angiotensinergic pressor response. Circ Res 2006;99:1125-1131.

102. Aronsson M, Almasan K, Fuxe K, et al. Evidence for the existence of angiotensinogen mRNA in magnocellular paraventricular hypothalamic neurons. Acta Physiol Scand 1988;132:585-586.

103. Palkovits M, Mezey E, Fodor M, et al. Neurotransmitters and neuropeptides in the baroreceptor reflex arc: connections between the nucleus of the solitary tract and the ventrolateral medulla oblongata in the rat. Clin Exp Hypertens 1995;17:101-113.

104. Lind RW, Swanson LW, Ganten D. Organization of angiotensin II immunoreactive cells and fibers in the rat central nervous system. An immunohistochemical study. Neuroendocrinology 1985;40:2-24.

105. Pickel VM, Chan J. Co-localization of angiotensin II and gamma-aminobutyric acid in axon terminals in the rat subfornical organ. Neurosci Lett 1995;193:89-92.

106. Grobe JL, Xu D, Sigmund CD. An intracellular renin-angiotensin system in neurons: fact, hypothesis, or fantasy. Physiology (Bethesda) 2008;23:187-193.

107. Fischer-Ferraro C, Nahmod VE, Goldstein DJ, Finkielman S. Angiotensin and renin in rat and dog brain. J Exp Med 1971;133:353-361.

108. Dzau VJ, Ingelfinger J, Pratt RE, Ellison KE. Identification of renin and angiotensinogen messenger RNA sequences in mouse and rat brains. Hypertension 1986;8:544-548.

109. Lavoie JL, Cassell MD, Gross KW, Sigmund CD. Adjacent expression of renin and angiotensinogen in the rostral ventrolateral medulla using a dual-reporter transgenic model. Hypertension 2004;43:1116-1119.

110. Lu H, Cassis LA, Kooi CW, Daugherty A. Structure and functions of angiotensinogen. Hypertens Res 2016;39:492-500.

111. Davisson RL, Oliverio MI, Coffman TM, Sigmund CD. Divergent functions of angiotensin II receptor isoforms in the brain. J Clin Invest 2000;106:103-106.

112. Gao L, Wang W, Wang W, Li H, Sumners C, Zucker IH. Effects of angiotensin type 2 receptor overexpression in the rostral ventrolateral medulla on blood pressure and urine excretion in normal rats. Hypertension 2008;51:521-527.

113. Harding JW, Cook VI, Miller-Wing AV, et al. Identification of an AII(3-8) [AIV] binding site in guinea pig hippocampus. Brain Res 1992;583:340-343.

114. Xu P, Sriramula S, Lazartigues E. ACE2/ANG-(1-7)/Mas pathway in the brain: the axis of good. Am J Physiol Regul Integr Comp Physiol 2011;300:R804-817.

115. Abbas A, Gorelik G, Carbini LA, Scicli AG. Angiotensin-(1-7) induces bradykinin-mediated hypotensive responses in anesthetized rats. Hypertension 1997;30:217-221.

116. Chappell MC, Brosnihan KB, Diz DI, Ferrario CM. Identification of angiotensin-(1-7) in rat brain. Evidence for differential processing of angiotensin peptides. J Biol Chem 1989;264:16518-16523.

117. Doobay MF, Talman LS, Obr TD, Tian X, Davisson RL, Lazartigues E. Differential expression of neuronal ACE2 in transgenic mice with overexpression of the brain renin-angiotensin system. Am J Physiol Regul Integr Comp Physiol 2007;292:R373-381.

118. Deshotels MR, Xia H, Sriramula S, Lazartigues E, Filipeanu CM. Angiotensin II mediates angiotensin converting enzyme type 2 internalization and degradation through an angiotensin II type I receptor-dependent mechanism. Hypertension 2014;64:1368-1375.

119. Xu J, Sriramula S, Xia H, et al. Clinical Relevance and Role of Neuronal AT1 Receptors in ADAM17-Mediated ACE2 Shedding in Neurogenic Hypertension. Circ Res 2017;121:43-55.

120. Shi P, Diez-Freire C, Jun JY, et al. Brain microglial cytokines in neurogenic hypertension. Hypertension 2010;56:297-303.

121. Nattie E. CO2, brainstem chemoreceptors and breathing. Prog Neurobiol 1999;59:299-331.

122. Dikalov SI, Nazarewicz RR. Angiotensin II-induced production of mitochondrial reactive oxygen species: potential mechanisms and relevance for cardiovascular disease. Antioxidants & redox signaling 2013;19:1085-1094.

123. Prabhakar NR. Sensory plasticity of the carotid body: role of reactive oxygen species and physiological significance. Respir Physiol Neurobiol 2011;178:375-380.

124. Hirooka Y, Kishi T, Sakai K, Takeshita A, Sunagawa K. Imbalance of central nitric oxide and reactive oxygen species in the regulation of sympathetic activity and neural mechanisms of hypertension. Am J Physiol Regul Integr Comp Physiol 2011;300:R818-826.

125. Prabhakar NR, Peng YJ, Kumar GK, Nanduri J. Peripheral chemoreception and arterial pressure responses to intermittent hypoxia. Comprehensive Physiology 2015;5:561-577.

126. Guyenet PG. The sympathetic control of blood pressure. Nat Rev Neurosci 2006;7:335-346.

127. Ichihara A. [Pathogenic mechanism of primary hypertension]. Nihon Rinsho 2015;73:1809-1814.

128. Klabunde RE. Cardiovascular Physiology Concepts, 2 ed: Lippincott Williams & Wilkins, 2011.

129. Jordan D. Arterial Chemoreceptors: Cell to System. New York: Plenum Press, 1994.

130. Guyenet PG. Lower Brainstem Mechanisms of Cardiorespiratory Integration. In: T. Douglas Bradley JSF, ed. Sleep Apnea: Implications in Cardiovascular and Cerebrovascular Disease. New York: Marcel Dekker, Inc., 2000: 84-90.

131. Colombari E, Sato MA, Cravo SL, Bergamaschi CT, Campos RR, Jr., Lopes OU. Role of the medulla oblongata in hypertension. Hypertension 2001;38:549-554.

132. Wyss JM. Central Nervous System in Arterial Pressure Regulation. In: Joseph L. Izzo DAS, Henry Richard Black, ed. Hypertension Primer, 4 ed. Dallas, Texas: American Heart Association, 2008: 116-119.

133. Tamra Llewellyn HZ, Xuefei Liu, Bo Xu, and Kaushik P. Patel. Median preoptic nucleus and subfornical organ drive renal sympathetic nerve activity via a glutamatergic mechanism within the paraventricular nucleus. American Journal of Physiology-Regulatory, Integrative and Comparative Physiology 2012;302:R424-R432.

134. Gabor A, Leenen FH. Central neuromodulatory pathways regulating sympathetic activity in hypertension. J Appl Physiol (1985) 2012;113:1294-1303.

135. Schreihofer AM, Guyenet PG. The baroreflex and beyond: control of sympathetic vasomotor tone by GABAergic neurons in the ventrolateral medulla. Clin Exp Pharmacol Physiol 2002;29:514-521.

136. Prabhakar NR, Peng YJ, Jacono FJ, Kumar GK, Dick TE. Cardiovascular alterations by chronic intermittent hypoxia: importance of carotid body chemoreflexes. Clin Exp Pharmacol Physiol 2005;32:447-449.

137. Bathina CS, Rajulapati A, Franzke M, Yamamoto K, Cunningham JT, Mifflin S. Knockdown of tyrosine hydroxylase in the nucleus of the solitary tract reduces elevated blood pressure during chronic intermittent hypoxia. American Journal of Physiology - Regulatory, Integrative and Comparative Physiology 2013;305:R1031-R1039.

138. Bathina CS, Rajulapati A, Franzke M, Yamamoto K, Cunningham JT, Mifflin S. Knockdown of tyrosine hydroxylase in the nucleus of the solitary tract reduces elevated blood pressure during chronic intermittent hypoxia. Am J Physiol Regul Integr Comp Physiol 2013;305:R1031-1039.

139. Knight WD, Little JT, Carreno FR, Toney GM, Mifflin SW, Cunningham JT. Chronic intermittent hypoxia increases blood pressure and expression of FosB/DeltaFosB in central autonomic regions. Am J Physiol Regul Integr Comp Physiol 2011;301:R131-139.

140. Shell B, Faulk K, Cunningham JT. Neural Control of Blood Pressure in Chronic Intermittent Hypoxia. Curr Hypertens Rep 2016;18:19.

141. Cunningham JT KW, Mifflin SW, Nestler EJ. an essential role for ΔFosB in the median preoptic nucleus in the sustained hypertensive effects of chronic intermittent hypoxia. Hypertension 2012;60:179-187.

142. W. David Knight AS, 2 Brent Shell,2 T. Prashant Nedungadi,2 Steven W. Mifflin,2 and J. Thomas Cunningham. Central losartan attenuates increases in arterial pressure and expression of FosB/ΔFosB along the autonomic axis associated with chronic intermittent hypoxia. American Journal of Physiology-Regulatory, Integrative and Comparative Physiology 2013;305:R1051-R1058.

143. Carmichael CY, Wainford RD. Hypothalamic signaling mechanisms in hypertension. Curr Hypertens Rep 2015;17:39.

144. Cunningham JT, Herrera-Rosales M, Martinez MA, Mifflin S. Identification of active central nervous system sites in renal wrap hypertensive rats. Hypertension 2007;49:653-658.

145. Zhang M, Qin DN, Suo YP, et al. Endogenous hydrogen peroxide in the hypothalamic paraventricular nucleus regulates neurohormonal excitation in high salt-induced hypertension. Toxicol Lett 2015;235:206-215.

146. Ribeiro N, Panizza Hdo N, Santos KM, Ferreira-Neto HC, Antunes VR. Salt-induced sympathoexcitation involves vasopressin V1a receptor activation in the paraventricular nucleus of the hypothalamus. Am J Physiol Regul Integr Comp Physiol 2015;309:R1369-1379.

147. Carmichael CY, Carmichael AC, Kuwabara JT, Cunningham JT, Wainford RD. Impaired sodium-evoked paraventricular nucleus neuronal activation and blood pressure regulation in conscious Sprague-Dawley rats lacking central Galphai2 proteins. Acta Physiol (Oxf) 2016;216:314-329.

148. Menani JV, Vieira AA, Colombari DSA, De Paula PM, Colombari E, De Luca LA, Jr. Preoptic-Periventricular Integrative Mechanisms Involved in Behavior, Fluid-Electrolyte Balance, and Pressor Responses. In: De Luca LA, Jr., Menani JV, Johnson AK, eds. Neurobiology of Body Fluid Homeostasis: Transduction and Integration. Boca Raton (FL)2014.

149. Llewellyn T, Zheng H, Liu X, Xu B, Patel KP. Median preoptic nucleus and subfornical organ drive renal sympathetic nerve activity via a glutamatergic mechanism within the paraventricular nucleus. Am J Physiol Regul Integr Comp Physiol 2012;302:R424-432.

150. Zalucky AA, Nicholl DD, Hanly PJ, et al. Nocturnal hypoxemia severity and renin-angiotensin system activity in obstructive sleep apnea. Am J Respir Crit Care Med 2015;192:873-880.

151. S. O. Mack PK, M. Wu, B. R. Coleman, F. P. Tolentino-Silva, M. A. Haxhiu. Paraventricular oxytocin neurons are involved in neural modulation of breathing. J Appl Physiol 2002;92:826-834.

CHAPTER II

SELECTIVELY INHIBITING THE MEDIAN PREOPTIC NUCLEUS ATTENUATES ANGIOTENSIN II AND HYPEROSMOTIC-INDUCED DRINKING BEHAVIOR AND VASOPRESSIN RELEASE IN ADULT MALE RATS

Alexandria B. Marciante, Lei A. Wang, George E. Farmer and J. Thomas Cunningham

The University of North Texas

Health Science Center at Fort Worth

3500 Camp Bowie Blvd.

Fort Worth, TX 76107

**published in* eNeuro, 2019. 6(2).

Visual Abstract

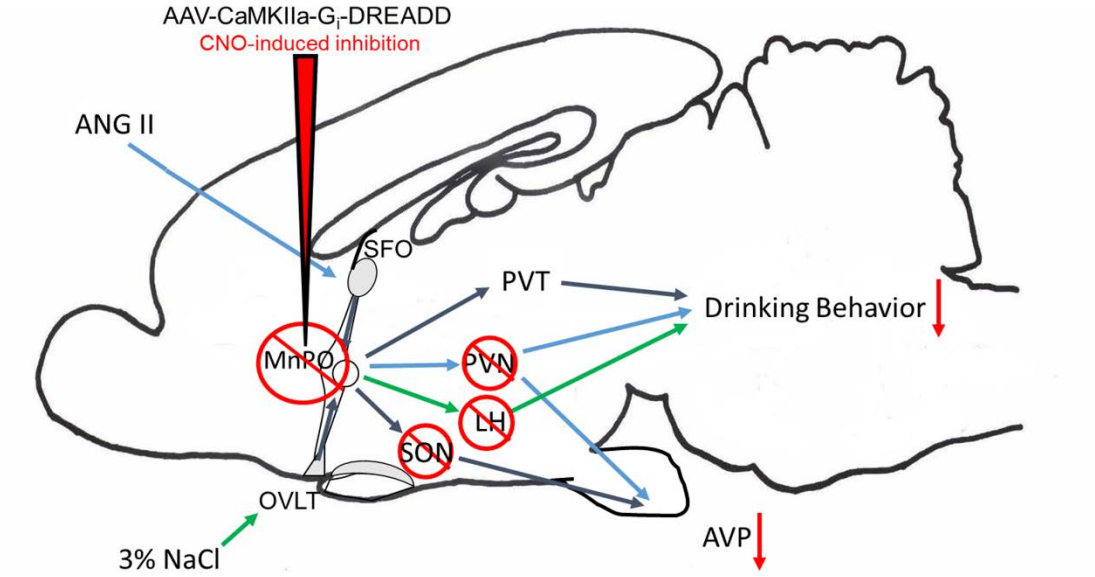

Abstract

The median preoptic nucleus (MnPO) is a putative integrative region that contributes to body fluid balance. Activation of the MnPO can influence thirst but it is not clear how these responses are linked to body fluid homeostasis. We used Designer Receptors Exclusively Activated by Designer Drugs (DREADDs) to determine the role of the MnPO in drinking behavior and vasopressin release in response to peripheral angiotensin II (ANG II) or 3% hypertonic saline in adult male Sprague-Dawley rats (250-300g). Rats were anesthetized with isoflurane and stereotaxically injected with an inhibitory DREADD (rAAV5-CaMKIIa-hM4D(G_i)-mCherry) or control (rAAV5-CaMKIIa-mCherry) virus in the MnPO. After 2 weeks' recovery, a subset of rats were used for extracellular recordings to verify functional effects of ANG II or hyperosmotic challenges in MnPO slice preparations. Remaining rats were used in drinking behavior studies. Each rat was administered either 10mg/kg of exogenous clozapine-N-oxide (CNO) to inhibit DREADD-expressing cells or vehicle ip followed by a test treatment with either 2mg/kg ANG II or 3% hypertonic saline (1mL/100g bw) sc, twice per week for two separate treatment weeks. CNO-induced inhibition during either test treatment significantly attenuated drinking responses compared to vehicle treatments and controls. Brain tissue processed for cFos immunohistochemistry showed decreased expression with CNO-induced inhibition during either test treatment in the MnPO and downstream nuclei compared to controls. CNO-mediated inhibition significantly attenuated treatment-induced increases in plasma vasopressin compared to controls. The results indicate inhibition of CaMKIIa-expressing MnPO neurons significantly reduces drinking and vasopressin release in response to ANG II or hyperosmotic challenge.

Significance Statement

The MnPO is an important regulatory center that influences thirst, cardiovascular and neuroendocrine function. Activation of different MnPO neuronal populations can inhibit or stimulate water intake. However, the role of the MnPO and its pathway-specific projections during ANG II and hyperosmotic challenges still have not yet been fully elucidated. These studies directly address this by using DREADDs to acutely and selectively inhibit pathway-specific MnPO neurons, and uses techniques that measure changes at the protein, neuronal, and overall physiological and behavioral level. More importantly, we have been able to demonstrate that physiological challenges related to extracellular (ANG II) or cellular (hypertonic saline) dehydration activate MnPO neurons that may project to different parts of the hypothalamus.

Introduction

The median preoptic nucleus (MnPO) is a midline nucleus that is part of the lamina terminalis, or anteroventral 3rd ventricle (AV3V) region. It plays an important role in receiving and integrating signals related to homeostasis and further propagating information to the hypothalamus (McKinley et al. 2015). Neurons in the MnPO contribute to the central regulation of sleep, core temperature, body fluid balance, hormone release, and autonomic function (McKinley et al. 2015). These studies focus on the role of the MnPO in regulating body fluid homeostasis through drinking behavior and vasopressin release.

The MnPO receives projections from two circumventricular organs (CVOs), the organum vasculosum of the lamina terminalis (OVLT) and the subfornical organ (SFO), that lie just ventral and dorsal to the MnPO along the anterior wall of the third ventricle, respectively. CVOs respond to fluctuations in plasma osmolality and other humoral factors, like angiotensin II (ANG II) (Johnson, Cunningham, and Thunhorst 1996). The OVLT and SFO project to several hypothalamic regions that contribute to homeostasis through behavioral, endocrine, and autonomic responses. These pathways include, but are not limited to, the supraoptic nucleus (SON), paraventricular nucleus of the hypothalamus (PVN) and the MnPO (Miselis 1982; McKinley et al. 2004). The MnPO has reciprocal connections with the OVLT and SFO and also projects to the SON and PVN (McKinley et al. 2015). Studies have also shown that the MnPO has projections to the lateral hypothalamus (LH) and paraventricular thalamus (PVT) to regulate drinking

behavior (Leib et al. 2017). The role, however, of the MnPO and its relationship to specific challenges regarding body fluid homeostasis are not completely understood.

Body fluid homeostasis involves orchestrated physiological responses to cellular or extracellular dehydration (Fitzsimons 1972; Adler and Verbalis 2006). Cellular dehydration results from changes in body fluid solute content that is detected by osmoreceptors in the peripheral and central nervous system (Bourque 2008). Extracellular dehydration is related to changes in body fluid volume that influence several hormonal and neural systems (Dampney 2016; Mecawi Ade et al. 2015). Changes in the function of these systems contribute to several pathophysiological states (Adler and Verbalis 2006). The contribution of the CNS to this physiology and pathophysiology has been the subject of previous investigations.

Lesions of the rat AV3V region produce a life threatening adipsia (Johnson, Cunningham, and Thunhorst 1996). If properly maintained, however, rats can recover some spontaneous water intake but do not respond to experimental challenges that mimic aspects of homeostatic thirst, such as ANG II or osmotic stimulation (Johnson, Cunningham, and Thunhorst 1996).

Studies using electrolytic or chemical lesions of the MnPO have produced conflicting results. For example, electrolytic lesions of the MnPO are reported to increase baseline drinking and prevent vasopressin release (Gardiner and Stricker 1985; Gardiner, Verbalis, and Stricker 1985). Excitotoxin lesions of the MnPO inhibit experimentally-induced drinking behavior without affecting basal water intake (Cunningham et al. 1992).

A recent study by Allen et al. (2017) used a new technique involving the induction of Fos in neurons, a measurement for acute neuronal activation, co-transfected with TRAP creating an in-frame fusion to characterize MnPO neurons based on their activation by water deprivation or changes in body temperature. This study showed that putative thirst-related neurons in the MnPO are different from those that respond to body temperature. However, water deprivation is a complex, progressive physiological challenge characterized by increased plasma osmolality, hypovolemia, and activation of the renin-angiotensin system. It is not clear if MnPO neuronal activation associated with water deprivation is segregated by the physiological stimulus or stimuli associated with water deprivation. The MnPO also contributes to other aspects of body fluid homeostasis in addition to thirst.

Recently developed chemogenetic and optogenetic techniques have been used to study neuronal circuitry responsible for mediating thirst in the lamina terminalis. A study by Augustine, et al. (2018) recently used these approaches to characterize MnPO neurons that stimulate or inhibit thirst. Their results provide important information about the neurochemical phenotype of these two cell populations, however, the physiological stimuli that regulate the activity of these cell types is not clear.

In the current study, AAV vectors with CaMKIIa promoters were used to express Designer Receptors Exclusively Activated by Designer Drugs (DREADDs) in the MnPO to inhibit CaMKIIa-expressing neurons with clozapine-N-oxide (CNO). Conscious rats were administered CNO during protocols that simulate extracellular (ANG II) or intracellular dehydration (hypertonic saline) to assess the role of the MnPO in behavioral and neuroendocrine responses to specific homeostatic challenges.

Materials and Methods

Animals

Adult male Sprague-Dawley rats (250-300 g bw), Charles River Laboratories, Wilmington, MA) were used for experiments. All rats were individually housed in a temperature-controlled (25 °C) room on a 12:12 light/dark cycle with light onset at 0700 h. Food and water was available *ad libitum* except on the day of perfusions. Rats were weighed daily and their food and water intake monitored. Experiments were performed according to the National Institute of Health guide for the care and use of laboratory animals and the Institutional Animal Care and Use Committee.

Microinjection Surgeries

Rats were anesthetized with 2% isoflurane and received stereotaxic microinjections of the inhibitory (AAV5-CaMKIIa-hM4D(G_i)-mCherry) Cre-independent DREADD or control (AAV5-CaMKIIa-mCherry-Cre) virus (both from the UNC VectorCore) into the MnPO (microinjector angled at 8º from medial to lateral to avoid the septum, 0.0 mm anterior, 0.9 mm lateral, -6.7 mm ventral from bregma). A burr hole was then drilled at the measured site and a 30-gauge stainless steel injection needle was lowered to the MnPO, where 200-300 nL of AAV was delivered at a rate of 200 nL/min. The injector was connected to a Hamilton 5 µL syringe (#84851, Hamilton, Reno, NV) by calibrated polyethylene tubing that was used to determine the injection volume. The injector remained in place for 5 minutes to allow for absorption and then slowly withdrawn. Gel foam was packed in to the drilled hole in the cranium. Absorbable antibiotic suture was used to close the incision site and minimize post-surgical infection.

Each rat was given carprofen (Rimadyl, Bio-Serv, 1 mg) orally to minimize pain following surgery. Rats were allowed time for recovery and viral transfection for two weeks.

In Situ Hybridization

In situ hybridization experiments were performed in order to characterize the neuronal phenotype of CaMKIIa-positive MnPO neurons transfected by the control virus. After the two-week recovery period, rats were anesthetized using 100 mg/kg inactin (Sigma-Aldrich, St. Louis, MO) ip and transcardially flushed first with RNase-free PBS. Rats were then perfused using 4% paraformaldehyde (PFA). Brains were dehydrated in RNase-free 30% sucrose. Twenty µm coronal sections of each brain were cut using a cryostat (Leica). Six sets of serial MnPO sections were collected in RNase-free PBS, mounted on to glass microscope slides, and left at room temperature overnight to dehydrate. Slides were then stored at -80ºC until used for *in situ* hybridization experiments. *In situ* hybridization was performed for vesicular glutamate transporter 2, or vGLUT2, (RNAScope, Advanced Cell Diagnostics Inc., Newark, CA) using a previously established protocol (Smith et al. 2014).

Electrophysiology

Slice Preparation. Hypothalamic slices containing the MnPO were prepared as previously described (Farmer et al. 2018). Experimental animals were anesthetized with isoflurane and decapitated. Coronal slices (300 µm) containing the MnPO were cut using a Microslicer DTK Zero 1 (Ted Pella, Inc.) in ice cold (0-1° C), oxygenated (95%

O_2, 5% CO_2) cutting solution consisting of (in mM): 3.0 KCl, 1.0 $MgCl_2$-$6H_2O$, 2.0 $CaCl_2$, 2.0 $MgSO_4$, 1.25 NaH_2PO_4, 26 $NaHCO_3$, 10 D-Glucose, 206 Sucrose (300 mOsm, pH 7.4). Slices were incubated at room temperature in oxygenated (95% O_2, 5% CO_2) artificial cerebrospinal fluid (aCSF) containing (in mM): 126 NaCl, 3.0 KCl, 2.0 $CaCl_2$, 2.0 $MgSO_4$, 1.25 NaH_2PO_4, 26 $NaHCO_3$, 10 and D-Glucose (300 mOsm, pH 7.4) for a minimum of 1 hour prior to recording.

Electrophysiology Protocols. Slices containing the MnPO were transferred to a submersion recording chamber and superfused with aCSF (31 ± 1°C). Slices were visualized using an upright epifluorescent microscope (BX50WI, Olympus, Center Valley, PA) with differential interference contrast optics.

Whole cell (intracellular) recordings were performed in current clamp mode and conducted in order to measure if CNO and DREADD-induced inhibition caused off-target effects that would influence the local circuitry. Recordings were obtained using borosilicate glass micropipettes (3-8 MΩ). The internal filling solution consisted of (in mM): 145 K-gluconate, 10 HEPES, 1.0 EGTA, 2.0 Na_2ATP, and 0.4 NaGTP (300 mOsm, pH 7.2). A tight gigaohm seal on MnPO neurons were made and had an access resistance of less than 25 MΩ. Neurons were slightly depolarized with current injection (2-5 pA) to generate a regular spiking activity (range, -50 to -40 mV), as previously described (Grob, Drolet, and Mouginot 2004). Loose patch voltage clamp (extracellular) recordings were obtained using borosilicate glass micropipettes (1-3 MΩ) containing aCSF as the internal solution. Voltage was clamped at 0 mV to measure changes in current.

Electrophysiological signals (voltage and current) were amplified and digitized using Multiclamp 200B and Digidata 1440A, respectively (Axon Instruments). Signals were filtered at 2 KHz and digitized at 10 KHz. Recordings from MnPO neurons were made by targeting both mCherry-expressing and non mCherry-expressing neurons in slices prepared from rats injected with the AAV. Electrophysiological signals were analyzed using 10s bins.

In the first set of experiments, intracellular or extracellular recordings were performed on MnPO neurons. Baseline membrane potential (for intracellular recordings) or action potential firing (for extracellular recordings) was recorded for 5 minutes. Then, CNO (10µM) was focally applied for 10s using a Pico spritzer (8 psi) with a patch pipette containing the drug placed 150-200 µm upstream of the recording electrode followed by an additional 10 min of recording. CNO (Tocris, Mineapolis, MN) was dissolved in DMSO and diluted in aCSF to final concentration of 10 µM (< 0.01% DMSO).

In the ANG II experiments, baseline action potential firing was recorded for 5 min in either an aCSF bath solution containing CNO (500 nM) or aCSF alone (for G_i DREADD-labeled neuronal controls). Then, ANG II (10 µM) was focally applied for 10s using a Pico spritzer (8 psi), as in the first set of electrophysiology experiments, followed by 10 min of recording. ANG II (A9525, Sigma-Aldrich) was dissolved and diluted in aCSF to a final concentration of 10 µM.

In the hyperosmotic challenge experiments, baseline action potential firing was recorded for 5 min in an aCSF bath solution containing CNO (500 nM). Then for 2 min, the bath solution was switched to CNO (500 nM) in hypertonic aCSF (HTN-aCSF; 330 mOsm) followed by 2 min of bath application of HTN-aCSF (330 mOsm). For the

remaining 5 min of recording, aCSF was bath applied. Bath application of hyperosmotic solution was used instead of focal application because it allowed for a more exact control of the extracellular NaCl concentration that would not be possible with focal application. To control for G_i DREADD-labeled neuronal activity, experiments were performed following the same time course, however the protocol was 5 min in aCSF bath, 4 min in HTN-aCSF (330 mOsm), then 5 min aCSF bath. Additional NaCl was dissolved in aCSF to raise osmolality to 330 mOsm.

Drinking Study—Angiotensin II

Prior to microinjections, rats were pretested with subcutaneous (sc) injection of ANG II twice, separated by 48-72 hr, to determine individual drinking response to peripherally administered ANG II (consume $\geq$ 5mL of water over the course of 3 h). Rats that responded were then microinjected with either the G_i DREADD or control virus and allowed recovery for two weeks. For each test, rats were intraperitoneally (ip) injected with 10 mg/kg CNO (dissolved in DMSO and diluted to the working concentration with 0.9% saline) or vehicle for CNO, VEH (DMSO and 0.9% saline in 1:4 ratio). Thirty minutes later, rats were administered ANG II (2 mg/kg sc diluted to the working concentration in 0.9% saline) or the same volume of 0.9% saline. Water consumption was measured over the course of 3 hr from the time ANG II was administered to measure drinking response and duration of CNO-induced inhibition. The substances injected for each test were administered in a randomized counter balanced order. The tests were separated by 48-72 hours and were repeated 2 and 3 weeks after microinjection surgeries.

Drinking Study—3% Hypertonic Saline

A separate group of rats was used for drinking studies with 3% hypertonic saline (3% HTN). Rats were pretested consistent with those in the ANG II drinking study to determine individual drinking response to peripherally administered 3% HTN (consume $\geq$ 5mL of water over the course of 3 hr). Rats that responded were microinjected with the G_i DREADD or control virus and allowed recovery for two weeks. After the recovery period, animals were injected ip with CNO or VEH and 3% HTN (1 mL per 100 g bw) or the same volume of 0.9% saline. Study design and duration was consistent with the ANG II drinking study.

Perfusions—Tissue and Body Fluid Collection

After the final treatment week for each drinking study, rats were administered ip CNO and sc ANG II or 3% hypertonic saline, and denied food and water access the following 90 minutes. Animals were then anesthetized using 100 mg/kg inactin (Sigma-Aldrich) ip. Blood was collected by cardiac puncture (3 mL) and transferred to an EDTA vacutainer containing 100 µL of Aprotinin (Catalog # RK-APRO, Phoenix Pharmaceuticals, Inc.) per mL of blood (300 µL total) immediately preceding the perfusion in order to measure plasma AVP and osmolality. Rats were transcardially flushed first with PBS and then perfused using 4% paraformaldehyde (PFA). Brain tissue was fixed overnight in 4% PFA before being dehydrated in 30% sucrose.

Arginine Vasopressin

Plasma AVP concentrations were measured by specific EIA (Phoenix Pharmaceuticals, Inc., Burlingame, CA) following peptide extraction, as recommended by the manufacturer (Catalog # EK-065-07, Phoenix Pharmaceuticals, Inc.). The volume of plasma used was 500 µL per sample for peptide extraction. One hundred µL from each sample was recovered from the extraction and assayed in duplicate (50 µL assayed). The total peptide concentration of each sample was calculated according to the directions provided by the manufacturer of the extraction kit. The intra- and inter-assay coefficients of variation averaged <10% and <15%, respectively, as provided by the manufacturer (Phoenix Pharmaceuticals, Inc.).

Immunohistochemistry

Forty µm coronal sections of each previously perfused brain were cut using a cryostat. Three sets of serial sections were separately collected in cryoprotectant (Hoffman, Smith, and Fitzsimmons 1992) and stored at -20 ^{o}C until they were processed for immunohistochemistry. Separate sets of serial sections from brains injected with DREADD or control virus were stained for cFos (sc-253-G, goat polyclonal anti-Fos antibody, Santa Cruz Biotechnology, 1:1000). After 48 hr, sections were washed using phosphate buffer solution (PBS) and transferred to a secondary antibody (BA-9500, biotinylated anti-goat, Vector Laboratories) for DAB reaction and labeling. After the DAB reaction, the sections were washed and placed in the primary antibody (ab167453, rabbit polyclonal anti-mCherry, Abcam 1:500) and incubated for an additional 48 hr followed by incubation with a CY3 conjugated anti-rabbit antibody (711-165-152, Jackson ImmunoResearch, West Grove, PA) for 4-5 hr. The sections were then

mounted on gelatin-coated slides, dried, and coverslipped with Permount for imaging. All antibodies were diluted to the final concentration with PBS diluent (0.25% Triton, 3% horse serum, and 96.75% PBS).

Sections were examined using light microscopy to identify Fos-positive cells. Excitation wavelengths of 550-570 nm were used for emission of mCherry immunofluorescence. Images were captured using an epifluorescent microscope (Olympus BX41, Olympus, Center Valley, PA, USA) equipped with a digital camera (Olympus DP70) to image sections. Care was taken to ensure that sections included in this study were sampled from the same plane in each brain section. Co-localization was determined by quenching produced in cells with nuclear fos staining and cytosolic mCherry staining, as previously described (Grindstaff et al. 2000). Brightfield and fluorescent images were merged for analysis of the MnPO using ImageJ (NIH). Fos-positive neurons and their co-localization in the MnPO was determined blind to experimental conditions of the subjects.

Statistics

Electrophysiology data were tested for differences in baseline activity, changes in peak firing rate (defined as the 10 s bin with the lowest firing rate), and percent change baseline firing rate using one-way analysis of variance (ANOVA) or two-way repeated measures ANOVA. Two-way repeated measures ANOVA was used to compare changes in water consumption between the G_i DREADD-injected group and control group and treatment (CNO vs. VEH), followed by Tukey's *post-hoc* test. Analyses of plasma vasopressin concentrations, plasma osmolality, and cell counts for neuronal

phenotyping were figured using one-way ANOVA followed by Tukey's *post-hoc* test. Tukey's *post-hoc* analysis was used when performing multiple comparisons. Holm-Sidak *post-hoc* test was used in order to perform comparisons to a determined control. Statistical significance is defined at an α level of 0.05 and exact p-values are reported. Values are reported as mean ± SEM. All statistics were performed in SigmaPlot.v.12.0 (Systat Software, San Jose, CA).

Results

CaMKIIa neurons in the MnPO signal through excitatory pathways

Experiments were conducted to determine the neurochemical phenotype of MnPO neurons that were targeted by the viral vectors with CaMKIIa promoters used in this study. *In situ* hybridization for vGLUT2 was used to identify putative excitatory MnPO neurons (*n* = 5 rats, 2-3 sections per rat). An example of vGLUT2 *in situ* hybridization and CaMKIIa immunohistochemistry in the dorsal MnPO is shown in Figure 1. The results show that 89.17±1.32% of CaMKIIa neurons that express the viral construct co-localize with vGLUT2 message, indicating that the CaMKIIa-expressing neurons in the MnPO are primarily glutamatergic and would likely be involved in excitatory signaling.

Electrophysiology Results

CNO significantly attenuates basal firing rate in G_i DREADD-expressing neurons

Intracellular Recordings: In order to verify that CNO was not having off-target effects, whole cell current clamp experiments (intracellular recordings) were conducted for more direct measurements on G_i DREADD (n = 5, 3 rats, 2 slices per rat) and G_i DREADDx

(n = 7, 4 rats, 2 slices per rat) neurons within the same section. As previously described (Grob, Drolet, and Mouginot 2004), neurons were slightly depolarized with current injection to generate a regular spiking activity (range, -50 to -40 mV) and allowed to stabilize in aCSF for 5 min before CNO exposure. There was a significant effect of treatment on neuron type (data not shown; $F(3, 20) = 21.175$, $p < 0.001$, one-way ANOVA). CNO exposure caused a significant membrane hyperpolarization in G_i DREADD neurons between aCSF baseline and peak response (-6.1 $\pm$ 0.9 mV; $p = 0.001$) but no significant change in membrane potential of the G_i DREADDx neurons in the presence of CNO compared to aCSF baseline (2.1 $\pm$ 0.9 mV; $p = 0.979$). These results indicate that CNO and the DREADD-induced inhibition of the G_i DREADD neurons did not have an effect on local circuitry.

Extracellular Recordings: Loose cell recordings were made from brain slices containing the MnPO two weeks after the rats were injected with AAVs containing either G_i DREADD or the control (CTRL) construct. Cells expressing the constructs were easily identifiable by expression of the mCherry reported (Figure 2A). There were no differences in the rates of spontaneous activity of MnPO neurons transfected with either virus (G_i DREADD, 3.37 $\pm$ 0.1 Hz; $n = 17$, 6 rats, 2 slices per rat; CTRL, 3.30 $\pm$ 0.5 Hz; $n = 13$, 6 rats, 2 slices per rat) or unlabeled cells in slices from rats injected in the MnPO with the G_i DREADD (G_i DREADDx, 3.45 $\pm$ 0.5 Hz; $n = 19$, 6 rats, 2 slices per rat; $F(2, 46) = 0.306$, $p = 0.970$, one-way ANOVA).

Focal CNO application (10μM) significantly decreased the spontaneous activity of the G_i DREADD MnPO neurons (Figure 2B; $F(1, 32) = 16.22$, $p < 0.001$, one-way

ANOVA). When calculated as a percent change from baseline, only G_i DREADD neurons showed a significant decrease in activity from baseline, or peak response (Peak; defined as the 10 s bin with the lowest firing rate), that recovered after 172.4 $\pm$ 37.8 s (Figure 2D; $F(2, 46) = 10.050$, $p = 0.001$, one-way ANOVA; Tukey's *post-hoc,* Baseline vs. Peak $p < 0.001$ and Baseline vs Recovery, $p = 0.024$). There was also a significant difference in peak response to CNO in the G_i DREADD neuron firing rate ($F(2, 46) = 10.832$, $p < 0.005$, one-way ANOVA) compared to CTRL ($p < 0.001$) and G_i DREADDx neurons ($p < 0.001$) using Holm-Sidak *post-hoc* test.

Analysis of the firing rates (Hz) of neurons from each group produced similar results (Figure 2C). Focal CNO application did not significantly influence the spontaneous activity of the G_i DREADDx ($F(2, 36) = 0.0808$, $p = 0.923$, one-way ANOVA) or CTRL neurons (Figure 2D; $F(2, 54) = 0.0119$, $p = 0.988$, one-way ANOVA). Additional experiments were therefore conducted to determine if CNO could block changes in activity in CaMKIIa MnPO neurons produced by either ANG II or HTN.

CNO blocks ANG II-induced excitation in G_i DREADD-expressing neurons

Next, the effects of CNO on ANG II evoked responses in G_i DREADD MnPO neurons were tested. In these experiments, focally applied ANG II (10 uM) was administered during bath applications of CNO (500 nM). Bath application of CNO containing aCSF significantly reduced the spontaneous activity of G_i DREADD neurons (*n* = 15, 6 rats, 2 slices per rat) as compared to aCSF alone (*n* = 7, 3 rats, 2 slices per rat). In contrast bath application of CNO did not affect the activity of G_i DREADDx neurons from the same slices (*n* = 15, 6 rats, 2 slices per rat). In the G_i DREADD

positive neurons, this inhibition of spontaneous activity by CNO bath application was significant at 170 s after the start of CNO exposure and was maintained throughout the duration of the protocol (Figure 3A and 3B; $F(2, 39) = 5.577$, $p = 0.007$, two-way repeated measures ANOVA). When analyzed as a percent change from aCSF baseline, the activity of G_i DREADD cells was significantly reduced to 20% of baseline during CNO bath application, whereas G_i DREADDx cells were not affected (Figure 3C and 3D; $F(58, 1131) = 4.221$, $p < 0.001$, two-way repeated measures ANOVA).

During aCSF bath application, focally applied ANG II significantly increased the firing rate of 7 out of 7 G_i DREADD neurons ($n = 7$, 3 rats, 2 slices per rat). The activity of G_i DREADDx neurons was increased by focal ANG II during CNO bath application ($F(3, 66) = 840.408$, $p < 0.001$, one-way ANOVA). However, CNO bath application blocked the responses of 10 out of 15 G_i DREADD labeled neurons to focally applied ANG II (Figure 3D; $p = 0.258$, Tukey's *post-hoc* test). There was no significant difference in baseline firing rates between G_i DREADD neurons prior to CNO exposure or G_i DREADDx neurons during CNO or aCSF exposure ($F(3, 51) = 2.253$, $p = 0.093$, one-way ANOVA).

CNO significantly attenuates excitation produced by hypertonic saline in G_i DREADD-expressing neurons

The effects of DREADD mediated inhibition on responses produced by bath application of hypertonic aCSF (HTN-aCSF; 330 mOsm) was tested using MnPO neurons transfected with G_i DREADD or unlabeled cells in the same brain slices (G_i DREADDx). The activity of 7 out of 7 G_i DREADD neurons was significantly increased

by HTN bath solution. As observed in the previous experiments, bath application of CNO decreased the basal activity of cells transfected with the G_i DREADD construct but did not affect the activity of G_i DREADDx cells (Figure 4A and 4B).

Bath application of CNO did not influence the spontaneous activity or prevent increases in firing rate produced by HTN-aCSF in G_i DREADDx neurons compared to aCSF baseline (Figures 4A). In contrast, CNO decreased spontaneous activity in G_i DREADD cells as compared to activity in normal aCSF (Figure 4A; $F(2, 41) = 112.004$, $p < 0.001$, Holm-Sidak *post-hoc* analysis). G_i DREADD neurons did not show a significant increase in firing rate associated with HTN-aCSF in the presence of CNO (Figure 4C). Although the G_i DREADD cells appeared to be more active during bath application of CNO and HTN-aCSF, their average firing frequency was not different from CNO alone (Figure 4C). The changes in firing rate of MnPO neurons was influenced by both the treatment and time as indicated by a statistically significant interaction ($F(89, 2609) = 2.712$, $p < 0.001$, two-way repeated measures ANOVA).

CNO bath application significantly attenuated changes in activity expressed as percent of baseline activity in G_i DREADD neurons ($n = 15$, 6 rats, 2 slices per rat, $p < 0.001$, Tukey's *post-hoc* analysis). This was not the case for G_i DREADDx neurons ($n = 14$, 6 rats, 2 slices per rat) compared to aCSF bath applied G_i DREADD neurons (Figures 4A and 4B; $n = 7$, 2 rats, 2 slices per rat). HTN-aCSF significantly increased the firing rate of unlabeled cells compared to baseline and aCSF recordings (Figure 4C; $F(3, 52) = 7.119$, $p < 0.001$, one-way ANOVA). G_i DREADDx neurons had significantly increased firing rates when exposed to HTN-aCSF with or without CNO (Figure 4C; $p < 0.001$, Tukey's *post-hoc* analysis). When the bath solution was changed to normal

aCSF from HTN-aCSF, the activity of G_i DREADDx cells significantly decreased to a rate that was no different from CNO and normal aCSF (Figure 4C; $p = 0.301$ baseline compared to aCSF). When G_i DREADD were exposed to HTN-aCSF without CNO, their firing rate significantly increased as compared to the aCSF baseline (Figure 4C; $p < 0.001$ for all time points, Tukey's *post-hoc* analysis) and compared to CNO ($p < 0.001$ for all time points, Tukey's *post-hoc* analysis), but not when compared to G_i DREADDx neurons exposed to CNO.

In G_i DREADD neurons, there was a significant decrease in firing rate during CNO and HTN exposure compared to aCSF bath application ($F(3, 56) = 30.084$; $p < 0.001$, one-way ANOVA; $p = 0.001$, Tukey's *post-hoc* analysis). Although there was a trend for increased activity in G_i DREADD neurons exposed to HTN-aCSF after CNO was washed out (Figure 4C), this change was not significantly different from CNO with HTN-aCSF ($p = 0.917$, Tukey's *post-hoc* analysis).

Drinking Responses

Based on the results of the electrophysiological studies, we tested the effects of ip CNO (10 mg/kg) on drinking responses produced by ANG II (2 mg/kg sc) in one group of rats and 3% HTN (1 ml/100 g bw sc) in a separate group of rats. Control experiments using equal volumes of 0.9% saline (SAL) tests were also conducted for each group.

Acute CNO-induced inhibition significantly attenuates ANG II-induced thirst responses

When rats were pretreated with CNO or VEH injections followed by ANG II treatment, there was an associated increase in water consumption by rats during the 3 hr time-period in both the G_i DREADD rats (n = 10) and CTRL rats (n = 10). Two-way repeated measures ANOVA analysis indicated a significant AAV variant dependent difference in water consumption (Figure 5A; $F(1, 18) = 18.925$, $p < 0.001$, two-way repeated measures ANOVA) and treatment (VEH or CNO) received ($F(5, 86) = 69.735$, $p < 0.001$, two-way repeated measures ANOVA). There was no significant difference between groups during the 0.9% SAL tests (first treatment $p = 0.989$, last treatment $p = 0.935$, first treatment vs last treatment $p = 0.999$ (CTRL) and $p = 0.998$ (G_i DREADD)) or during VEH and ANG II test ($p = 0.074$) in the first treatment. During the CNO and ANG II test, however, the G_i DREADD group had approximately a 50% reduction in water consumed over the 3 hr period compared to the CTRL group ($p < 0.001$, first treatment). This was also the case compared to the VEH and ANG II exposure ($p = 0.005$, first treatment). Independent of VEH or CNO treatment, ANG II still resulted in significantly elevated drinking response compared to physiological saline volume control studies (all groups, $p < 0.001$, Tukey's *post-hoc* analysis).

One week later, ANG II significantly increased drinking behavior in the same manner compared to 0.9% SAL tests (all groups $p < 0.001$, Tukey's *post-hoc* analysis). There was no significant difference in thirst response between G_i DREADD or CTRL groups during VEH and ANG II exposure ($p = 0.292$, last treatment). During the CNO and ANG II treatment, however, the G_i DREADD group had approximately a 50% reduction in water consumed over the 3 hr period compared to the CTRL group, similar to what was observed in the first treatment ($p < 0.001$, last treatment).

Acute CNO-induced inhibition significantly attenuates hypertonic saline-induced thirst

A separate cohort of rats were injected in the MnPO with either G_i DREADD (*n* = 6 rats) or CTRL (*n* = 6 rats) virus and used to test whether or not CNO pretreatment would block the effects of 3% HTN injections on drinking behavior. As in the ANG II drinking studies, there was a significant interaction between AAV variant, pretreatment and 3% HTN exposure (Figure 5B; $F(5, 71) = 3.317$, $p = 0.015$, two-way repeated measures ANOVA). When either of the groups were pretreated with VEH followed by 3% HTN, rats drank a significant amount of water over the 3 hr time period compared to 0.9% SAL tests (Figure 5B; Tukey's *post-hoc* analysis, 0.9% SAL vs. CTRL + VEH + 3% HTN $p < 0.001$, 0.9% SAL vs. G_i DREADD + VEH + 3% HTN $p < 0.001$, CTRL + VEH + 3% HTN vs. G_i DREADD + VEH + 3% HTN group $p = 0.794$). However, when groups were pretreated with CNO prior to 3% HTN, the drinking response of the rats injected with G_i DREADD were significantly attenuated as compared to their responses to VEH and 3% HTN treatment (Figure 5B; Tukey's *post-hoc* analysis; 0.9% SAL vs. CTRL + CNO + 3% HTN $p < 0.001$, 0.9% SAL vs. DREADD + CNO + 3% HTN $p < 0.001$, CTRL + CNO + 3% HTN vs. DREADD + CNO + 3% HTN $p = 0.011$). Rats were injected with the same volume of 0.9% SAL and this treatment did not significantly affect water intake between groups (Figure 5B; $p = 0.799$, Tukey's *post-hoc* analysis).

After one week, the same rats were retested. Injections of HTN significantly increased water intake compared to 0.9% SAL tests (all groups, $p < 0.001$, Tukey's *post-hoc* analysis). There was no significant difference in water intake between groups during VEH and 3% HTN exposure ($p = 0.319$, last treatment). During the CNO and 3%

HTN treatment, the G_i DREADD group had approximately a 50% reduction in water consumed over the 3 hr period compared to the CTRL group, similar to what was observed during the first treatment ($p = 0.028$, last treatment).

Arginine Vasopressin Responses

Two days after completing the last drinking tests, rats were injected with VEH or CNO (10 mg/kg ip) followed by either ANG II (2 mg/kg sc), 3% HTN (1 ml/100 g bw sc) or 0.9% SAL (volume control) 30 minutes later, as described in the drinking tests. Blood samples were taken and analyzed for plasma AVP concentrations.

CNO-induced inhibition significantly attenuates ANG II-induced plasma vasopressin release

The effects of DREADD inhibition in the MnPO on ANG II-induced AVP release was tested. Rats injected in the MnPO with the control vector (CTRL) that were pretreated with CNO and administered ANG II (CTRL + CNO + ANG II) had significantly increased plasma AVP (Figure 6A; $F(2, 23) = 44.963$, $p < 0.001$, one-way ANOVA). This increase in plasma AVP associated with ANG II treatment was significantly decreased by CNO-induced inhibition in the G_i DREADD (G_i DREADD + CNO + ANG II) group ($p < 0.001$, Tukey's *post-hoc* analysis). However, the changes in plasma AVP observed in the G_i DREADD + CNO + ANG II were significantly increased compared to the vehicle control group (CTRL + CNO + 0.9% SAL) suggesting the ANG II-induced AVP release was significantly attenuated, but not reduced to control levels by MnPO inhibition (Figure 6A; $p < 0.001$).

CNO-induced inhibition blocks hypertonic saline-induced plasma vasopressin release

Plasma AVP concentration was significantly different between groups treated with 3% HTN compared to 0.9% SAL (Figure 6B; $F(2,15) = 6.443$, $p = 0.010$, one-way ANOVA), as well. Subcutaneous injection of 3% HTN significantly increased plasma AVP levels in the CTRL + CNO + 3% HTN from the vehicle controls (CTRL + CNO + 0.9% SAL) group ($p = 0.016$; Tukey's *post-hoc* analysis). Consistent with the ANG II plasma AVP results, CNO-pretreatment significantly attenuated this increase in the G_i DREADD + CNO + 3% HTN group ($p = 0.008$, Tukey's *post-hoc* analysis). There was no significant difference in plasma AVP concentrations between the CTRL + CNO + 0.9% SAL and the G_i DREADD + CNO + 3% HTN group ($p = 0.893$, Tukey's *post-hoc* analysis).

Functional Neuroanatomy

Brains harvested from perfusions were analyzed for Fos and mCherry expression associated with the AAVs. MnPO injections were verified by detecting the presence of mCherry immunofluorescence (Figure 7A). Rats included in the study had mCherry expression isolated to the MnPO. Rats with injections or mCherry labeling outside of the MnPO were excluded from the study.

CNO-induced inhibition during ANG II exposure significantly blocks CaMKIIa$^+$ Fos expression in the MnPO

In rats treated with the control vector injections of CNO followed by sc injection of 0.9% saline (CTRL + CNO + 0.9% SAL) produced Fos staining in the MnPO that was not different from Fos staining associated with VEH injections paired with 0.9% saline sc (CTRL + VEH + 0.9% SAL; Figure 7B & Table 1). Rats treated with the control vector and injected with CNO and ANG II (CTRL + CNO + ANG II) had a significant increase in Fos staining in the MnPO ($F(3, 24) = 32.575$, $p < 0.001$, one-way ANOVA, Figure 7B & Table 1).

In the Gi DREADD + CNO + ANG II group (n = 10, 2-4 MnPO sections per rat), the increase in Fos staining in the MnPO was significantly decreased as compared to the CTRL + CNO + ANG II group (n = 10, 2-4 MnPO sections per rat; Tukey's post-hoc analysis, $p < 0.001$) but not different from the Fos staining observed in CTRL + VEH + 0.9% SAL ($p = 0.170$) or CTRL + CNO + 0.9% SAL($p = 0.531$) rats. Fos staining in the MnPO was significantly increased in CTRL + CNO + ANG II rats compared to either the CTRL + VEH + 0.9% SAL ($p < 0.001$) or CTRL + CNO + VEH ($p < 0.001$) rats. Elevated MnPO Fos expression was blunted in Gi DREADD + CNO + ANG II rats ($p < 0.001$). There was no significant difference between CTRL groups treated with either VEH or CNO ($p = 0.916$) and 0.9% SAL.

Table 1. *Colocalization of ANG II-induced Fos expression with CaMKIIa neurons in the MnPO*

Treatment	***Total cFos+***	***Total CaMKIIa+***	***Total DL Cells***	***% DL cFos+***
Control				
CNO + 0.9% SAL	*21.0 ± 10.0*	*182.8 ± 54.8*	*8.8 ± 1.25*	*50.2 ± 17.9%*

Control VEH + 0.9% SAL	*25.8 ± 7.8*	*181.5 ± 37.5*	*15.1 ± 3.4*	*60.0 ± 4.8%*
Control CNO + ANG II	***79.8 ± 8.7******	*195.0 ± 57.6*	***44.0 ± 7.8******	*54.4± 6.7%*
G_i DREADD CNO + ANG II	*41.9 ± 7.2*	*206.5 ± 41.0*	*2.9 ± 1.0*	***6.5 ± 2.9%******

CaMKIIa neuron inhibition in the MnPO significantly decreases ANG II-evoked effects in downstream nuclei

As expected, ANG II significantly increased Fos staining in $CaMKIIa^+$ neurons ($F(3, 12) = 17.430$, $p < 0.001$, one-way ANOVA). The numbers of Fos and CaMKIIa labeled in MnPO were significantly higher in the CTRL + CNO + ANG II group compared to the CTRL + VEH + 0.9% SAL (*n* = 4, 2-4 MnPO sections per rat; $p < 0.001$) and CTRL + CNO + 0.9% SAL (*n* = 4, 2-4 MnPO sections per rat; $p = 0.003$) groups. About half (54.4%) of the Fos positive cells in the MnPO were also CaMKIIa positive in the CTRL + CNO + ANG II rats. The percentages of Fos and CaMKIIa positive cells were 50.2% and 60.0% for CTRL + CNO + 0.9% SAL and CTRL + VEH + 0.9% SAL rats, respectively. The increase in Fos and CaMKIIa staining cells associated with ANG II was significantly attenuated in the G_i DREADD+ CNO + ANG II rats (Figure 7B; *n* = 4, 2-4 MnPO sections per rat; $p < 0.001$). The percentage of Fos positive cells that were also CaMKIIa positive was reduced to 6.5%. This result indicates that over 90% of the remaining Fos positive cells in the MnPO of rats injected with G_i DREADD were not CaMKIIa positive cells, which is significantly greater than the other three treatment groups (Figure 7B and Table 1; $F(3, 12) = 6.010$, $p = 0.010$, one-way ANOVA;

Tukey's *post-hoc* analysis, all $p < 0.001$). Since these cells do not appear to express CaMKIIa they would not have been transfected with the AAV vector used in this study. There was no significant difference in CaMKIIa-positive neurons between any of the 4 groups ($F(3, 12) = 0.0901$, $p = 0.964$, one-way ANOVA)

G_i DREADD-mediated inhibition of the MnPO also influenced Fos staining associated with ANG II in regions connected to the MnPO (G_i DREADD + CNO + ANG II group: n = 6-10, 2-4 sections per nucleus per rat; CTRL + CNO + ANG II group: n = 4-10, 2-4 sections per nucleus per rat). In rats injected with the CTRL AAV vector and pretreated with CNO, ANG II significantly increased Fos staining in each region that we examined (Figure 8). However, the effects of G_i DREADD MnPO inhibition on ANG II induced Fos staining varied as a function of region. In the rats injected with G_i DREADD, CNO pretreatment did not significantly affect ANG II induced Fos staining in SFO, OVLT, LH, or PVT (Figure 8B).

In other regions G_i DREADD-mediated inhibition of the MnPO did influence Fos staining. In the SON, CNO pretreatment in rats injected in the MnPO with G_i DREADD was associated with a significant decrease in ANG II-induced Fos (Figures 8A and 8B; $F(3, 24) = 19.328$, $p < 0.001$, one-way ANOVA). Fos staining in the SON of CTRL + CNO + ANG II rats was significantly higher as compared to all of the other groups (Figures 8A and 8B; Tukey's *post-hoc* analysis, all $p < 0.001$). Similar results were seen in the RVLM (Figures 8A and 8B). ANG II injections significantly increased Fos staining in the CTRL + CNO + ANG II rats but not in the G_i DREADD + CNO + ANG II rats ($F(3, 16) = 29.480$, $p < 0.001$, one-way ANOVA).

In the PVN, CNO and ANG II significantly increased Fos staining in CTRL rats and there was a statistical trend for decreased Fos staining in the G_i DREADD + CNO + ANG II as compared to CTRL + CNO + ANG II ($F(3, 24) = 18.302$, $p < 0.001$, one-way ANOVA; Tukey's *post-hoc* analysis, $p = 0.084$). However, significant effects of G_i DREADD-mediated inhibition on Fos staining were observed in specific subregions of the PVN (Figure 8C). For example, the posterior magnocellular (PM) part of PVN Fos staining was significantly increased by ANG II in CTRL rats while CNO significantly decreased Fos staining associated with ANG II in G_i DREADD rats ($F(3, 22) = 49.423$, $p < 0.001$, one-way ANOVA; Tukey's *post-hoc* analysis, CTRL + CNO + ANG II; $p < 0.001$ from all other groups). Fos staining in the PM of G_i DREADD + CNO + ANG II rats was still significantly higher when compared to Fos staining in rats pretreated with either CNO or VEH followed by 0.9% SAL (Tukey's *post-hoc* analysis; $p = 0.05$ and $p = 0.097$, respectively). DREADD-mediated Inhibition of the MnPO influenced Fos staining in the medial parvocellular region (MP) of the PVN as well. In the medial parvocellular (MP) part of the PVN, Fos staining associated with CNO and ANG II injections in CTRL rats was significantly greater than Fos staining observed in any of the other groups ($F(3, 22) = 13.789$, $p < 0.001$, one-way ANOVA; Tukey's *post-hoc* analysis, all $p < 0.001$). The Fos staining in the MP of G_i DREADD + CNO + ANG II rats was not significantly different from the CTRL rats pretreated with either CNO or VEH followed by 0.9% SAL (Tukey's *post-hoc* analysis; $p = 0.097$ and $p = 0.050$, respectively). This suggested that in the MP region of the PVN inhibition of the MnPO reduced ANG II-induced Fos staining comparably to control levels. Similar results were observed in the ventrolateral parvocellular region (vlp). Fos staining was increased in CTRL + CNO + ANG II rats and

this increase was significantly different from all of the other groups ($F(3, 22) = 3.734$, $p = 0.026$, one-way ANOVA). Fos staining in the dorsal parvocellular part of the was increased by ANG II ($F(3, 22) = 11.903$, $p < 0.001$, one-way ANOVA) but CNO-induced inhibition did not significantly decrease it (CTRL + CNO + ANG II vs G_i DREADD + CNO + ANG II, $p = 0.258$, Tukey's *post-hoc* analysis).

CNO-induced inhibition in the MnPO and Fos staining associated with 3% HTN

In rats treated with the control vector, Fos staining in the MnPO was significantly increased by 3% HTN (CTRL + VEH + HTN and CTRL + CNO + HTN; Figures 9A & B; $F(3, 16) = 4.982$, $p = 0.002$, one-way ANOVA). Half of the cells that were Fos positive were also positive for CaMKIIa (Table 2) suggesting that HTN affected cells that were not transfected with the vector.

Unlike our results with ANG II, Fos staining associated with 3% HTN in the MnPO was not significantly decreased by CNO pretreatment in G_i DREADD rats (Gi DREADD + CNO + HTN). Fos staining in the MnPO of the G_i DREADD + CNO + HTN group (n = 6 rats, 2-4 MnPO sections per rat) was significantly increased as compared to either of the CTRL groups injected with 0.9% SAL (CTRL + CNO + 0.9% SAL, n = 6 rats, 2-4 MnPO sections per rat; CTRL + VEH + 0.9% SAL, n = 6 rats, 2-4 MnPO sections per rat; $p = 0.019$ and $p = 0.006$, respectively). Fos staining in the Gi DREADD + CNO + HTN was not different from CTRL + CNO + 3% HTN rats ($p = 0.893$, Tukey's *post-hoc* analysis).

In contrast, the number of Fos positive cells that were also labeled for CaMKIIa was significantly decreased (Table 2). As indicated above, half of the Fos positive cells

were CaMKIIa-positive in the CTRL + CNO + 3% HTN rats. In the G_i DREADD + CNO + 3% HTN rats, only 5% of the Fos positive cells were also positive for CaMKIIa meaning 95% of the cells had a different phenotype and may have intrinsic osmotic sensitivity. There were no significant differences in the numbers CaMKIIa-positive neurons between any of the 4 groups (Table 2; $F(3, 12) = 0.287$, $p = 0.834$, one-way ANOVA). This suggests that the apparent lack of CNO inhibition on HTN-mediated Fos staining in the MnPO was due to activation of non-CaMKIIa expressing cells.

Table 2. *Colocalization of hypertonic saline-induced Fos expression with CaMKIIa neurons in the MnPO*

Treatment	***Total cFos+***	***Total CaMKIIa+***	***Total DL Cells***	***% DL cFos+***
Control CNO + 0.9% SAL	*16.1 ± 3.7*	*226.4 ± 50.9*	*8.6 ± 2.2*	*63.3 ± 16.9%*
Control VEH + 0.9% SAL	*22.1 ± 4.0*	*202.9 ± 47.3*	*11.3 ± 2.1*	*74.6 ± 1.3%*
Control CNO + 3% HTN	***74.4 ± 17.6****	*194.3 ± 59.4*	***30.0 ± 8.3***	*49.5 ± 16.7%*
G_i DREADD CNO + 3% HTN	***64.6 ± 6.5****	*165.4 ± 22.1*	*3.4 ± 1.0*	***5.4 ± 1.9%****

CaMKIIa neuron inhibition in the MnPO significantly decreases 3% HTN-evoked effects in select downstream nuclei

Analysis of Fos staining was performed in the same downstream nuclei as in the ANG II experiments above. While all of the regions except the SFO showed significant increases in Fos staining associated with the 3% HTN injections, only the SON and LH were affected by G_i DREADD-mediated inhibition of the MnPO (Figure 9). In the SONs of CTRL + CNO + 3% HTN rats, Fos staining was significantly increased compared to all of the other groups (Figure 9A and B; $F(3, 16) = 52.418$, $p < 0.001$, one-way ANOVA; all $p < 0.001$, Tukey's *post-hoc* analysis). In the SONs of G_i DREADD rats, CNO pretreatment significantly reduced Fos staining associated with 3% HTN as compared to CTRL + CNO + 3% HTN rats ($p = 0.012$, Tukey's *post-hoc* analysis) but did not reduce the staining to control levels (vs. CTRL + VEH + 0.9% SAL, $p < 0.001$; vs. CTRL + CNO + 0.9% SAL, $p < 0.001$).

Similar results were observed in the LH. Rats in the CTRL + CNO + 3% HTN group had significantly more Fos staining in the LH compared to the other three groups (Figure 9B; $F(3, 16) = 18.937$, $p < 0.001$, one-way ANOVA;all $p < 0.001$, Tukey's *post-hoc* analysis). Fos staining in the LH of G_i DREADD + CNO + 3% HTN rats had significantly less Fos expression than the CTRL + CNO + 3% HTN treated rats (Figure 9B; $p = 0.001$, Tukey's *post-hoc* analysis) and significantly higher than both the 0.9% SAL treated groups (Figure 9B; both $p < 0.001$, Tukey's *post-hoc* analysis). For the remaining regions (OVLT, PVN, PVT, and RVLM) Fos staining associated with CNO and 3% HTN was not different between the CTRL virus and G_i DREADD-injected rats and both of these groups were significantly increased as compared to the two CTRL

groups that received the 0.9% SAL injection (Figure 9A and B). This result was also observed in the posterior magnocellular and medial parvocellular regions of the PVN (Figure 9C) while 3% HTN did not influence Fos staining in either the dorsal or ventrolateral parvocellular regions.

Discussion

These studies tested the role of putative excitatory MnPO neurons in behavioral and physiological responses produced by peripheral administration of ANG II or 3% HTN. The virally-mediated chemogenetic inhibition was employed in these studies in order to remotely and selectively reduce the activity of CaMKIIa-expressing MnPO neuronal population in the least invasive manner. These experiments showed that acutely inhibiting the CaMKIIa-expressing neurons in the MnPO significantly attenuated water intake and vasopressin release produced by either ANG II or 3% HTN. The results, however, suggest several differences in how the MnPO contributes to these responses.

In previous studies of the lamina terminalis and its role in water consumption, the SFO and OVLT have been linked to body fluid homeostasis. Studies performed in sheep using electrolytic lesions placed along the ventral lamina terminalis, including the OVLT, decreased water intake stimulated by cellular dehydration (McKinley et al. 1999). Chemogenetic activation of the CaMKIIa neuronal phenotype in the SFO has also been shown to influence drinking behavior (Nation et al. 2016). Studies performed by Oka, et al. showed that 48-hour water deprivation induced Fos immunoreactivity and were able to identify that in the SFO all of the neurons expressing Fos co-localized with CaMKIIa and nNOS (Oka, Ye, and Zuker 2015). The SFO and the OVLT both project to the MnPO as well as other regions involved in body fluid homeostasis (McKinley et al. 2004). Recent studies conducted by Augustine, et al. (2018) implicated the $MnPO^{nNOS}$ neuronal phenotype in regulating drinking behavior stimulated by water deprivation and salt-loading. The current study shows that CNO-induced inhibition of DREADD-

transfected CaMKIIa MnPO neurons significantly attenuates extracellular and cellular thirst. The result of the Fos studies indicate, however, that the homeostatic responses could involve different pathways from the MnPO.

These studies specifically targeted CaMKIIa neurons in the MnPO, which as shown in the *in situ* hybridization studies, is highly co-localized with vGLUT2. This indicates that CaMKIIa neurons in the MnPO are primarily glutamatergic. This is an important consideration since the MnPO has been shown to contain cells that can stimulate or inhibit water intake (Oka, Ye, and Zuker 2015). The results of the current study extend the observations of Oka et al. (2015) by demonstrating that water intake related to extracellular and cellular dehydration is mediated by putative excitatory neurons in MnPO.

The CaMKIIa MnPO neurons transfected by the virus were sensitive to both ANG II and HTN-aCSF. The design of the experiments prevented us from being able to test the same cells with both ANG II and HTN-aCSF. Previous studies have defined a set of sodium sensitive MnPO neurons that likely contribute to body fluid balance (Grob, Drolet, and Mouginot 2004) and additionally characterized ANG II-sensitive MnPO neurons in earlier experiments, consistent with our findings (Bai and Renaud 1998). The relationship between ANG II and HTN-aCSF in the regulation of the MnPO neurons will be the focus of future investigations.

The CNO-mediated inhibition of CaMKIIa-positive neurons in the MnPO completely blocked ANG II-induced excitatory responses. However, during osmotic challenges, CNO-mediated inhibition was only able to significantly attenuate osmotic-induced excitatory response, in contrast to the complete inhibition of ANG II-induced

excitation. This is consistent with studies conducted by Grob, et al. (2004) describing a specific MnPO neuronal phenotype with intrinsic sodium sensitivity. Recordings performed in the current experiments also verify that G_i DREADDx neurons, or MnPO neurons that do not express CaMKIIa, are also sensitive to ANG II and osmotic challenges (Grob, Drolet, and Mouginot 2004).

Results from these Fos studies further support the electrophysiology findings and suggest that ANG II and 3% HTN mediated responses could involve different populations of CaMKIIa-expressing MnPO neurons. Fos immunohistochemistry and its co-localization with CaMKIIa in the MnPO was analyzed. Neurons in the MnPO both expressing CaMKIIa and Fos were significantly elevated in groups injected with the control virus and administered ANG II or 3% hypertonic saline. During DREADD-mediated inhibition using CNO, however, there were significantly reduced numbers of CaMKIIa-positive cells that were also positive for Fos in the MnPO. While this lead to a significant decrease in the total number of Fos positive cells associated with ANG II, the overall decrease in the MnPO was not significant after hypertonic saline. This could be related to the electrophysiology data showing that CNO did not completely block the hyperosmotically-stimulated excitation as strongly as the ANG II responses in the G_i DREADD-transfected neurons.

The differences observed for Fos staining in the MnPO could be related to the nonspecific effects of the hypertonic saline injections. While hypertonic saline is widely used as an osmotic stimulus, Fos staining associated with its administration may be a result of visceral pain related to the route of injection, and therefore, not specific. However, a study conducted by Xu, et al. (2003) compared Fos staining produced by ip

versus iv administration of 2.0 M NaCl in several of the regions included in the current study (MnPO, OVLT, PVN, and SON). They concluded that the increases in Fos staining observed in areas such as the MnPO were related osmotic stimulation and fluid balance and not nociception. Similar conclusions were made about Fos staining in the LH produced ip administration of 1.5 M NaCl (Pirnik, Mravec, and Kiss 2004). It should be noted that the concentration of NaCl used in the current study are approximately four times lower than the concentration used by Xu et al. (2003) and that this study used sc injections to avoid producing visceral pain associated with ip injections. Therefore, the Fos staining produced by hypertonic saline is more likely related to osmotic stimulation but the contribution of nociceptive stimulation at the injection site cannot be ruled out.

There were also observed differences in Fos staining in several other regions that receive projections from the MnPO that were stimulus-dependent. In rats administered ANG II, CNO-induced inhibition of G_i DREADD was associated with significant decreases in Fos staining in the SON, PVN, and RVLM. When rats were injected with hypertonic saline, G_i DREADD mediated inhibition of the MnPO significantly attenuated Fos staining in the SON and LH but not the PVN or RVLM. The central effects of ANG II and hypertonic saline are mediated by circumventricular organs (Ferguson 2014). These regions project not only to the MnPO but also to the SON, PVN, and LH (Ferguson 2014; McKinley et al. 2004; McKinley et al. 2015). This creates a series of redundant pathways from the lamina terminalis to regions contributing to hormone release and water intake. Our results suggest that, despite these possible redundancies, the MnPO significantly contributes to the activation of SON, PVN, and LH in a stimulus dependent manner.

As shown in these studies, G_i DREADD inhibition of the MnPO was associated with significant decreases in Fos staining in the SON after either ANG II or 3% HTN. These results are consistent with observed reductions in AVP release associated with G_i DREADD inhibition of the MnPO during ANG II or 3% HTN exposure, with ANG II inducing a greater release of AVP than 3% HTN between groups. This may be due to how each stimulus induces its effects in the local circuitry. In ANG II-treated rats, G_i DREADD inhibition of the MnPO reduced Fos staining in the PVN and RVLM, while these regions were not influenced by MnPO inhibition in hypertonic saline treated rats. Fos staining in the LH that was associated with hypertonic saline was significantly decreased by G_i DREADD inhibition. Recent studies suggest that the PVN, PVT, and LH receive projections from the MnPO that are related to water intake (Leib et al. 2017). Results from the current study are generally consistent with these findings and suggest that these pathways might be differentially regulated by extracellular dehydration versus cellular dehydration (Fitzsimons 1972). Differences in MnPO neurons that contribute to extracellular versus cellular was first proposed based on the results of studies using excitotoxins (Cunningham et al. 1991). The current results provide evidence that MnPO neurons mediating water intake associated with extracellular dehydration project to the PVN while MnPO neurons participating in cellular thirst project to the LH. These data also suggest that there are MnPO neurons participating in both extracellular and cellular dehydration that project to the SON.

Findings from the current study also demonstrate that Fos expression was significantly decreased in the RVLM during ANG II, but not hypertonic saline exposure during G_i DREADD-mediated inhibition. The RVLM contains sympathetic motor neurons

that contribute to blood pressure regulation. These results suggest that the MnPO may contribute to increases in sympathetic tone related to activation of the Renin-Angiotensin System but not high salt. This is consistent with previous studies on the role of the lamina terminalis in ANG II-dependent models of hypertension (Collister et al. 2014; Ployngam and Collister 2007; Shell, Faulk, and Cunningham 2016). The decreased Fos staining in the RVLM could be related to the decreased Fos expression observed in the PVN, which has also been linked to hypertension (Basting et al. 2018; Llewellyn et al. 2012). Lesions of the AV3V have been shown prevent or reverse several ANG II dependent models of hypertension (Brody et al. 1978). The results of the current study suggest that CaMKIIa neurons in the MnPO that project to the PVN could contribute to this aspect of AV3V function.

Interestingly, ANG II was much more effective at inducing differential Fos expression, water intake, and AVP release compared to 3% HTN. Studies by Fitzsimons showed that water consumption associated with hypovolemic dehydration can result in a greater volume of water intake as compared to cellular dehydration of similar magnitude (Fitzsimons 1998). While it is difficult to determine the equivalence of extracellular versus cellular dehydration, the differences in the magnitude of the response could be related to the position of the doses used in their respective dose-response curves.

It is important to note how increases in arterial pressure associated with ANG II may alter its dipsogenic effects. Early studies addressing ANG II in relation to arterial pressure and thirst have been conducted. Rettig and Johnson (1985) studied the role of ANG II, among other stimuli, on drinking in sinaortic denervated rat models to

hypovolemia, and found no effect on water intake (Rettig and Johnson 1986). In other studies conducted by Evered et al. (1988), the interaction between the dipsogenic and pressor effects of ANG II at various concentrations were tested using diazoxide, a vasodilator, to counteract the increases in blood pressure (Evered, Robinson, and Rose 1988). It was concluded from these studies that intravenous infusions of ANG II in water-replete rats stimulate thirst in a dose-dependent manner, but water intake may be attenuated due to the concurrent increase in blood pressure. The rise in arterial pressure may also produce increases in urinary water and solute excretion, resulting in dehydration that could eventually contribute to thirst as well (Evered, Robinson, and Rose 1988). Most physiological situations characterized by activation of the renin-angiotensin system include hypovolemia and hypotension. In this context, the increase in blood pressure produced by ANG II may allow the rats to be behaviorally competent enough to ingest water (Evered, Robinson, and Rose 1988).

In summary, these studies used ANG II and hypertonic saline injections to simulate aspects of extracellular and cellular dehydration in order to better understand the contribution of the MnPO to the integrative physiology of body fluid homeostasis. Both of these stimuli act through circumventricular organs to affect the MnPO, Additionally, hypertonic saline can directly influence the activity of sodium sensitive MnPO neurons. The chemogenetic inhibition of putative excitatory MnPO neurons inhibited vasopressin release and drinking behavior produced by either ANG II or hypertonic saline. In contrast, the effects of inhibiting CaMKIIa MnPO neurons was associated with different patterns of Fos staining. Fos staining in the SON, PVN, and RVLM associated with ANG II injections was significantly decreased by chemogenetic

inhibition of the MnPO. After injections of hypertonic saline, MnPO inhibition affected the LH and SON. Thus, extracellular and cellular dehydration appear to influence different populations of CaMKIIa-expressing MnPO neurons based on their afferent projections but can result in converging behavioral outcomes.

Acknowledgments

The authors would like to acknowledge and thank the technical assistance of M. Bachelor, J. T. Little and J. Kiehlbauch.

Sources of Funding

This work was supported by NIH grants R01 HL142341, P01 HL088052 and T32 AG020494.

Conflict of Interest/Disclosures

Authors report no conflict of interest.

Figure 1. *CaMKIIa-positive MnPO neurons are glutamatergic*. Representative image of the dorsal MnPO (dMnPO) with CaMKIIa-positive MnPO neurons (red) and colocalization with vGLUT2 (green), as indicated in the inset by white arrows. Scale bar for inset, 25 µm. Main figure scale bar, 100 µm. Anterior commissure, a.c.

Figure 1.

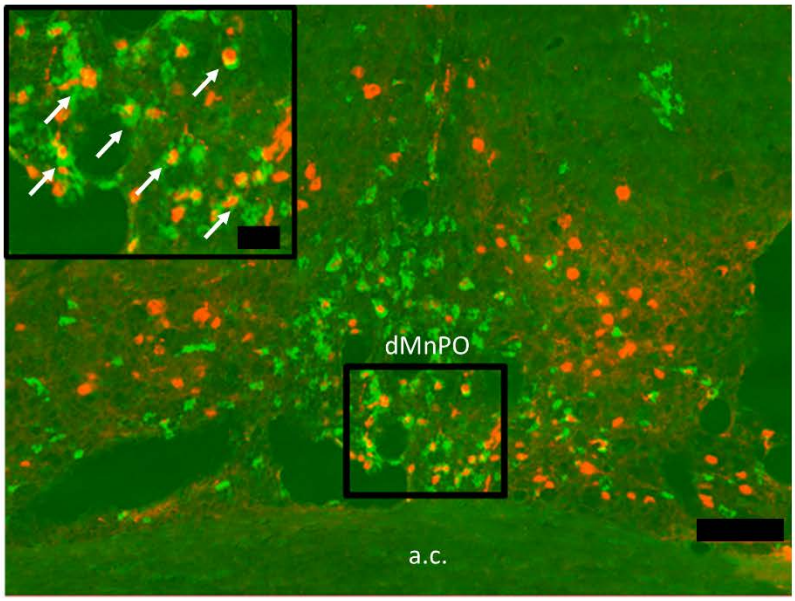

Figure 2. *CNO-mediated inhibition significantly attenuates basal firing rate in G_i DREADD-labeled neurons*. ***A***, Representative image showing loose-cell patch recording of a G_i DREADD-labeled (G_i DREADD) neuron (red). Scale bar, 20 µm. ***B***, Representative raw trace recordings of a control (CTRL) neuron (top, *n* = 13 neurons, 6 rats), G_i DREADD-unlabeled (G_i DREADDx) neuron (middle, *n* = 19 neurons, 6 rats), and G_i DREADD neuron (bottom, *n* = 17 neurons, 6 rats). Scale bar, 10 s. ***C***, CNO-mediated inhibition significantly attenuated basal firing rate of G_i DREADD neurons (peak response) compared to baseline and recovery, and compared to CTRL and G_i DREADDx. ***D***, CNO-mediated inhibition significantly attenuated basal firing rate of G_i DREADD neurons (peak response), represented as a percent baseline, compared to G_i DREADDx and CTRL neurons. *$p < 0.050$, compared to peak response between groups; #$p < 0.050$, compared to baseline within group. Data are presented as mean and SEM.

Figure 2.

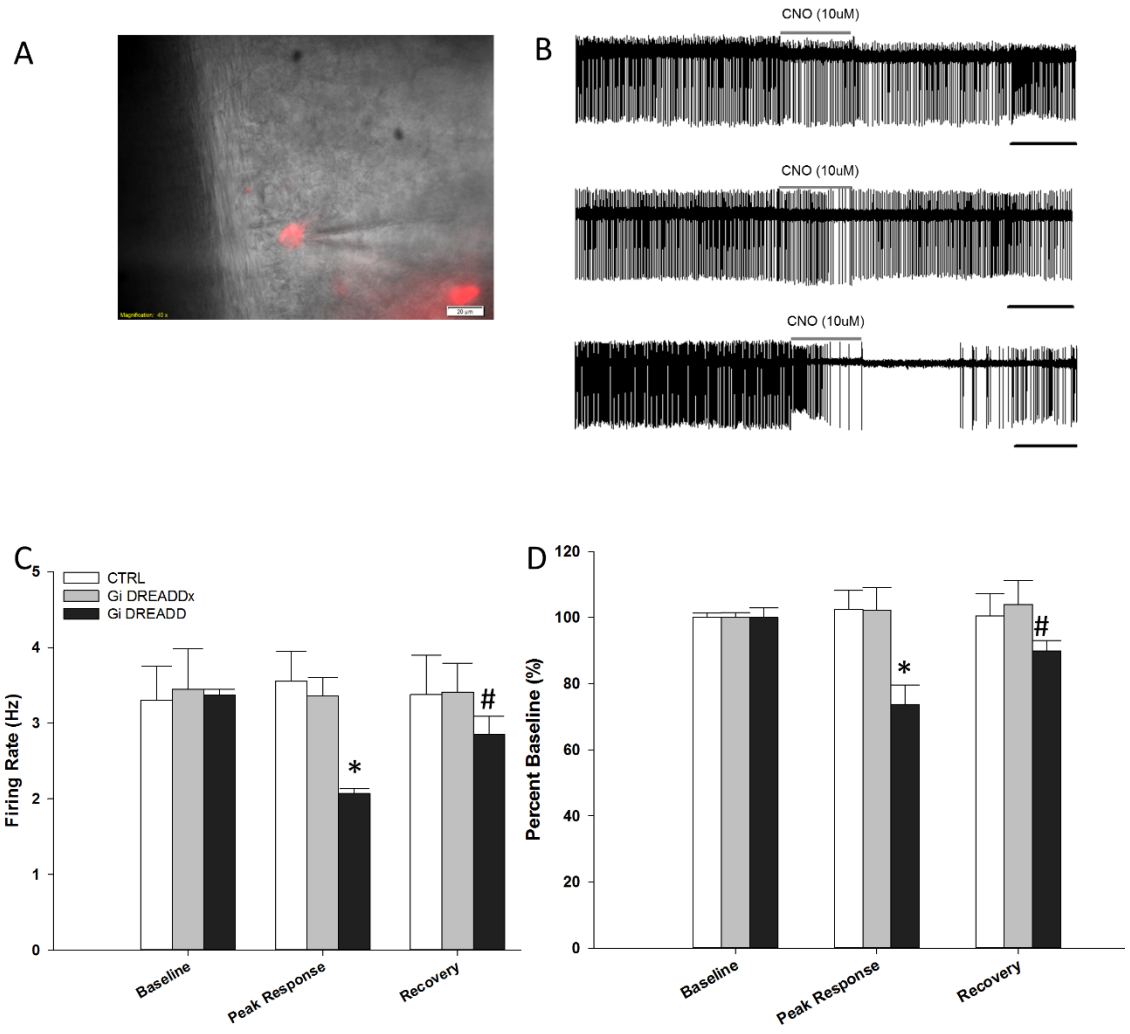
A
B
CNO (10uM)
CNO (10uM)
CNO (10uM)
C
CTRL
Gi DREADDx
Gi DREADD
Firing Rate (Hz)
0
1
2
3
4
5
*
#
Baseline
Peak Response
Recovery
D
Percent Baseline (%)
0
20
40
60
80
100
120
*
#
Baseline
Peak Response
Recovery

Figure 3. *CNO-mediated inhibition blocks ANG II-induced excitation*. ***A***, CNO bath application significantly inhibits basal firing rate of G_i DREADD neurons (*n* = 15 neurons, 6 rats), but does not affect spontaneous activity in control (*n* = 7 neurons, 3 rats) or G_i DREADD-unlabeled (G_i DREADDx) neurons (*n* = 15 neurons, 6 rats). **p < 0.050 compared to each group. ***B***, G_i DREADD neurons during CNO bath application reduced firing rate to 20% of percent aCSF baseline but did not affect baseline of G_i DREADDx neurons. ***C***, Representative raw trace recordings of a G_i DREADD neuron during aCSF (control conditions) exposure (top), G_i DREADDx neuron (middle) and G_i DREADD neuron (bottom) with the two latters exposed to CNO during baseline. Scale bar, 10 s. ***D***, Focal ANG II application significantly increased firing rate of G_i DREADDx neurons during CNO exposure and G_i DREADD neurons during aCSF exposure. ‡p < 0.001. CNO-mediated inhibition blocked ANG II excitation of G_i DREADD neurons and displayed significantly reduced firing rate compared to G_i DREADDx neurons. *p < 0.001. Data are presented as mean and SEM.

Figure 3.

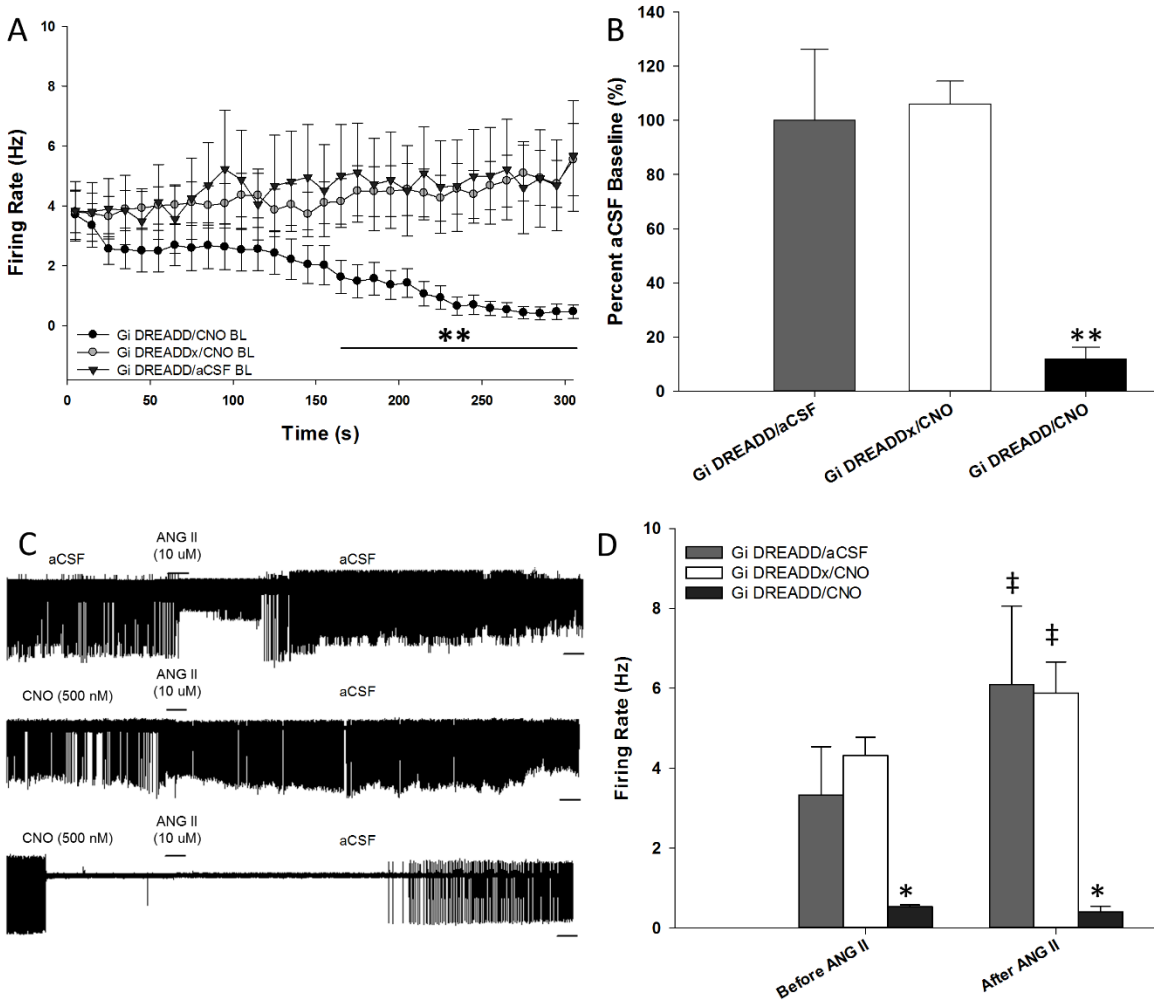
A
Firing Rate (Hz)
Time (s)
Gi DREADD/CNO BL
Gi DREADDx/CNO BL
Gi DREADD/aCSF BL
**
B
Percent aCSF Baseline (%)
Gi DREADD/aCSF
Gi DREADDx/CNO
Gi DREADD/CNO
**
C
aCSF
ANG II (10 uM)
aCSF
CNO (500 nM)
ANG II (10 uM)
aCSF
CNO (500 nM)
ANG II (10 uM)
aCSF
D
Gi DREADD/aCSF
Gi DREADDx/CNO
Gi DREADD/CNO
Firing Rate (Hz)
‡
‡
*
*
Before ANG II
After ANG II

Figure 4. *CNO-mediated inhibition attenuates firing rate during hyperosmotic challenges*. ***A***, Representative raw trace recordings of a G_i DREADD neuron in the absence of CNO, using aCSF for control conditions (top), G_i DREADD-unlabeled (G_i DREADDx) neuron (middle) and G_i DREADD neuron (bottom), both latter neurons exposed to CNO. Scale bar, 10 s. Hypertonic aCSF, HTN-aCSF. ***B***, CNO significantly inhibits basal firing rate compared to percent aCSF baseline of G_i DREADD neurons. ***C***, Hyperosmotic challenges significantly increased firing frequency of G_i DREADD neurons during aCSF exposure and G_i DREADDx neurons during CNO exposure (unaffected). CNO significantly attenuated firing rate of G_i DREADD neurons compared to G_i DREADDx neurons. There was an observed increase in firing rate in the absence of CNO during HTN-aCSF bath application, which became significant during aCSF bath application. *$p < 0.001$ compared to G_i DREADDx neurons exposed to CNO and G_i DREADD neurons during aCSF exposure, #$p < 0.050$ compared to time points within group. Data are presented as mean and SEM.

Figure 4.

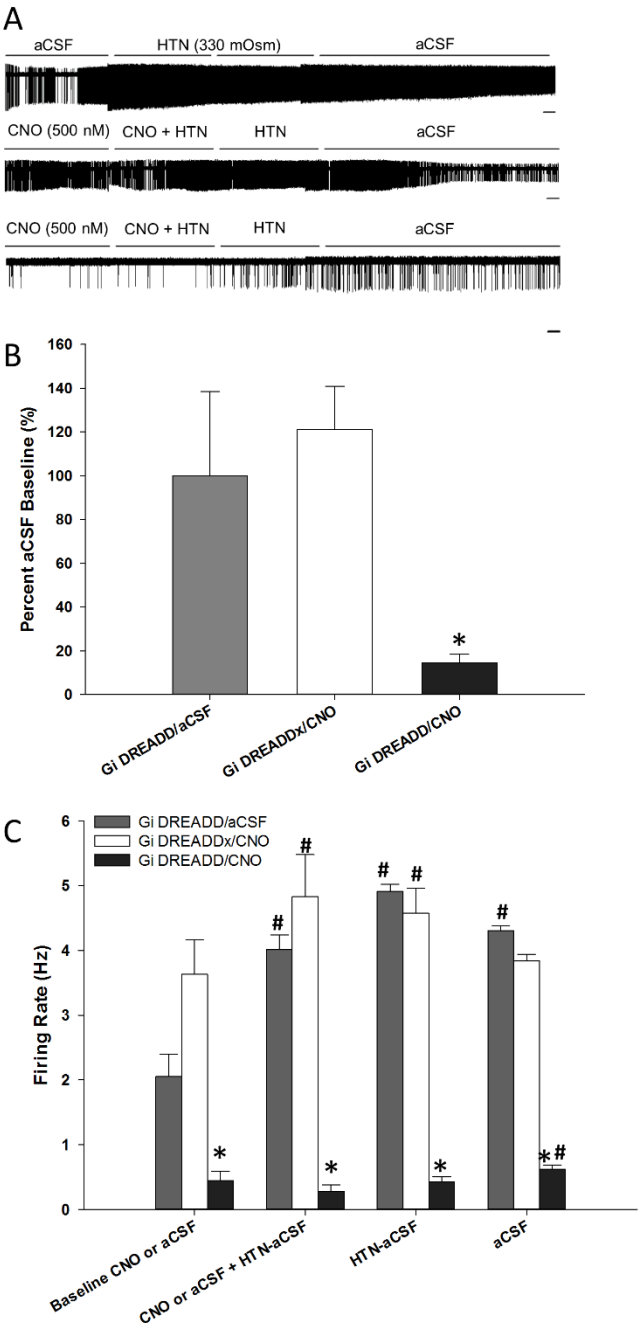
A
aCSF
HTN (330 mOsm)
aCSF
CNO (500 nM)
CNO + HTN
HTN
aCSF
CNO (500 nM)
CNO + HTN
HTN
aCSF
B
Percent aCSF Baseline (%)
160
140
120
100
80
60
40
20
0
*
Gi DREADD/aCSF
Gi DREADDx/CNO
Gi DREADD/CNO
C
Gi DREADD/aCSF
Gi DREADDx/CNO
Gi DREADD/CNO
Firing Rate (Hz)
6
5
4
3
2
1
0
#
#
#
#
#
*
*
*
*#
Baseline CNO or aCSF
CNO or aCSF + HTN-aCSF
HTN-aCSF
aCSF

Figure 5. *Acute MnPO inhibition attenuates evoked drinking responses.* ***A***, ANG II significantly increased water consumption compared to volume control tests (VEH + 0.9% SAL) in both G_i DREADD and CTRL (VEH + ANG II) rats (*n* = 10 rats). CNO-mediated inhibition significantly attenuated this increase in G_i DREADD (CNO + ANG II) rats (*n* = 10 rats). B, Hypertonic saline (3% HTN) significantly increased water consumption compared to VEH + 0.9% SAL tests in both G_i DREADD and CTRL (VEH + 3% HTN) rats (*n* = 6 rats) and CNO-mediated inhibition significantly attenuated this increase in G_i DREADD rats (*n* = 6 rats). *p < 0.005 compared to VEH + 0.9% SAL in respective group (A or B), ‡p = < 0.050 compared to VEH and ANG II (A) and 3% HTN (B) exposure in respective group, #p < 0.015 compared to CTRL + CNO + ANG II (A) and CTRL + CNO + 3% HTN (B). Data are presented as mean and SEM.

Figure 5.

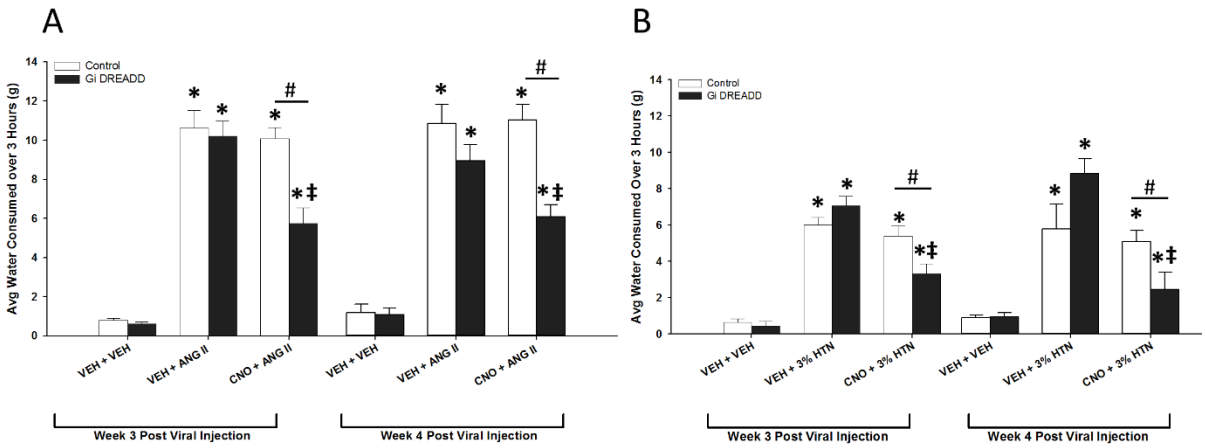
A
Control
Gi DREADD
Avg Water Consumed over 3 Hours (g)
VEH + VEH
VEH + ANG II
CNO + ANG II
VEH + VEH
VEH + ANG II
CNO + ANG II
Week 3 Post Viral Injection
Week 4 Post Viral Injection
B
Control
Gi DREADD
Avg Water Consumed Over 3 Hours (g)
VEH + VEH
VEH + 3% HTN
CNO + 3% HTN
VEH + VEH
VEH + 3% HTN
CNO + 3% HTN
Week 3 Post Viral Injection
Week 4 Post Viral Injection

Figure 6. *CNO-induced inhibition of CaMKIIa MnPO neurons significantly attenuates evoked increases of plasma AVP*. ***A***, ANG II significantly increased plasma AVP concentration in CTRL rats (CTRL + CNO + ANG II), but this increase was significantly attenuated during CNO-mediated inhibition in G_i DREADD (G_i DREADD + CNO + ANG II) rats. ***B***, Hypertonic saline (3% HTN) significantly increased plasma AVP concentration, but this increase was blocked during CNO-mediated inhibition in G_i DREADD (G_i DREADD + CNO + 3%HTN) rats. *$p < 0.020$ compared to respective controls (CTRL +CNO + 0.9% SAL), ‡$p < 0.050$ compared to VEH and 3% HTN exposure, #$p < 0.001$ compared to CTRL +CNO + ANG II. Data are presented as mean and SEM.

Figure 6.

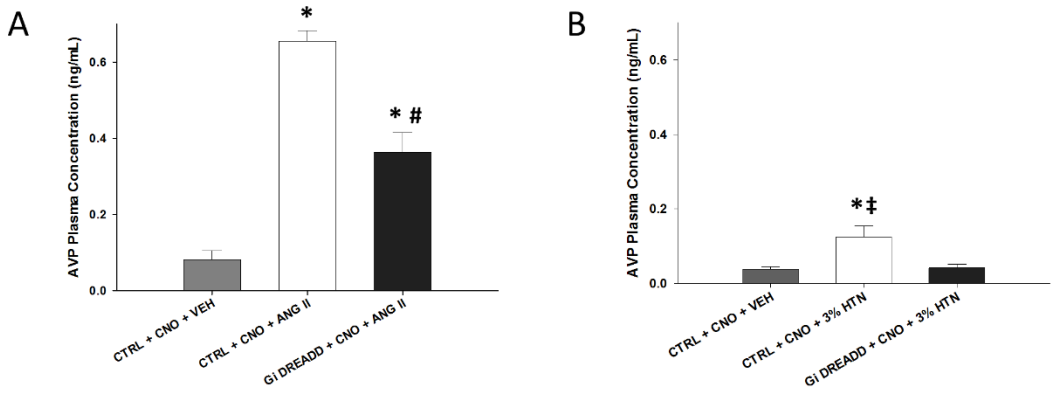
A
AVP Plasma Concentration (ng/mL)
0.0
0.2
0.4
0.6
*
* #
CTRL + CNO + VEH
CTRL + CNO + ANG II
Gi DREADD + CNO + ANG II
B
AVP Plasma Concentration (ng/mL)
0.0
0.2
0.4
0.6
*‡
CTRL + CNO + VEH
CTRL + CNO + 3% HTN
Gi DREADD + CNO + 3% HTN

Figure 7. *ANG II significantly increases Fos expression in the MnPO in control virus-injected rats, but is blocked during CNO-mediated inhibition in G_i DREADD-injected rats.* ***A***, Diagram showing representative mCherry labeling from AAV transfection in the MnPO. Scale bar, 250 µm. Third ventricle, 3V; anterior commissure, a.c.; dorsal MnPO, dMnPO; ventral MnPO, vMnPO. ***B***, Representative Fos staining in the dMnPO of control virus-injected (CTRL) rats treated with CNO vehicle (VEH) and ANG II vehicle (0.9% SAL; *n* = 4, 2-4 sections per rat), upper left panel, CTRL rats treated with CNO and 0.9% SAL (*n* = 4, 2-4 sections per rat), upper right panel, CTRL rats treated with CNO and ANG II (*n* = 10, 2-4 sections per rat), lower left panel, and G_i DREADD-injected rats treated with CNO and ANG II (*n* = 10, 2-4 sections per rat), lower right panel. Scale bar, 100 µm.

Figure 7.

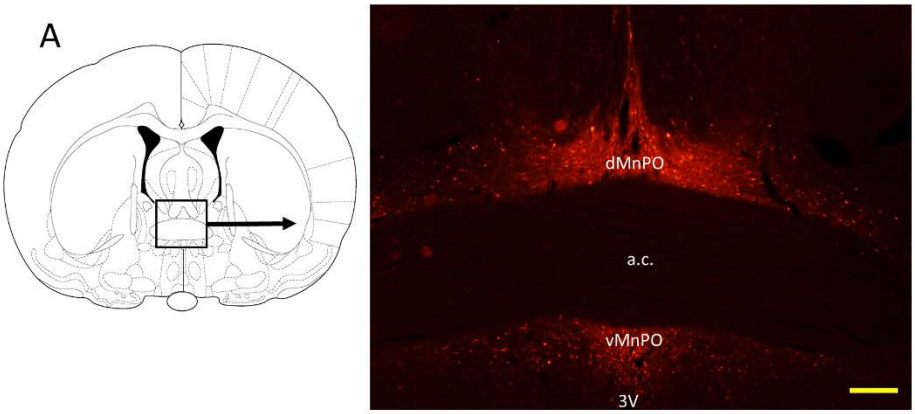
A
dMnPO
a.c.
vMnPO
3V

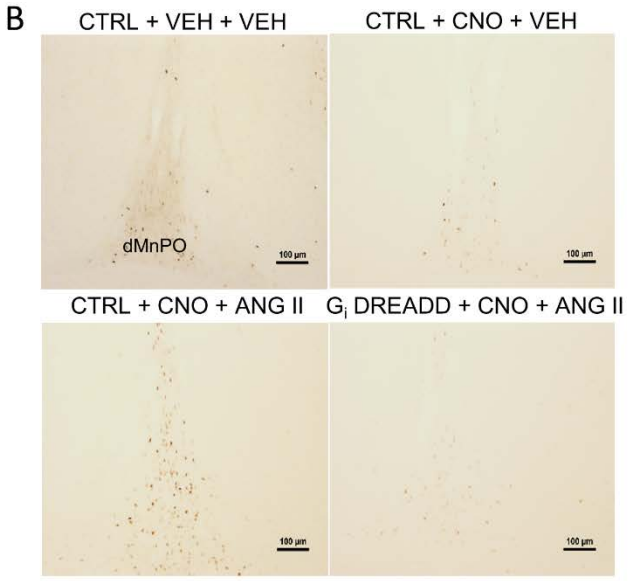
B
CTRL + VEH + VEH
CTRL + CNO + VEH
dMnPO
100 µm
100 µm
CTRL + CNO + ANG II
G$_i$ DREADD + CNO + ANG II
100 µm
100 µm

Figure 8. *ANG II significantly increases Fos expression in regions downstream of the MnPO compared to controls and is blunted during CNO-induced inhibition in G_i DREADD-injected rats.* ***A***, Representative Fos staining in the SON (top row), PVN (middle row), and RVLM (bottom row) for each group tested. Scale bar, 100 µm. Supraoptic nucleus, SON; optic tract, ot: paraventricular nucleus, PVN; posterior magnocellular, pm; dorsal parvocellular, dp; medial parvocellular, mp; ventral lateral parvocellular, vlp; rostral ventral lateral medulla, RVLM. ***B***, ANG II significantly increases Fos expression in the SFO, OVLT, PVN, and PVT but this increase was significantly attenuated during CNO-mediated inhibition in the MnPO, SON, LH, and RVLM. Subfornical organ, SFO; organum vasculosum of the lamina terminalis, OVLT; paraventricular thalamus, PVT; lateral hypothalamus, LH.***C***, ANG II significantly increases Fos staining in cardiovascular and neuroendocrine-regulating regions of the PVN, but is significantly attenuated by CNO-mediated inhibition in the pm and mp subregions.*$p < 0.005$ compared to VEH (CTRL + VEH + 0.9% SAL) and CNO (CTRL + CNO + 0.9% SAL) controls, #$p < 0.001$ G_i DREADD-injected rats compared to control virus-injected rats treated with CNO and ANG II (G_i DREADD + CNO + ANG II and CTRL + CNO + ANG II, respectively). Data are presented as mean and SEM.

Figure 8.

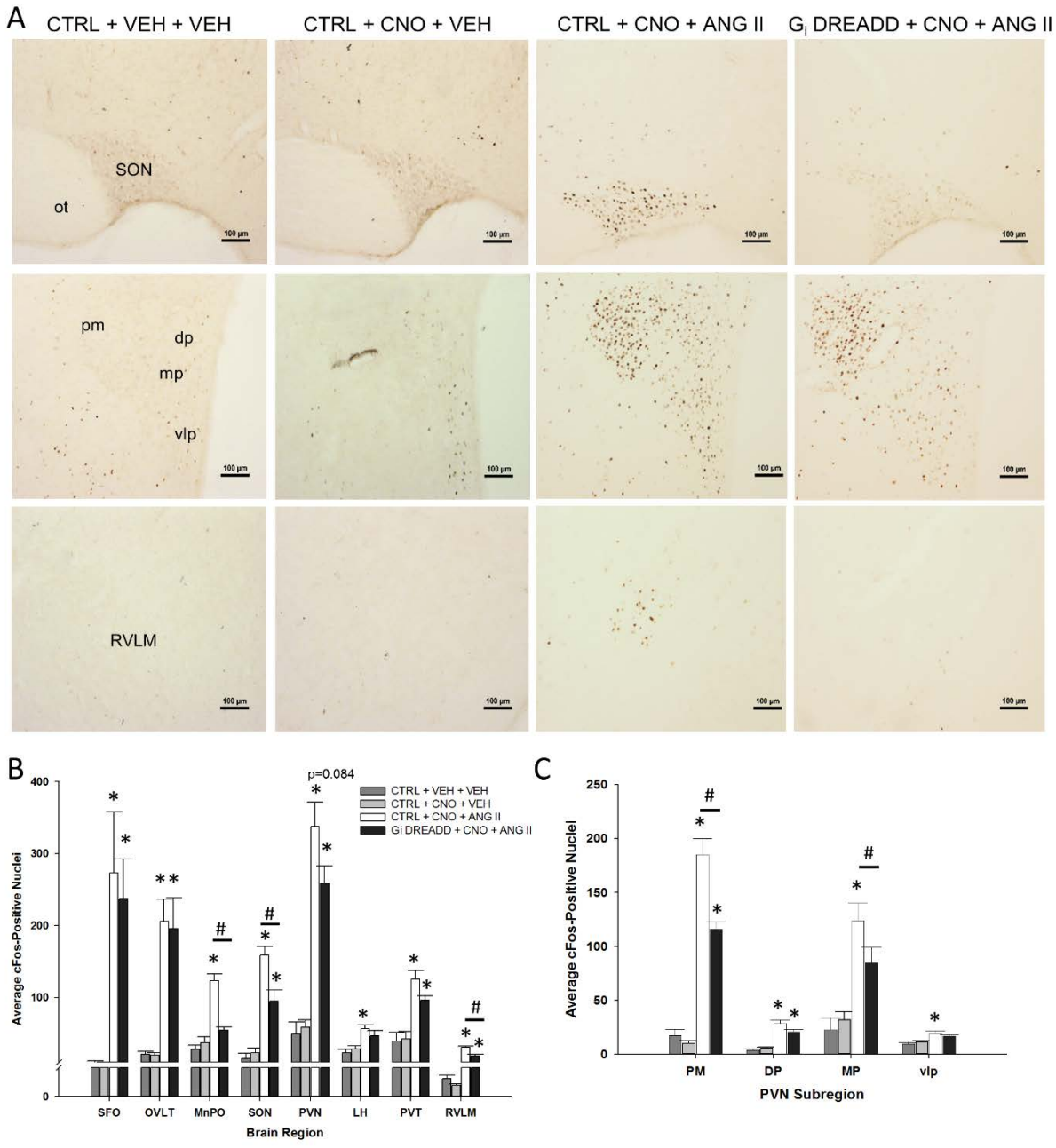
A
CTRL + VEH + VEH
CTRL + CNO + VEH
CTRL + CNO + ANG II
Gi DREADD + CNO + ANG II
SON
ot
pm
dp
mp
vlp
RVLM
100 µm
B
p=0.084
CTRL + VEH + VEH
CTRL + CNO + VEH
CTRL + CNO + ANG II
Gi DREADD + CNO + ANG II
Average cFos-Positive Nuclei
SFO
OVLT
MnPO
SON
PVN
LH
PVT
RVLM
Brain Region
C
Average cFos-Positive Nuclei
PM
DP
MP
vlp
PVN Subregion

Figure 9. *Hypertonic saline significantly increases Fos expression in the MnPO and in regions downstream, but is attenuated during CNO-induced inhibition in G_i DREADD-injected rats*. ***A***. Representative Fos staining in control virus-injected (CTRL) rats (*n* = 6, 2-4 sections per rat), left, and G_i DREADD rats (*n* = 6, 2-4 sections per rat), right, treated with CNO and 3% hypertonic saline (3% HTN); dMnPO (top row), SON (second row), PVN (third row), RVLM (bottom row) . ***B***, 3% HTN significantly increases Fos expression in the OVLT, MnPO, PVN and PVT but this increase was significantly attenuated during CNO-mediated inhibition in the SON and LH. Scale bar, 100 µm. Subfornical organ, SFO; organum vasculosum of the lamina terminalis, OVLT; paraventricular thalamus, PVT; lateral hypothalamus, LH.***C***, 3% HTN significantly increases Fos staining in cardiovascular and neuroendocrine-regulating regions of the PVN, the pm and mp subregions.*$p < 0.005$ compared to VEH (CTRL + VEH + 0.9% SAL) and CNO (CTRL + CNO + 0.9% SAL) controls, #$p < 0.001$ G_i DREADD rats compared to CTRL rats treated with CNO and 3% HTN (G_i DREADD + CNO + 3% HTN and CTRL + CNO + 3% HTN, respectively). Data are presented as mean and SEM.

Figure 9.

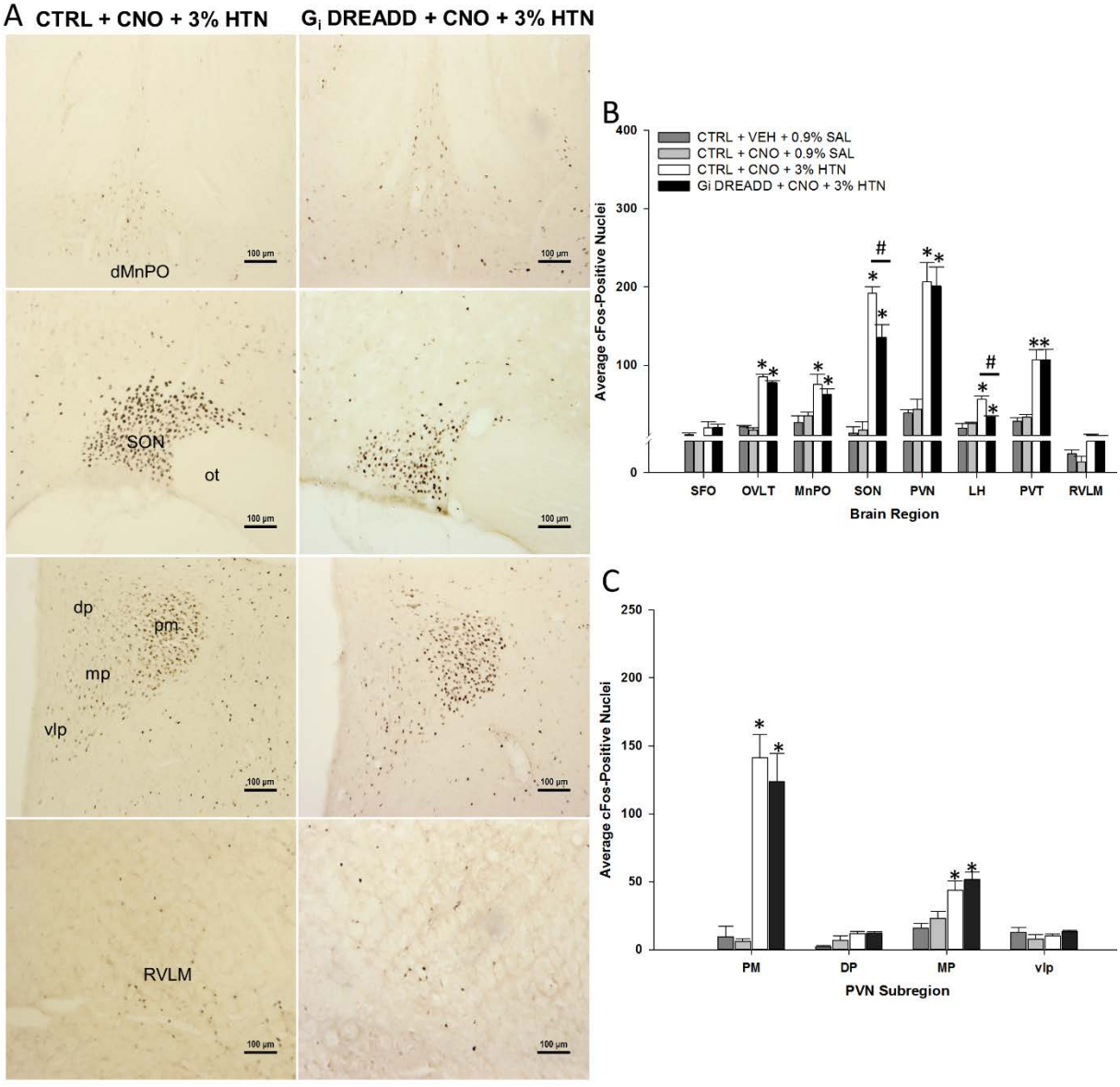
A
CTRL + CNO + 3% HTN
Gi DREADD + CNO + 3% HTN
dMnPO
SON
ot
dp
pm
mp
vlp
RVLM
100 µm
B
CTRL + VEH + 0.9% SAL
CTRL + CNO + 0.9% SAL
CTRL + CNO + 3% HTN
Gi DREADD + CNO + 3% HTN
Average cFos-Positive Nuclei
0
100
200
300
400
SFO
OVLT
MnPO
SON
PVN
LH
PVT
RVLM
Brain Region
C
Average cFos-Positive Nuclei
0
50
100
150
200
250
PM
DP
MP
vlp
PVN Subregion

Table 1. ANG II exposure significantly increases Fos expression in the MnPO, specifically in CaMKIIa-positive neurons. CNO-mediated inhibition significantly attenuated ANG II-induced Fos expression in the MnPO in G_i DREADD-injected rats, with inhibition of the CaMKIIa neuronal phenotype. **p < 0.001 compared to all groups. Data are presented as mean ± SEM.

Table 2. Hypertonic saline exposure significantly increases Fos expression in the MnPO, not only in CaMKIIa-positive neurons, but also other neuronal phenotypes. CNO-mediated inhibition did not significantly attenuate total hypertonic saline-induced Fos expression in the MnPO in G_i DREADD-injected rats. *p < 0.050 compared to vehicle controls. **p < 0.001 compared to all groups. Data are presented as mean ± SEM.

References

Adler, S. M., and J. G. Verbalis. 2006. 'Disorders of body water homeostasis in critical illness', *Endocrinol Metab Clin North Am*, 35: 873-94, xi.

Allen, W. E., L. A. DeNardo, M. Z. Chen, C. D. Liu, K. M. Loh, L. E. Fenno, C. Ramakrishnan, K. Deisseroth, and L. Luo. 2017. 'Thirst-associated preoptic neurons encode an aversive motivational drive', *Science*, 357: 1149-55.

Augustine, V., S. K. Gokce, S. Lee, B. Wang, T. J. Davidson, F. Reimann, F. Gribble, K. Deisseroth, C. Lois, and Y. Oka. 2018. 'Hierarchical neural architecture underlying thirst regulation', *Nature*, 555: 204-09.

Bai, D., and L. P. Renaud. 1998. 'ANG II AT1 receptors induce depolarization and inward current in rat median preoptic neurons in vitro', *Am J Physiol*, 275: R632-9.

Basting, T., J. Xu, S. Mukerjee, J. Epling, R. Fuchs, S. Sriramula, and E. Lazartigues. 2018. 'Glutamatergic neurons of the paraventricular nucleus are critical contributors to the development of neurogenic hypertension', *J Physiol*.

Bourque, C. W. 2008. 'Central mechanisms of osmosensation and systemic osmoregulation', *Nat Rev Neurosci*, 9: 519-31.

Brody, M. J., G. D. Fink, J. Buggy, J. R. Haywood, F. J. Gordon, and A. K. Johnson. 1978. 'The role of the anteroventral third ventricle (AV3V) region in experimental hypertension', *Circulation Research*, 43: I2-I13.

Collister, J. P., M. Bellrichard, D. Drebes, D. Nahey, J. Tian, and M. C. Zimmerman. 2014. 'Over-expression of copper/zinc superoxide dismutase in the median preoptic nucleus attenuates chronic angiotensin II-induced hypertension in the rat', *Int J Mol Sci*, 15: 22203-13.

Cunningham, J. T., T. Beltz, R. F. Johnson, and A. K. Johnson. 1992. 'The effects of ibotenate lesions of the median preoptic nucleus on experimentally-induced and circadian drinking behavior in rats', *Brain Res*, 580: 325-30.

Cunningham, J. T., M. J. Sullivan, G. L. Edwards, R. Farinpour, T. G. Beltz, and A. K. Johnson. 1991. 'Dissociation of experimentally induced drinking behavior by ibotenate injection into the median preoptic nucleus', *Brain Res*, 554: 153-8.

Dampney, R. A. 2016. 'Central neural control of the cardiovascular system: current perspectives', *Adv Physiol Educ*, 40: 283-96.

Evered, M. D., M. M. Robinson, and P. A. Rose. 1988. 'Effect of arterial pressure on drinking and urinary responses to angiotensin II', *Am J Physiol*, 254: R69-74.

Farmer, G. E., K. Balapattabi, M. E. Bachelor, J. T. Little, and J. T. Cunningham. 2018. 'AT1a influences GABAa mediated inhibition through the regulation of KCC2 expression', *Am J Physiol Regul Integr Comp Physiol*.

Ferguson, A. V. 2014. 'Frontiers in Neuroscience

Circumventricular Organs: Integrators of Circulating Signals Controlling Hydration, Energy Balance, and Immune Function.' in L. A. De Luca, Jr., J. V. Menani and A. K. Johnson (eds.), *Neurobiology of Body Fluid Homeostasis: Transduction and Integration* (CRC Press/Taylor & Francis

(c) 2014 by Taylor & Francis Group, LLC.: Boca Raton (FL)).

Fitzsimons, J. T. 1972. 'Thirst', *Physiological reviews*, 52: 468-561.

———. 1998. 'Angiotensin, thirst, and sodium appetite', *Physiol Rev*, 78: 583-686.

Gardiner, T. W., and E. M. Stricker. 1985. 'Hyperdipsia in rats after electrolytic lesions of nucleus medianus', *Am J Physiol*, 248: R214-23.

Gardiner, T. W., J. G. Verbalis, and E. M. Stricker. 1985. 'Impaired secretion of vasopressin and oxytocin in rats after lesions of nucleus medianus', *Am J Physiol*, 249: R681-8.

Grindstaff, R. J., R. R. Grindstaff, M. J. Sullivan, and J. T. Cunningham. 2000. 'Role of the locus ceruleus in baroreceptor regulation of supraoptic vasopressin neurons in the rat', *Am J Physiol Regul Integr Comp Physiol*, 279: R306-19.

Grob, M., G. Drolet, and D. Mouginot. 2004. 'Specific Na+ sensors are functionally expressed in a neuronal population of the median preoptic nucleus of the rat', *J Neurosci*, 24: 3974-84.

Hoffman, G. E., M. S. Smith, and M. D. Fitzsimmons. 1992. 'Detecting steroidal effects on immediate early gene expression in the hypothalamus', *Neuroprotocols*, 1: 55-66.

Johnson, A. K., J. T. Cunningham, and R. L. Thunhorst. 1996. 'Integrative role of the lamina terminalis in the regulation of cardiovascular and body fluid homeostasis', *Clin Exp Pharmacol Physiol*, 23: 183-91.

Leib, D. E., C. A. Zimmerman, A. Poormoghaddam, E. L. Huey, J. S. Ahn, Y. C. Lin, C. L. Tan, Y. Chen, and Z. A. Knight. 2017. 'The Forebrain Thirst Circuit Drives Drinking through Negative Reinforcement', *Neuron*, 96: 1272-81 e4.

Llewellyn, Tamra, Hong Zheng, Xuefei Liu, Bo Xu, and Kaushik P. Patel. 2012. 'Median preoptic nucleus and subfornical organ drive renal sympathetic nerve activity via a glutamatergic mechanism within the paraventricular nucleus', *American Journal of Physiology - Regulatory, Integrative and Comparative Physiology*, 302: R424-R32.

McKinley, M. J., M. L. Mathai, R. M. McAllen, R. C. McClear, R. R. Miselis, G. L. Pennington, L. Vivas, J. D. Wade, and B. J. Oldfield. 2004. 'Vasopressin secretion: osmotic and hormonal regulation by the lamina terminalis', *J Neuroendocrinol*, 16: 340-7.

McKinley, M. J., M. L. Mathai, G. Pennington, M. Rundgren, and L. Vivas. 1999. 'Effect of individual or combined ablation of the nuclear groups of the lamina terminalis on water drinking in sheep', *Am J Physiol*, 276: R673-83.

McKinley, M. J., S. T. Yao, A. Uschakov, R. M. McAllen, M. Rundgren, and D. Martelli. 2015. 'The median preoptic nucleus: front and centre for the regulation of body fluid, sodium, temperature, sleep and cardiovascular homeostasis', *Acta Physiol (Oxf).* 214: 8-32. doi: 10.1111/apha.12487. Epub 2015 Apr 1.

Mecawi Ade, S., S. G. Ruginsk, L. L. Elias, W. A. Varanda, and J. Antunes-Rodrigues. 2015. 'Neuroendocrine Regulation of Hydromineral Homeostasis', *Compr Physiol*, 5: 1465-516.

Miselis, R. R. 1982. 'The subfornical organ's neural connections and their role in water balance', *Peptides*, 3: 501-2.

Nation, H. L., M. Nicoleau, B. J. Kinsman, K. N. Browning, and S. D. Stocker. 2016. 'DREADD-induced activation of subfornical organ neurons stimulates thirst and salt appetite', *J Neurophysiol*, 115: 3123-9.

Oka, Y., M. Ye, and C. S. Zuker. 2015. 'Thirst driving and suppressing signals encoded by distinct neural populations in the brain', *Nature*, 520: 349-52.

Pirnik, Z., B. Mravec, and A. Kiss. 2004. 'Fos protein expression in mouse hypothalamic paraventricular (PVN) and supraoptic (SON) nuclei upon osmotic stimulus: colocalization with vasopressin, oxytocin, and tyrosine hydroxylase', *Neurochem Int*, 45: 597-607.

Ployngam, T., and J. P. Collister. 2007. 'An intact median preoptic nucleus is necessary for chronic angiotensin II-induced hypertension', *Brain Res*, 1162: 69-75.

Rettig, R., and A. K. Johnson. 1986. 'Aortic baroreceptor deafferentation diminishes saline-induced drinking in rats', *Brain Res*, 370: 29-37.

Shell, B., K. Faulk, and J. T. Cunningham. 2016. 'Neural Control of Blood Pressure in Chronic Intermittent Hypoxia', *Curr Hypertens Rep.*, 18: 19. doi: 10.1007/s11906-016-0627-8.

Smith, J. A., L. Wang, H. Hiller, C. T. Taylor, A. D. de Kloet, and E. G. Krause. 2014. 'Acute hypernatremia promotes anxiolysis and attenuates stress-induced activation of the hypothalamic-pituitary-adrenal axis in male mice', *Physiol Behav*, 136: 91-6.

Xu, Z., J. Torday, and J. Yao. 2003. 'Functional and anatomic relationship between cholinergic neurons in the median preoptic nucleus and the supraoptic cells', *Brain Res*, 964: 171-8.

CHAPTER III

CASPASE LESIONS OF PVN-PROJECTING MNPO NEURONS BLOCKS THE SUSTAINED COMPONENT OF CIH-INDUCED HYPERTENSION IN ADULT MALE RATS

Alexandria B. Marciante, Lei A. Wang, Joel T. Little and J. Thomas Cunningham

The University of North Texas

Health Science Center at Fort Worth

3500 Camp Bowie Blvd.

Fort Worth, TX 76107

**revisions requested by* Hypertension, 2019.

Abstract

Obstructive Sleep Apnea (OSA) is characterized by interrupted breathing that leads to cardiovascular sequelae including chronic hypertension that persists into waking hours. Previous studies have shown that chronic intermittent hypoxia (CIH) associated with OSA is sufficient to cause a sustained increase in blood pressure that involves the central nervous system. The median preoptic nucleus (MnPO) is an integrative forebrain region that contributes to blood pressure regulation and projects to the paraventricular nucleus (PVN). The PVN contains pre-autonomic neurons that project to regions in the hindbrain regulating sympathetic outflow. We hypothesized that pathway-specific lesions of the projection from the MnPO to the PVN would attenuate the sustained component of CIH-induced hypertension. Adult male Sprague-Dawley rats (250-300g) were anesthetized with isoflurane and stereotaxically injected bilaterally in the PVN with a retrograde Cre-containing AAV (AAV9.CMV.HI.eGFP-Cre.WPRE.SV40) and injected in the MnPO with caspase-3 (AAV5-flex-taCasp3-TEVp) or control virus (AAV5-hSyn-DIO-mCherry) before 7 days of CIH. During CIH, controls developed a diurnal hypertension that was blunted in rats with caspase lesions. Brain tissue processed for FosB immunohistochemistry showed decreased staining with caspase-induced lesions of MnPO and downstream autonomic-regulating nuclei. CIH significantly increased plasma advanced oxidative protein products levels in controls but this increase was blocked in caspase-lesioned rats. Caspase lesions of the MnPO significantly reduced changes in AT_1aR expression associated with CIH compared to CIH controls. The results indicate that PVN-projecting MnPO neurons play a significant role in blood pressure regulation in the development of persistent CIH-induced hypertension.

Introduction

Obstructive Sleep Apnea (OSA) is characterized by cessations in respiration that leads to reductions in airflow sufficient to cause significant arterial hypoxemia [1]. Reoxygenation following the obstructed respiration causes mechanical stress on the vasculature and inappropriately elevated sympathetic nerve activity (SNA) that leads to hypertension and other cardiovascular morbidities [2]. As OSA progresses, the hypertension observed during the intermittent hypoxic sleep cycle begins to manifest into the normoxic waking hours even during normal respiratory patterns. Subsequently, this can lead to the development of sustained systemic hypertension and cardiovascular disease [3, 4].

In order to fully understand the pathogenesis of hypertension associated with OSA, it is important to use a model that affords the study of its development. Chronic intermittent hypoxia (CIH) is a rodent model designed to mimic the intermittent hypoxemia experienced in OSA [5]. Exposure to CIH is sufficient to cause chronic hypertension and other cardiovascular comorbidities consistent with patients suffering from OSA [3, 4]. Hypertension associated with CIH is linked to several CNS mechanisms such as changes in chemoreceptor reflex sensitivity [6, 7],baroreceptor reflex function [8, 9], altered cardio-respiratory coupling [10], and catecholamine neurons in the nucleus of the solitary tract in the hindbrain [11]. However, additional mechanisms that include the forebrain may contribute to the sustained component of CIH hypertension, which occurs in normoxic components of the diurnal cycle.

During the initiation of CIH hypertension, chemoreceptors become sensitized stimulating the hindbrain, which increases sympathetic outflow and plasma renin

angiotensin [4, 12-15]. Our working hypothesis is that increased circulating angiotensin II (ANG II) activates the forebrain, thereby increasing sympathetic drive, creating a vicious cycle [4, 16]. Peripheral ANG II could be sensed by forebrain circumventricular organs (CVOs)—the subfornical organ (SFO) and organum vasculosum of the lamina terminalis (OVLT)—and relayed to downstream sympatho-regulatory regions [4].

The median preoptic nucleus (MnPO) is a region in the forebrain that lies in the anteroventral 3rd ventricle (AV3V) region and plays an important role in receiving and integrating afferent signals, as well as propagating information to the hypothalamus [17]. Neurons in the MnPO are involved in thermoregulation, osmoregulation, sleep, body fluid balance and cardiovascular and autonomic function [17-20]. The MnPO receives afferent signals from the CVOs that lie just dorsal and ventral to the MnPO on the AV3V, respectively, responding to fluctuations in plasma osmolality or other humoral factors, including ANG II through Angiotensin type 1a receptors (AT1aRs) [17, 19-22]. The MnPO has projections to the paraventricular nucleus (PVN) of the hypothalamus [4, 16, 17, 23]. The PVN contains pre-autonomic neurons involved in blood pressure regulation, SNA, and the hypothalamic-pituitary-adrenal axis [4, 5]. Through these efferent projections, the PVN can influence activity in sympatho-regulatory regions of the hindbrain, specifically the rostral ventrolateral medulla (RVLM) that regulates sympathetic outflow. Studies have shown that the MnPO influences sympathetic responses through a glutamatergic input to the PVN that connect to sympathetic vasoconstrictor pathways [17, 23] and that hypertension relies on elevated sympathetic tone and ongoing PVN neuronal activity [5, 16]. Along with other adaptations, this feed

forward loop could maintain increased sympathetic outflow, resulting in sustained hypertension [3, 16, 24-26].

Studies show that the MnPO can contribute to activation of sympathetic outflow [21, 23, 27]. Our work suggests that the MnPO is necessary for hypertension produced by CIH [28] and that the MnPO neurons that project to the PVN have an excitatory effect on PVN activity [5, 29]. The role and phenotype of the neurons involved in the MnPO-PVN pathway during CIH-induced hypertension, however, have not yet been fully elucidated.

We hypothesized that a pathway-specific lesion of the MnPO-PVN projections would attenuate the hypertension that persists into the normoxic period, or the sustained component, of CIH-induced hypertension. A caspase-3 lesion approach was used to selectively eliminate MnPO neurons projecting to PVN. Each rat was injected bilaterally in the PVN with a retrograde adeno-associated virus (rAAV) that contained Cre recombinase. This caused Cre expression in neurons projecting to PVN. The MnPO was injected with an adeno-associated virus (AAV) containing caspase-3 and TEV protease with a flex promotor, which would allow the constructs to be translated only in cells expressing Cre [30]. This approach results in apoptosis in MnPO neurons projecting to the PVN. The study used a 7-day CIH protocol to study the early events involved in the initiation and maintenance of CIH hypertension, without potential confounding effects of end-organ damage.

Methods

Animals

Adult male Sprague-Dawley rats (250-300 g bw, Charles River Laboratories) were individually housed in a temperature-controlled (25 °C) room on a 12:12 light/dark cycle

with light onset at 0700 h. Food and water was available *ad libitum* except on the day of perfusions. Rats were weighed daily and their food and water intake monitored. Experiments were performed according to the National Institute of Health *Guide for the Care and Use of Laboratory Animals* and approved by the University of North Texas Health Science Center Institutional Animal Care and Use Committee. Detailed methods and associated references are available in the online-only Supplement.

All rats were anesthetized with isoflurane (2-3%) and injected bilaterally in the PVN (-1.8 mm anterior, ±0.4 mm lateral, 7.6 mm ventral from bregma) [31] with retrograde AAV containing Cre (AAV9.CMV.HI.eGFP-Cre.WPRE.SV40; Penn State Vector Core). One set of rats was used for histology to phenotype PVN-projecting MnPO neurons. These brains were processed for vesicular glutamate transporter 2 (vGLUT2) *in situ* hybridization (ISH; n=5) and nitric oxide synthase 1 (NOS1) immunohistochemistry (IHC; n=4).

Other rats received caspase-3 (AAV5-flex-taCasp3-TEVp) or control (AAV5-hSyn-DIO-mCherry) virus (UNC VectorCore) injected into the MnPO (microinjector angled at 8º from medial to lateral, coordinates: 0.0 mm anterior, 0.9 mm lateral, 6.7 mm ventral from bregma) [28] in the same surgery. Rats injected with caspase-3 were also used for NOS1 IHC (n=4).

The other rats from five total cohorts injected with caspase-3 or control virus received aortic radio telemetry implants (n=54) to measure mean arterial pressure (MAP), systolic and diastolic arterial pressure (SAP and DAP, respectively), heart rate (HR) and body temperature (BT). Hemodynamic measurements were recorded for a 5-day baseline period before some of the rats were exposed to 7 days of CIH. On the

morning of day 8 following CIH, animals were anesthetized with inactin (100 mg/kg ip) and transcardially perfused. In three cohorts of rats (n=30), brains were harvested for FosB and AAV9-GFP IHC. In two additional cohorts of rats (n=24), brains were harvested for angiotensin type 1a receptor (AT_1aR) ISH. Additionally, methyl green staining was used to verify injection sites. At least 3 mL of blood was collected to assay advanced oxidative protein products (AOPP), plasma osmolality and hematocrit. Inclusion criteria for rats in data analysis were dependent on valid injection sites, quality of blood collection (for blood plasma analysis) and accurately recorded hemodynamic measurements.

Statistics

Student's t-tests were performed when comparing AAV9-GFP labeling in control versus caspase virus-injected rats, vGLUT2 and NOS1 analysis. One-way ANOVA was used for comparing plasma measurements (e.g. hematocrit, plasma osmolality, and AOPP levels), neuronal phenotyping dependent on CIH exposure and virus (e.g. FosB, AAV9-GFP labeling, and AT_1aR expression), body temperature, and body weight changes. Baseline data for telemetry recordings were analyzed for between group differences using two-way mixed effects ANOVA. The baseline measurements were averaged for each rat and within group differences for each condition were analyzed using separate repeated measures (RM) ANOVA followed by Holm-Sidak *post hoc* test to compare against baseline conditions. Effects of CIH on MAP, SAP, DAP, HR, and BT during the dark phase (1800-0600 h) and during the 8 h CIH exposure period (0800-1600 h) were analyzed separately by two-way repeated measures ANOVA. *Post hoc* analysis on between group differences was performed using the Student Newman-Keuls (SNK) test.

Statistical significance is defined at an α level of 0.05 and exact p-values are reported. Values are reported as mean ± SEM. All statistics were performed using SigmaPlot.v.12.0 (Systat Software, San Jose, CA).

Results

MnPO neurons projecting to the PVN are excitatory

In situ hybridization experiments for vGLUT2 were performed to determine if the AAV-retrograde virus injected into the PVN was labeling putative excitatory MnPO neurons (Figure 1B). The results indicate that 89.3 ± 1.4% of MnPO neurons (n=5, 2-3 MnPO sections per rat) that project to the PVN (green) are glutamatergic (red).

Immunohistochemistry was performed on a separate set of sections containing the MnPO (n=4, 2-3 MnPO sections per rat) for NOS1 to further identify the phenotype of MnPO neurons that project to the PVN (Figure 1C). The results indicate that 42.3 ± 3.0% of MnPO neurons that project to the PVN (green) are also NOS1 positive (red). In rats with caspase-3 lesions (n=4, 2-3 MnPO sections per rat), the number of NOS1 positive cells significantly decreased by 30% to 30.1 ± 2.5% ($t(6) = -3.112$, $p = 0.021$, Student's t-test). Experiments with glia fibrillary acidic protein staining suggest that the AAV mediated caspase-3 apoptosis does not affect astrocytes (Figure S1).

Injection Verification

Immunohistochemistry was performed after the 7-day CIH protocol for AAV-retrograde to verify the injection sites and caspase lesions (n=6 for each group). The PVN was analyzed to verify bilateral rAAV injections and the MnPO was assessed to verify the caspase lesions (Figure 2B). Additionally, methyl green staining was used to identify injector tracks in the MnPO and PVN to further verify successful microinjections

(Figure 2A). Overall, the numbers of GFP-positive neurons in the MnPO of caspase-injected rats was significantly reduced compared to rats injected with control virus (caspase 106.3 $\pm$ 8.0; control 269.6 $\pm$ 8.3; Figure 2C, $t(10) = 33.303$, $p < 0.001$, Student's t-test).

Any rats with unsuccessful rAAV bilateral PVN or MnPO injection were eliminated from analysis (n=11). Rats exposed to CIH with successful rAAV bilateral PVN but unsuccessful MnPO injection of caspase, referred to as the 'miss' group, were used as an additional control only in hemodynamic and AOPP analyses (n=6). Rats with successful rAAV injections, but instrumented with faulty telemetry or inaccurately recorded hemodynamics were only included in neuroanatomy studies (n=6).

Caspase-induced inhibition of PVN-projecting MnPO neurons blocks CIH increases in MAP

To determine if CIH-induced hypertension could be blunted by selectively eliminating MnPO neurons that project to the PVN, hemodynamic measurements were assessed after a 5-day baseline period and 7 days of CIH for each rat in each group (n=6-9). During the baseline period, there were no significant differences among treatment groups for baseline MAP, SAP, DAP, HR, or BT (Table S1). This suggests MnPO neurons that project to the PVN do not significantly contribute to basal MAP, SAP, DAP or HR.

During CIH exposure from 0800 to 1600 h, the average daily changes in MAP varied significantly among the treatment groups (Figure 3A, $F(4, 32) = 5.293$, $p = 0.002$, two-way RM ANOVA). During the normoxic dark phase (1800 to 0600 h), significant differences were also detected between treatment groups ($F(4, 32) = 7.313$, $p < 0.001$,

two-way RM ANOVA). There was also a statistically significant interaction between day of exposure and treatment during the normoxic dark phase ($F(28, 295) = 1.713$, $p = 0.018$, two-way RM ANOVA).

During the CIH period, rats exposed to CIH and injected with the control virus (CTRL CIH) had significantly increased MAP compared to normoxic controls (vs CTRL NORM: $p = 0.013$, vs CASP NORM: $p = 0.009$; SNK; Figure 4A). This is also true for the 'miss' group exposed to CIH (CASP CIH MISS) compared to normoxic controls (vs CTRL NORM: $p = 0.020$, vs CASP NORM: $p = 0.026$; SNK), but not the CIH exposed rats injected successfully in the MnPO with caspase (CASP CIH). Similarly, MAP during the normoxic dark period continues to be significantly elevated in the CTRL CIH group (vs CTRL NORM: $p = 0.001$, vs CASP NORM: $p = 0.005$; SNK) and CASP CIH MISS (vs CTRL NORM: $p = 0.013$, vs CASP NORM: $p = 0.018$; SNK) compared to normoxic controls. With successful caspase injections, however, CIH-exposed rats did not display this same increase in MAP (CASP CIH vs CTRL CIH: $p = 0.002$, vs CASP CIH MISS: $p = 0.023$; SNK), and maintained MAP comparable to normoxic controls (CASP CIH vs CTRL NORM: $p = 0.915$, vs CASP NORM: $p = 0.915$; SNK). These results indicate that diurnal increases in MAP produced by CIH in the control virus-injected group and the caspase 'miss' group, was significantly blocked by successful caspase lesions in the MnPO neurons that project to the PVN.

Related to this, systolic and diastolic arterial pressure (SAP and DAP, respectively) were also analyzed for the CIH period and normoxic dark period for each group. Exposure to CIH and treatment significantly affected SAP (Figure 3B and 4B) and DAP (Figure 3C and 4C). Significant differences were found between groups for

changes in SAP during the CIH period ($F(4, 32) = 4.500$, $p = 0.005$, two-way RM ANOVA) and dark period ($F(4, 32) = 5.834$, $p = 0.001$, two-way RM ANOVA). Results were consistent to those related to changes in MAP during the CIH period (CTRL CIH vs CTRL NORM: $p = 0.032$, vs CASP NORM: $p = 0.011$; CASP CIH MISS vs CASP NORM: $p = 0.026$; SNK) and dark period (CTRL CIH vs CTRL NORM: $p = 0.005$, vs CASP NORM: $p = 0.010$, vs CASP CIH: $p = 0.006$; SNK).

Significant differences were found between groups for changes in DAP during the CIH period ($F(4, 32) = 3.737$, $p = 0.013$, two-way RM ANOVA) and dark period ($F(4, 32) = 4.513$, $p = 0.005$, two-way RM ANOVA). This was due to significant differences in DAP changes during the dark period between CTRL CIH vs CTRL NORM: $p = 0.017$, vs CASP NORM: $p = 0.044$, and vs CASP CIH: $p = 0.024$; SNK. When analyzing overall average change in DAP, there was a significant effect of treatment between groups during the CIH period ($F(4, 32) = 42.035$, $p < 0.001$, one-way ANOVA) and normoxic dark period ($F(4, 32) = 48.214$, $p < 0.001$, one-way ANOVA). These results were consistent with results from SAP. This was due to significant increases in DAP during CIH exposure (CTRL CIH, CASP CIH, CASP CIH MISS: $p < 0.010$ for each group compared to normoxic controls, SNK). Although DAP was significantly augmented compared to controls, this increase was significantly decreased in CASP CIH vs CTRL CIH and vs CASP CIH MISS ($p < 0.001$, SNK). Increases in SAP were maintained into the dark period only by the CTRL CIH and CASP CIH MISS groups compared to normoxic controls and CASP CIH ($p < 0.001$ for each group, SNK). Increases in DAP were maintained into the dark period only by the CTRL CIH and CASP CIH MISS groups compared to normoxic controls and CASP CIH ($p < 0.001$ for each group, SNK).

No significant differences were found among any of the groups for daily changes in HR or BT (Figure S2A & S2B), however, there were significant overall average changes (Figure S3A & S3B).

CIH exposure significantly increases oxidative stress but is blocked by caspase lesions

As previously reported [32], 7 days of CIH exposure significantly increased circulating AOPP (uM) levels (Figure 4D, $F(4, 35) = 8.337$, $p < 0.001$, one-way ANOVA). However, this was only the case for CIH-exposed rats injected with the control virus (CTRL CIH vs CTRL NORM: $p = 0.005$, vs CASP NORM: $p = 0.005$; SNK) and those that did not have successful caspase transfection (CASP CIH MISS vs CTRL NORM: $p = 0.002$, vs CASP NORM: $p = 0.001$; SNK). The increase in AOPP due to CIH exposure, was blocked in the CIH-exposed caspase lesion group (CASP CIH vs CTRL CIH: $p = 0.003$, vs CASP CIH MISS: $p < 0.001$; SNK) to levels comparable to normoxic controls (CASP CIH vs CTRL NORM: $p = 0.681$, vs CASP NORM: $p = 0.655$; SNK).

CIH exposure significantly increased hematocrit, however, rats with successful caspase lesions had hematocrit levels comparable to normoxic control rats (CTRL NORM: 43.1 $\pm$ 0.4%, CASP NORM: 42.8 $\pm$ 0.5%, CTRL CIH: 45.4 $\pm$ 0.3%, CASP CIH: 43.2 $\pm$ 0.4%, CASP CIH MISS: 45.7 $\pm$ 0.9%). There were no significant differences in osmolality (CTRL NORM: 289.3 $\pm$ 1.6 mOsmol/l, CASP NORM: 289.5 $\pm$ 1.9 mOsmol/l, CTRL CIH: 292.9 $\pm$ 1.1 mOsmol/l, CASP CIH: 289.7 $\pm$ 1.4 mOsmol/l, CASP CIH MISS: 293.5 $\pm$ 2.5 mOsmol/l).

Caspase lesions influence FosB staining

Caspase lesions of MnPO influenced FosB staining associated with CIH in a region specific manner (Figure 5B). In the SFO, FosB staining associated by CIH was not influenced by caspase lesion of MnPO-PVN neurons, however, FosB staining in the SFO was influenced by the 7-day exposure ($F(3, 20) = 9.821$, $p < 0.001$, one-way ANOVA). There was a trend for an effect of CIH on FosB staining in the OVLT ($F(3, 20) = 3.301$, $p = 0.041$, one-way ANOVA), however, SNK did not detect significance between groups.

In MnPO, CIH significantly increased FosB staining in rats injected with the control vector and this increase was blocked by the caspase lesions (Figure 5A, $F(3, 20) = 5.606$, $p = 0.006$, one-way ANOVA). FosB staining in the MnPO of the CTRL CIH group was significantly increased as compared to the other groups (Figure 6B; vs. CTRL NORM, $p = 0.007$; vs. CASP NORM, $p = 0.008$, SNK and vs. CASP CIH, $p = 0.018$, all SNK). There were no significant differences between the CASP CIH group compared to either normoxic control group (vs. CTRL NORM, $p = 0.829$; vs. CASP NORM, $p = 0.728$) groups. There was no effect of CIH or virus on FosB expression in the SON (Figure 5B, $F(3, 20) = 1.497$, $p = 0.246$, one-way ANOVA).

Caspase lesions attenuated FosB expression in the PVN associated with CIH. In PVN, FosB staining was significantly affected by CIH and caspase lesions ($F(3, 20) = 7.579$, $p = 0.001$, one-way ANOVA). The CTRL CIH group had significantly elevated FosB expression in the PVN compared to the CTRL NORM ($p = 0.010$, SNK), CASP NORM ($p = 0.001$, SNK), and CASP CIH ($p = 0.015$, SNK) groups. Subregions of the PVN were also analyzed (Figure 5C). There was a significant effect of CIH and virus on FosB expression in the medial parvocellular (MP) PVN neurons ($F(3, 20) = 13.229$, $p <$

0.001, one-way ANOVA). The CTRL CIH group had significantly elevated FosB expression in only the MP of the PVN compared to the CTRL NORM ($p < 0.001$, SNK), CASP NORM ($p < 0.001$, SNK), and CASP CIH ($p = 0.002$, SNK) groups.

The RVLM was also analyzed for FosB expression as it is a major regulatory region for autonomic function. CIH and caspase lesions also had a significant effect on FosB expression in the RVLM (Figure 5B, $F(3, 20) = 9.691$, $p < 0.001$, one-way ANOVA). FosB expression was significantly elevated in the CTRL CIH group in the RVLM compared to the CTRL NORM ($p = 0.001$, SNK) and CASP NORM ($p < 0.001$, SNK) groups. This increase was again blocked by caspase lesions of MnPO in the CASP CIH ($p = 0.005$, SNK) group. Rats that did not have successful injections into the MnPO or PVN were excluded from anatomy studies.

Caspase-induced inhibition knocks down AT_1aR expression in CIH-exposed rats

Expression of AT_1aR in the MnPO after CIH was studied in two cohorts of rats that were separate from those used for FosB immunohistochemistry (n=3-5, 2-4 MnPO sections per rat). As previously reported, CIH increased mRNA for the AT_1aR in the MnPO. Control virus-injected rats exposed to CIH had a significantly increased AT_1aR expression in the MnPO compared to normoxic controls (CTRL NORM: $p < 0.001$; CASP NORM: $p < 0.001$) and compared to the caspase-injected group exposed to CIH ($p < 0.001$, SNK). This increase in AT_1aR message in the MnPO associated with CIH was significantly blocked by caspase-lesions of MnPO-PVN neurons (Figure 5E and 5F, $F(3, 10) = 31.336$, $p < 0.001$, one-way ANOVA).

Discussion

These studies tested the role of MnPO neurons that project to the PVN in the regulation of the sustained component of CIH-induced hypertension. The MnPO to PVN projection was studied in this context based on previous studies conducted by our lab and others. The MnPO neurons that project to the PVN have an excitatory effect on PVN activity and elevated MAP relies on elevated sympathetic tone, as well as ongoing PVN neuronal activity [5, 16]. However, studies had not yet been conducted to demonstrate the role of the MnPO to PVN projection in the development of hypertension associated with CIH. Therefore, we used caspase-3 to selectively lesion the MnPO neurons that project to the PVN and were able to effectively block the sustained component of CIH hypertension. Associated with this, rats injected with the caspase-3 virus in the MnPO and exposed to CIH also had circulating oxidative by-products no different from the normoxic controls levels. Furthermore, we were able to identify the phenotypes of these neurons implicated in driving excitatory signaling from the forebrain to the hindbrain.

After 7 days of CIH, transcription factor FosB is significantly increased in the MnPO [25]. FosB is part of the activator protein-1 (AP-1) complex that regulates gene expression [33]. Blocking the transcriptional effects of FosB with a dominant negative inhibitory construct injected in the MnPO attenuated the sustained component of CIH hypertension [28]. Our lab has also shown that CIH significantly increases AT_1aR mRNA expression in the MnPO and by using shRNA knockdown of AT_1aR, we were able to effectively attenuate the sustained component of hypertension as well. However, it has not yet fully elucidated which MnPO neuronal phenotypes contribute to CIH hypertension. These results indicate that PVN projecting MnPO neurons are necessary for CIH hypertension.

Caspase-3 was the preferred viral construct over the diphtheria toxin A or tBid because of its higher efficacy in committing a cell to apoptosis and killing adult neurons *in vivo*, while minimizing toxicity to adjacent non-Cre-expressing cells [30]. There were no changes in GFAP expression (Online Supplement Data), indicating the AAV5-caspase-3 flex viral construct induced apoptosis specific to neurons.

In the current study, the phenotype of PVN-projecting MnPO neurons was characterized. Of roughly 270 AAV9-GFP positive MnPO neurons, about 90% of these neurons were glutamatergic indicating they are involved in excitatory signaling. Additionally, about 44% of PVN-projecting MnPO neurons were positive for NOS1. This is important as previous studies have indicated a potential role for NOS1 during CIH exposure [28]. When caspase-3 was used to trigger cell-autonomous apoptosis of MnPO neurons projecting to the PVN, AAV9-GFP positive MnPO neurons was significantly reduced by approximately 60% and NOS1-expressing neurons by 25%. These initial findings are significant when considering the results for the FosB and AT_1aR studies.

The 7-day CIH protocol used in previous studies [25, 28, 34], significantly increased FosB-positive nuclei in the SFO, MnPO, PVN and RVLM. However, rats in the CASP CIH group had attenuated FosB expression comparable to that in normoxic control groups in the MnPO. Similar effects were seen in PVN and RVLM. Caspase lesion also influences AT_1aR expression in the MnPO. Both CASP groups had about 60% less AAV9-GFP expression in the MnPO while the numbers of single-labeled AT_1aR neurons was comparable to CTRL NORM. However, when comparing AT_1aR expression co-localization with AAV9-GFP, the percentage in CTRL NORM group was significantly greater than the CASP groups, indicating that caspase-3 apoptosis targets cells

expressing AT_1aR. Additionally, after 7 days of CIH exposure, the CTRL CIH group had significantly increased AT_1aR expression in AAV9-GFP neurons. These results suggest that after 7 days of CIH exposure, AT_1aR expression significantly increases in MnPO neurons, specifically that project to the PVN.

Over the 7-day CIH protocol, CIH exposure significantly increased MAP in the CTRL CIH and CASP CIH MISS groups compared to nomoxic controls. Interestingly, this significant increase was not observed for the CASP CIH group on a day-to-day basis, indicating that PVN-projecting MnPO neurons contribute to CIH hypertension during both the intermittent hypoxia and the sustained, normoxic phase. SAP and DAP were also analyzed to better assess cardiovascular health associated with changes in CIH [35]. This pattern was observed for SAP and DAP as well.

Similarly, when analyzing AOPP, the CTRL CIH and CASP CIH MISS groups had significantly increased plasma concentrations compared to normoxic controls. The CIH-induced AOPP increase was blocked in the CASP CIH group and comparable to concentrations observed in normoxic controls. These results suggest that oxidative stress associated with CIH hypertension also was mitigated by lesioning PVN-projecting MNPO neurons.

Related to this, caspase-3 mediated apoptosis of PVN-projecting MnPO neurons decreased putative excitatory neurons that also expressed NOS1 and AT_1aR. Because of the decrease in signaling from the MnPO to pre-autonomic centers in the PVN, there may have been a reduced stimulus to areas in the hindbrain, i.e. RVLM—as observed with FosB expression—resulting in reduced sympathetic outflow. Thus, the observed decrease in the sustained component of CIH-induced hypertension and the blocked

CIH-induced increase in AOPP concentration. This indicates that CIH hypertension and its associated increase in oxidative stress are dependent of the integrity of PVN-projecting MnPO neurons. Therefore, it can speculated that the presence of functional AT_1aRs in MnPO may be a key component in the brain RAS activation and that excitatory signaling to the PVN are necessary for CIH hypertension and increased oxidative stress.

Interestingly, we observed CIH may have an effect on thermoregulation (Supplement Data). The glutamatergic neurons in the MnPO have been shown to be involved in thermoregulation [36, 37]. Body heat of groups exposed to CIH had a decreasing trend during the CIH period. And, although not a large increase, CIH exposure caused body heat to be significantly elevated from baseline compared to both of the NORM groups during the normoxic period. Future studies should be focused on understanding how CIH could potentially effect body temperature in the context of MnPO neuron regulation.

This study highlights the critical role of the MnPO neurons that project to the PVN in the sustained component of CIH-induced hypertension. Many studies have indicated the importance and necessity of the MnPO in the development of hypertension [21, 25, 27, 28, 34] as well as how the PVN contributes to increased sympathetic outflow [5, 16]. These studies effectively show how the MnPO to PVN projection and specific neuronal phenotypes may contribute to the sustained, diurnal increases in blood pressure due to CIH.

Perspectives

OSA is a disease that can go unnoticed in patients for extensive lengths of time, until secondary symptoms become more prominent. Despite efforts in studying OSA, the pathogenesis of this disease is still not fully understood. Early in OSA pathophysiology, hypertension and oxidative stress can be identified [3]. The 7-day CIH model used in these studies allows us to examine early adaptations and events that could contribute to the development of neurogenic hypertension. Previous studies have identified several mechanisms that could contribute to CIH hypertension, such as long-term facilitation, chemoreflex sensitivity, baroreflex desensitization, and the peripheral RAS [4, 6, 12, 16, 24, 38]. Other recent studies suggest that the brain RAS that may also contribute to increased sympathetic outflow [4, 34, 39]. The current study not only supports a role for the brain RAS in this form of hypertension but also uses a novel approach that identifies a projection-specific mechanism in the forebrain that connects the brain RAS to downstream autonomic regulatory pathways.

Acknowledgments

The authors would like to acknowledge and thank the technical assistance of M. Bachelor and J. Kiehlbauch. The AAV-flex-taCasp3-TEVp was a gift from Drs. N. Shah and J. Wells (Addgene plasmid #45580)

Sources of Funding

This work was supported by NIH grants P01 HL088052 and T32 AG020494.

Conflict of Interest/Disclosures

Authors report no conflict of interest.

Novelty and Significance

What is new?

- MnPO neurons that project to the PVN are largely excitatory. Selective lesions of these phenotypes (vGLUT2, NOS1, and/or AT_1aR-positive) interrupts the drive for sustained hypertension.
- Caspase-3 lesions in MnPO neurons that project to the PVN blocks the sustained component of CIH hypertension, causing a reduction in circulating oxidative protein products.

What is relevant?

- The hypothalamus has been extensively studied as a major area of autonomic regulation. Investigators have hypothesized how the sustained component of hypertension in CIH associated with OSA, with ANG II being the peptide hormone that potentiates increased sympathetic activity. However, it had not been fully elucidated how the hypothalamus bridges ANG II activation in the forebrain to mechanisms that drive blood pressure through the hindbrain. In these experiments, we show that this is a mechanism dependent on MnPO neurons that project to the PVN.

Summary

Caspase-3 lesions of MnPO neurons projecting to the PVN blocks the sustained component of CIH hypertension, returning blood pressure to normoxic control levels and effectively reducing oxidative by-product. These studies provide evidence that the MnPO to PVN projection provides the bridge in how the forebrain may be exacerbating

the pathophysiology in CIH and potentiates sustained hypertension associated with OSA.

Figure 1. *MnPO neurons that project to the PVN are mainly glutamatergic and NOS1-positive*. A, Representative illustration of a coronal section from a rat outlining the median preoptic nucleus (MnPO, adapted Paxinos, et al. [40]). B, From left to right, representative single channel AAV9-GFP labeling, vGLUT 2 labeling, and merged image of vGLUT2 *in situ* hybridization (red) and AAV9-GFP retrograde labeling (green) in the MnPO. C, From left to right, representative single-channel AAV9-GFP labeling, NOS1 labeling and merged image of NOS1 staining (red) and AAV9-GFP retrograde labeling (green) in the MnPO. White arrows indicate double-labeled neurons. Anterior commissure, ac. Scale bar, 100 µM.

Figure 1.

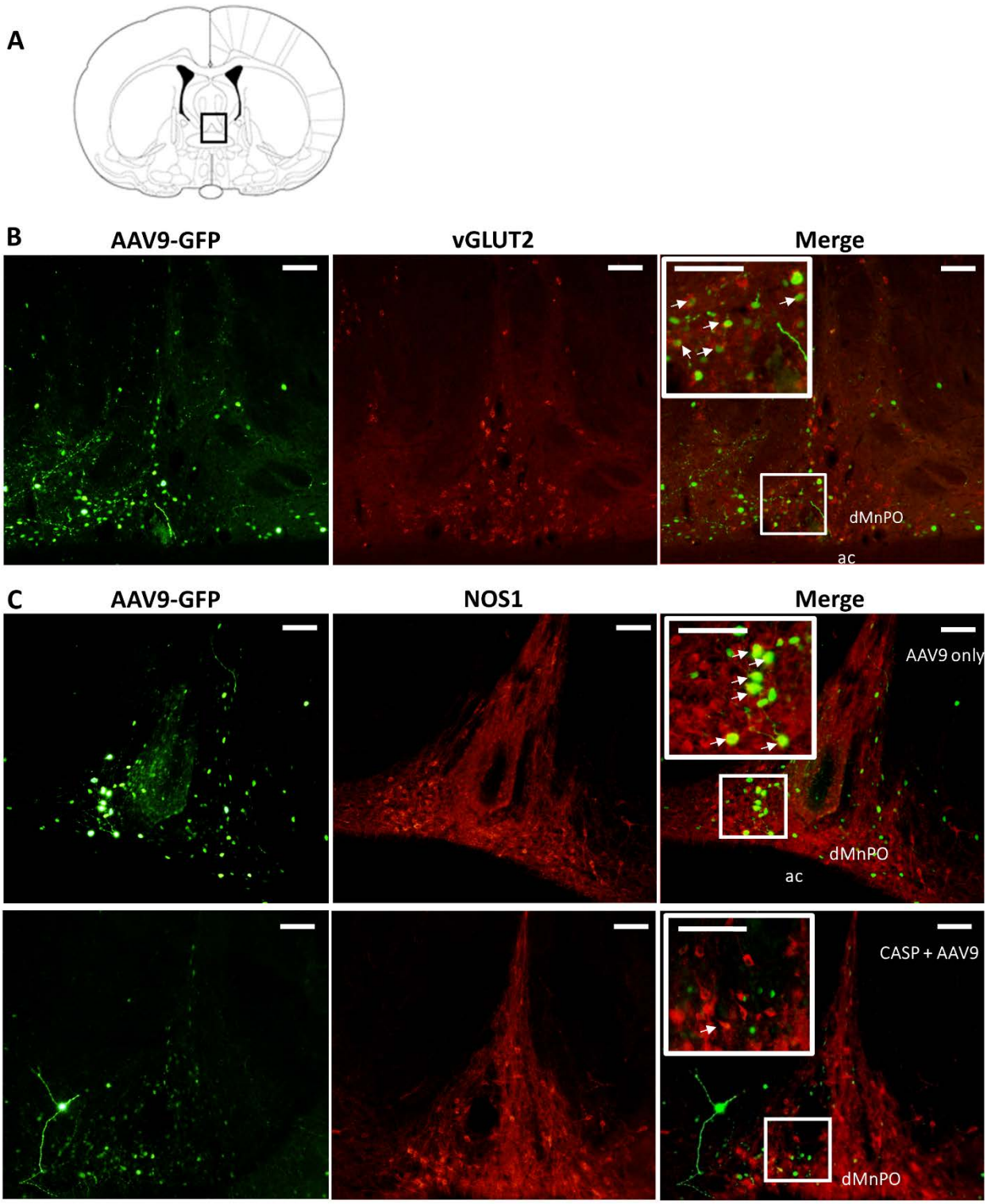
A
B
AAV9-GFP
vGLUT2
Merge
dMnPO
ac
C
AAV9-GFP
NOS1
Merge
AAV9 only
dMnPO
ac
CASP + AAV9
dMnPO

Figure 2. *Caspase lesions significantly decreases retrograde labeling in the MnPO.* A, Representative images of methyl green staining in the median preoptic nucleus (MnPO, left) and paraventricular nucleus (PVN, right); injection sites indicated by the black arrow. B, Representative images of rAAV retrograde labeling in the MnPO (left) and PVN (right) of animals injected with the control (CTRL, top row) or caspase-3 (CASP, bottom row) virus. C, Rats injected with the CASP virus had significantly less rAAV retrograde labeling in the MnPO than CTRLs (*$p < 0.050$ compared to CTRL). Scale bar, 100 µM. Data are expressed as mean + SEM.

Figure 2.

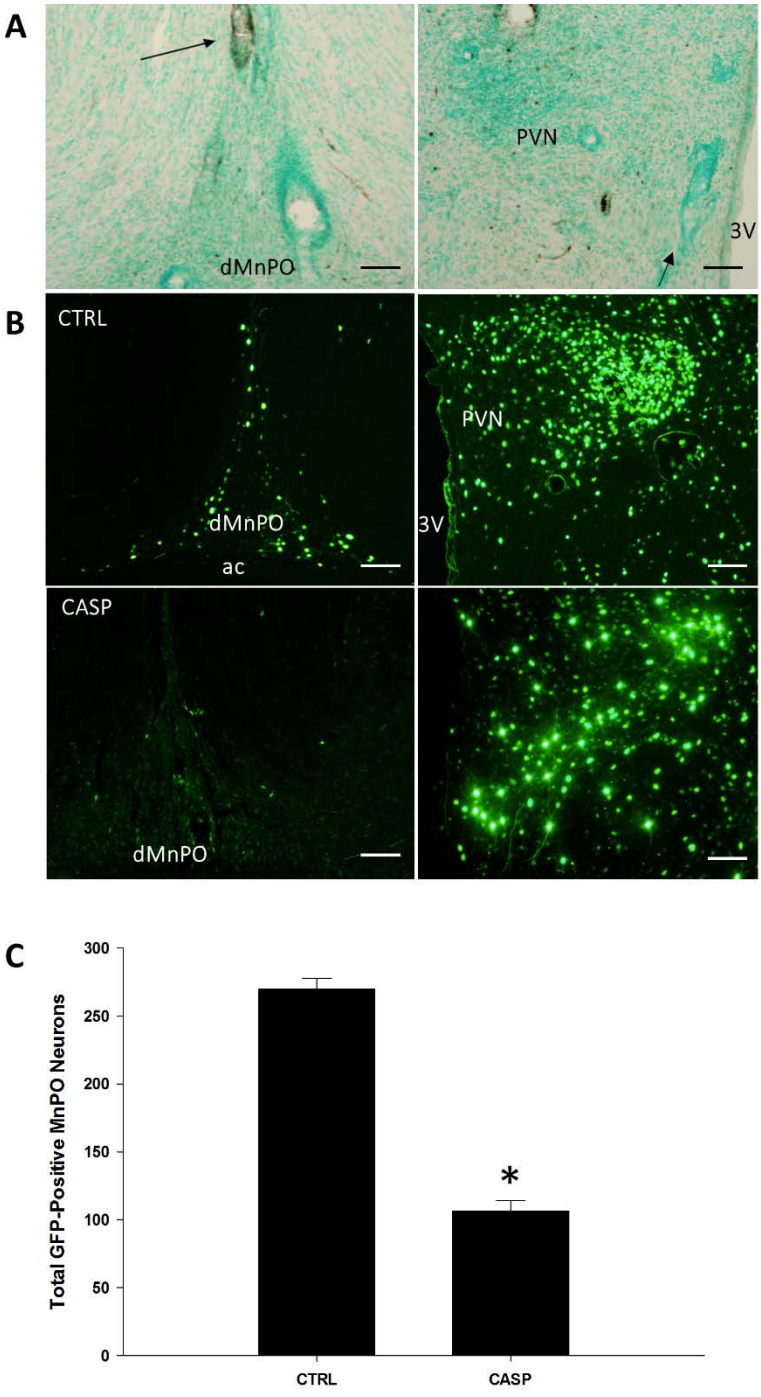
A
dMnPO
PVN
3V
B
CTRL
dMnPO
ac
PVN
3V
CASP
dMnPO
C
Total GFP-Positive MnPO Neurons
300
250
200
150
100
50
0
*
CTRL
CASP

Figure 3. *CIH-induced diurnal hypertension was significantly attenuated with caspase lesions of PVN-projecting MnPO neurons.* Left column, chronic intermittent hypoxia (CIH) period; right column, dark period (1800-0600). Average daily change in mean arterial pressure (A, MAP), systolic arterial pressure (B, SAP), and diastolic arterial pressure (C, DAP) from baseline period. Control-injected rats exposed to normoxia (CTRL NORM) or hypoxia (CTRL CIH); caspase-injected rats exposed to normoxia (CASP NORM), hypoxia (CASP CIH), or misses (CASP CIH MISS); *$p < 0.050$, CASP CIH MISS compared to CTRL NORM and CASP NORM; **$p < 0.050$, CTRL CIH compared to CASP NORM; ***$p < 0.050$, CTRL CIH or CASP CIH MISS compared to CTRL NORM, CASP NORM, and CASP CIH. Data are expressed as mean $\pm$ SEM.

Figure 3.

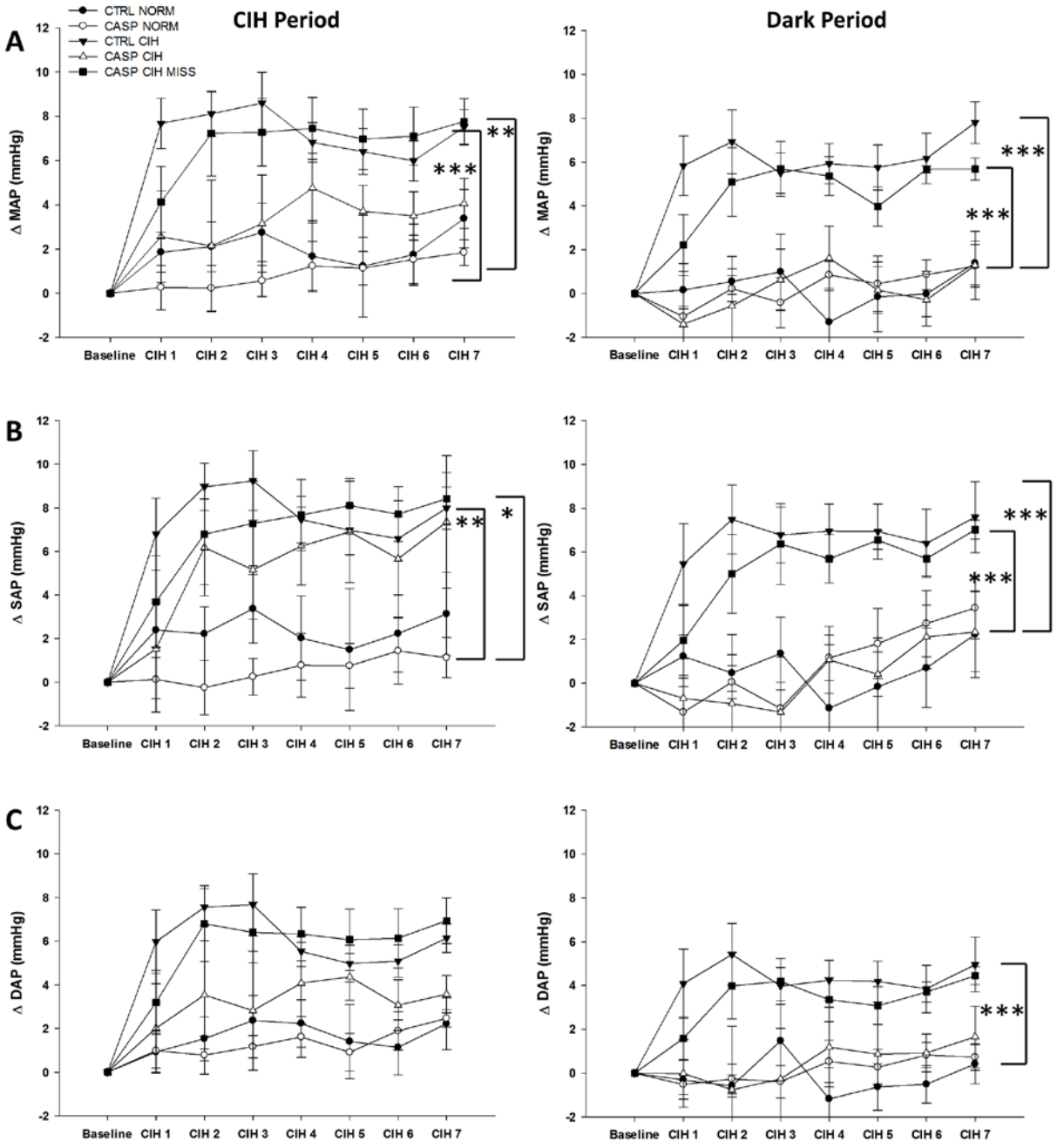
A
B
C
CTRL NORM
CASP NORM
CTRL CIH
CASP CIH
CASP CIH MISS
CIH Period
Dark Period
Δ MAP (mmHg)
Δ SAP (mmHg)
Δ DAP (mmHg)
Baseline
CIH 1
CIH 2
CIH 3
CIH 4
CIH 5
CIH 6
CIH 7
*
**
***

Figure 4. *Overall increases in arterial pressure and plasma oxidative protein concentration induced by CIH was blocked with caspase lesions of PVN-projecting MnPO neurons.* Overall change in mean arterial pressure (A, MAP), systolic arterial pressure (B, SAP) and diastolic arterial pressure (C, DAP). D, CIH increases in plasma advanced oxidative protein product (AOPP) concentration is blocked by caspase lesions of PVN-projecting MnPO neurons. Control-injected rats exposed to normoxia (CTRL NORM) or hypoxia (CTRL CIH); caspase-injected rats exposed to normoxia (CASP NORM), hypoxia (CASP CIH), or misses (CASP CIH MISS); **p < 0.050, compared to CTRL NORM and CASP NORM; ***p < 0.050, compared to CTRL NORM, CASP NORM and CASP CIH during the CIH period; #p < 0.050, compared to CTRL NORM, CASP NORM and CASP CIH during the dark period. *p < 0.050, AOPP compared to CTRL NORM, CASP NORM and CASP CIH. Data are expressed as mean + SEM.

Figure 4.

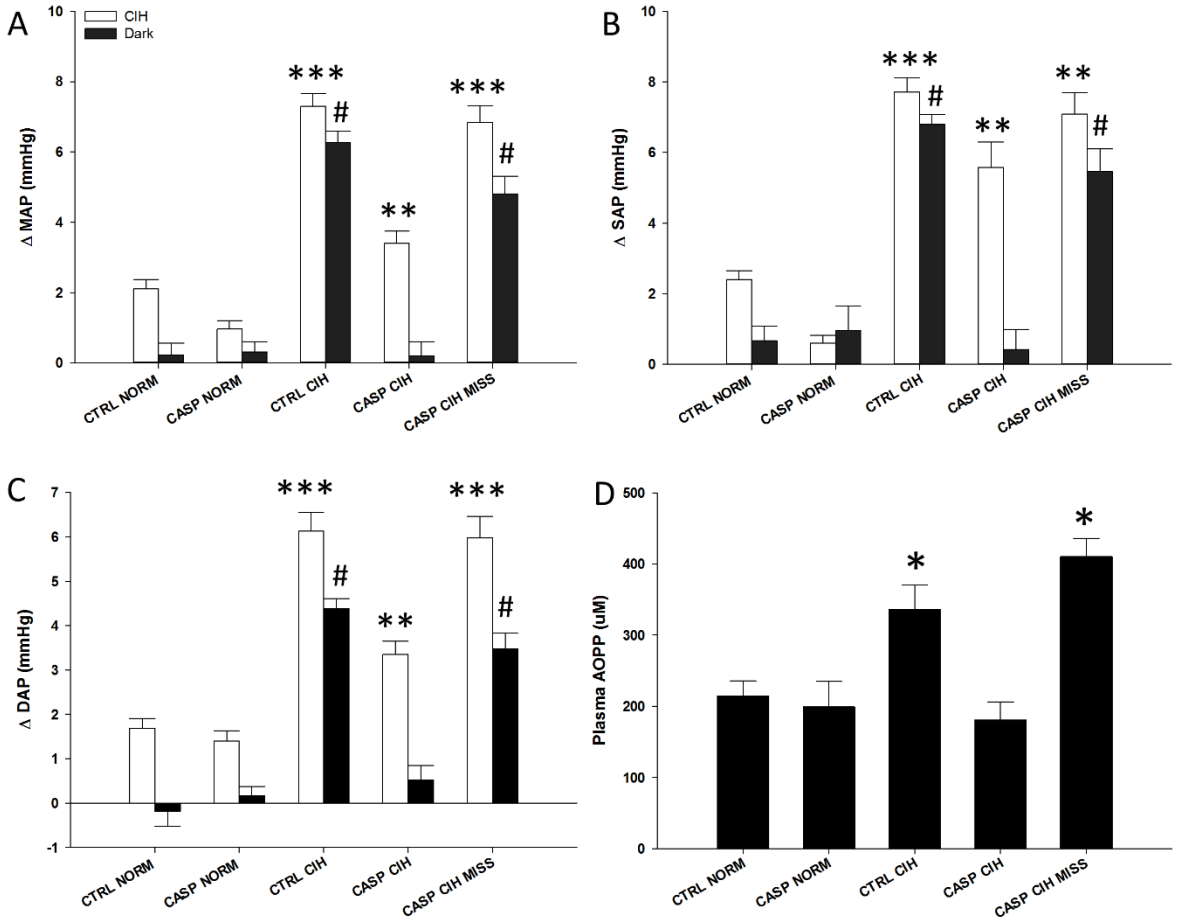
A
CIH
Dark
Δ MAP (mmHg)
B
Δ SAP (mmHg)
C
Δ DAP (mmHg)
D
Plasma AOPP (uM)
CTRL NORM
CASP NORM
CTRL CIH
CASP CIH
CASP CIH MISS

Figure 5. *Caspase lesions of PVN-projecting MnPO neurons blocks CIH-induced increases in FosB and AT_1aR expression.* A, Representative images of FosB staining in the dorsal median preoptic nucleus (dMnPO) of control-injected rats exposed to normoxia (CTRL NORM) or hypoxia (CTRL CIH) and caspase-injected rats exposed to normoxia (CASP NORM) or hypoxia (CASP CIH); scale bar, 100 µM. B, Average FosB positive nuclei in regions upstream (OVLT, SFO) and downstream (SON, PVN, RVLM) of the MnPO; organum vasculosum of the lamina terminalis, OVLT; subfornical organ, SFO; supraoptic nucleus, SON; rostral ventral lateral medulla, RVLM. C, Average FosB positive nuclei in PVN subregions; posterior magnocellular, PM; dorsal parvocellular, DP; medial parvocellular, MP; ventral lateral parvocellular, vlp. D, Representative images AT_1aR (white) expression and rAAV retrograde labeling (green) in the MnPO; single-labeled AT_1aR neurons, purple arrows; single-labeled GFP neurons, yellow arrows; double-labeled AT_1aR and GFP neurons, white arrows; scale bar, 25 µM. E, Proportion of average single- or double-labeled AT_1aR or GFP MnPO neurons. F, Percent double-labeled AT_1aR and GFP MnPO neurons; ***$p < 0.050$, compared to CTRL NORM, CASP NORM and CASP CIH. **$p < 0.050$, compared to CTRL NORM and CASP NORM; ***$p < 0.050$, compared to CTRL NORM, CASP NORM and CASP CIH. Data are expressed as mean + SEM.

Figure 5.

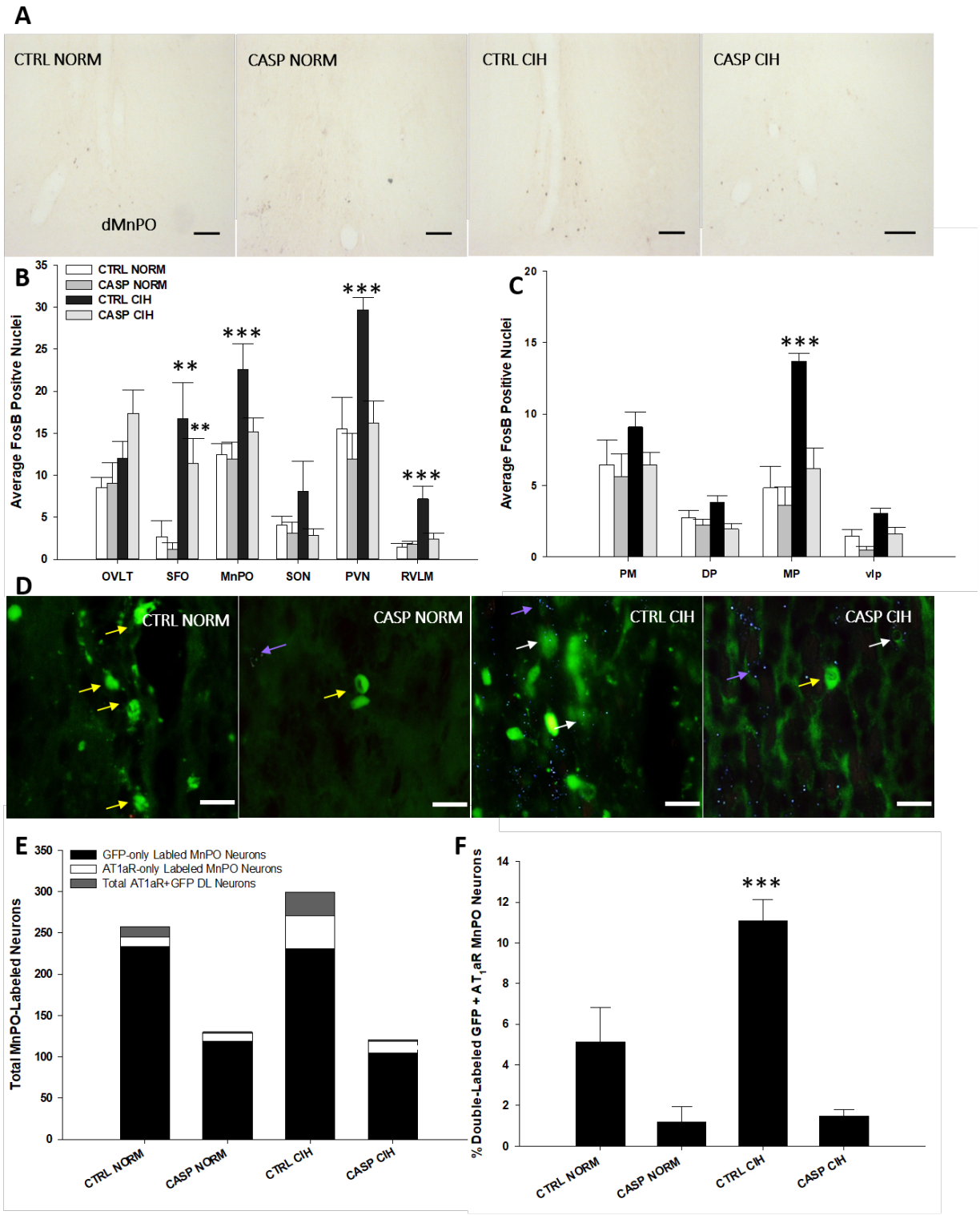
A
CTRL NORM
CASP NORM
CTRL CIH
CASP CIH
dMnPO
B
CTRL NORM
CASP NORM
CTRL CIH
CASP CIH
Average FosB Positive Nuclei
OVLT
SFO
MnPO
SON
PVN
RVLM
C
Average FosB Positive Nuclei
PM
DP
MP
vlp
D
CTRL NORM
CASP NORM
CTRL CIH
CASP CIH
E
GFP-only Labled MnPO Neurons
AT1aR-only Labeled MnPO Neurons
Total AT1aR+GFP DL Neurons
Total MnPO-Labeled Neurons
CTRL NORM
CASP NORM
CTRL CIH
CASP CIH
F
% Double-Labeled GFP + AT1aR MnPO Neurons
CTRL NORM
CASP NORM
CTRL CIH
CASP CIH

References

1. Zhang W, Si LY. Obstructive sleep apnea syndrome (OSAS) and hypertension: pathogenic mechanisms and possible therapeutic approaches. Ups J Med Sci 2012;117:370-382.

2. Jean-Louis G, Zizi F, Clark LT, Brown CD, McFarlane SI. Obstructive sleep apnea and cardiovascular disease: role of the metabolic syndrome and its components. J Clin Sleep Med 2008;4:261-272.

3. Dempsey JA, Veasey SC, Morgan BJ, O'Donnell CP. Pathophysiology of sleep apnea. Physiol Rev 2010;90:47-112.

4. Shell B, Faulk K, Cunningham JT. Neural Control of Blood Pressure in Chronic Intermittent Hypoxia. Curr Hypertens Rep 2016;18:19.

5. Sharpe AL, Calderon AS, Andrade MA, Cunningham JT, Mifflin SW, Toney GM. Chronic intermittent hypoxia increases sympathetic control of blood pressure: role of neuronal activity in the hypothalamic paraventricular nucleus. Am J Physiol Heart Circ Physiol 2013;305:H1772-1780.

6. Prabhakar NR, Peng YJ, Jacono FJ, Kumar GK, Dick TE. Cardiovascular alterations by chronic intermittent hypoxia: importance of carotid body chemoreflexes. Clin Exp Pharmacol Physiol 2005;32:447-449.

7. Fletcher EC, Lesske J, Behm R, Miller CC, Stauss H, Unger T. Carotid chemoreceptors, systemic blood pressure, and chronic episodic hypoxia mimicking sleep apnea. Journal of applied physiology (Bethesda, Md : 1985) 1992;72:1978-1984.

8. Silva AQ, Schreihofer AM. Altered sympathetic reflexes and vascular reactivity in rats after exposure to chronic intermittent hypoxia. The Journal of physiology 2011;589:1463-1476.

9. Bathina CS, Rajulapati A, Franzke M, Yamamoto K, Cunningham JT, Mifflin S. Knockdown of tyrosine hydroxylase in the nucleus of the solitary tract reduces elevated blood pressure during chronic intermittent hypoxia. American Journal of Physiology - Regulatory, Integrative and Comparative Physiology 2013;305:R1031-R1039.

10. Zoccal DB, Simms AE, Bonagamba LGH, et al. Increased sympathetic outflow in juvenile rats submitted to chronic intermittent hypoxia correlates with enhanced expiratory activity. The Journal of physiology 2008;586:3253-3265.

11. Bathina CS, Rajulapati A, Franzke M, Yamamoto K, Cunningham JT, Mifflin S. Knockdown of tyrosine hydroxylase in the nucleus of the solitary tract reduces elevated blood pressure during chronic intermittent hypoxia. Am J Physiol Regul Integr Comp Physiol 2013;305:R1031-1039.

12. Marcus NJ, Li YL, Bird CE, Schultz HD, Morgan BJ. Chronic intermittent hypoxia augments chemoreflex control of sympathetic activity: role of the angiotensin II type 1 receptor. Respir Physiol Neurobiol 2010;171:36-45.

13. Fletcher EC. Effect of episodic hypoxia on sympathetic activity and blood pressure. Respiration Physiology 2000;119:189-197.

14. Fletcher EC, Bao G, Li R. Renin activity and blood pressure in response to chronic episodic hypoxia. Hypertension 1999;34:309-314.

15. Fletcher EC, Orolinova N, Bader M. Blood pressure response to chronic episodic hypoxia: the renin-angiotensin system. J Appl Physiol 2002;92:627-633.

16. Mifflin S, Cunningham JT, Toney GM. Neurogenic mechanisms underlying the rapid onset of sympathetic responses to intermittent hypoxia. J Appl Physiol (1985) 2015;119:1441-1448.

17. McKinley MJ, Yao ST, Uschakov A, McAllen RM, Rundgren M, Martelli D. The median preoptic nucleus: front and centre for the regulation of body fluid, sodium, temperature, sleep and cardiovascular homeostasis. Acta Physiol (Oxf) 2015;214:8-32.

18. Cunningham JT, Beltz T, Johnson RF, Johnson AK. The effects of ibotenate lesions of the median preoptic nucleus on experimentally-induced and circadian drinking behavior in rats. Brain Res 1992;580:325-330.

19. Johnson AK, Cunningham JT, Thunhorst RL. Integrative role of the lamina terminalis in the regulation of cardiovascular and body fluid homeostasis. Clin Exp Pharmacol Physiol 1996;23:183-191.

20. Allen WE, DeNardo LA, Chen MZ, et al. Thirst-associated preoptic neurons encode an aversive motivational drive. Science 2017;357:1149-1155.

21. Ployngam T, Collister JP. Role of the median preoptic nucleus in chronic angiotensin II-induced hypertension. Brain Res 2008;1238:75-84.

22. Saxena A, Little JT, Nedungadi TP, Cunningham JT. Angiotensin II type 1a receptors in subfornical organ contribute towards chronic intermittent hypoxia-

associated sustained increase in mean arterial pressure. Am J Physiol Heart Circ Physiol 2015;308:H435-446.

23. Llewellyn T, Zheng H, Liu X, Xu B, Patel KP. Median preoptic nucleus and subfornical organ drive renal sympathetic nerve activity via a glutamatergic mechanism within the paraventricular nucleus. Am J Physiol Regul Integr Comp Physiol 2012;302:R424-432.

24. Guyenet PG. The sympathetic control of blood pressure. Nat Rev Neurosci 2006;7:335-346.

25. Knight WD, Little JT, Carreno FR, Toney GM, Mifflin SW, Cunningham JT. Chronic intermittent hypoxia increases blood pressure and expression of FosB/DeltaFosB in central autonomic regions. Am J Physiol Regul Integr Comp Physiol 2011;301:R131-139.

26. Menani JV, Vieira AA, Colombari DSA, De Paula PM, Colombari E, De Luca LA, Jr. Preoptic-Periventricular Integrative Mechanisms Involved in Behavior, Fluid-Electrolyte Balance, and Pressor Responses. In: De Luca LA, Jr., Menani JV, Johnson AK, eds. Neurobiology of Body Fluid Homeostasis: Transduction and Integration. Boca Raton (FL)2014.

27. Ployngam T, Collister JP. An intact median preoptic nucleus is necessary for chronic angiotensin II-induced hypertension. Brain Res 2007;1162:69-75.

28. Cunningham JT, Knight WD, Mifflin SW, Nestler EJ. An essential role for ΔFosB in the median preoptic nucleus in the sustained hypertensive effects of chronic intermittent hypoxia. Hypertension 2012;60:179-187.

29. Cunningham JT, Knight WD, Mifflin SW, Nestler EJ. An Essential role for DeltaFosB in the median preoptic nucleus in the sustained hypertensive effects of chronic intermittent hypoxia. Hypertension 2012;60:179-187.

30. Yang CF, Chiang MC, Gray DC, et al. Sexually dimorphic neurons in the ventromedial hypothalamus govern mating in both sexes and aggression in males. Cell 2013;153:896-909.

31. Shi P, Martinez MA, Calderon AS, Chen QH, Cunningham JT, Toney GM. Intra-carotid hyperosmotic stimulation increases Fos staining in forebrain organum vasculosum laminae terminalis neurones that project to the hypothalamic paraventricular nucleus. Journal Of Physiology-London 2008;586:5231-5245.

32. Snyder B, Shell B, Cunningham JT, Cunningham RL. Chronic intermittent hypoxia induces oxidative stress and inflammation in brain regions associated with early-stage neurodegeneration. Physiol Rep 2017;5.

33. Herdegen T, Leah JD. Inducible and constitutive transcription factors in the mammalian nervous system: control of gene expression by Jun, Fos and Krox, and CREB/ATF proteins. Brain Res Brain Res Rev 1998;28:370-490.

34. Faulk KE, Nedungadi TP, Cunningham JT. Angiotensin converting enzyme 1 in the median preoptic nucleus contributes to chronic intermittent hypoxia hypertension. Physiol Rep 2017;5.

35. Latha Palaniappan LAS, Judith Simons, Yechiel Friedlander, and John McCallum. Comparison of Usefulness of Systolic, Diastolic, and Mean Blood Pressure and Pulse Pressure as Predictors of Cardiovascular Death in Patients >60 Years of Age (The Dubbo Study). Am J Cardiol 2002;90:1398-1401.

36. McKinley MJ, Yao ST, Uschakov A, McAllen RM, Rundgren M, Martelli D. The median preoptic nucleus: front and centre for the regulation of body fluid, sodium, temperature, sleep and cardiovascular homeostasis. Acta Physiol (Oxf) 2015;214:8-32. doi: 10.1111/apha.12487. Epub 12015 Apr 12481.

37. Abbott SBG, Saper CB. Median preoptic glutamatergic neurons promote thermoregulatory heat loss and water consumption in mice. J Physiol 2017;595:6569-6583.

38. Silva AQ, Schreihofer AM. Altered sympathetic reflexes and vascular reactivity in rats after exposure to chronic intermittent hypoxia. The Journal of Physiology 2011;589:1463-1476.

39. Knight WD, Saxena A, Shell B, Nedungadi TP, Mifflin SW, Cunningham JT. Central losartan attenuates increases in arterial pressure and expression of FosB/DeltaFosB along the autonomic axis associated with chronic intermittent hypoxia. Am J Physiol Regul Integr Comp Physiol 2013;305:R1051-1058.

40. Paxinos GaCW. The Rat Brain in Stereotaxic Coordinates, 4th Edition ed1998.

Online Supplement

Caspase Lesions of PVN-Projecting MnPO Neurons Blocks the Sustained Component of CIH-Induced Hypertension in Adult Male Rats

Alexandria B. Marciante, Lei A. Wang, Joel T. Little and J. Thomas Cunningham

University of North Texas Health Science Center, Department of Physiology and Anatomy

CORRESPONDENCE

Dr. J. Thomas Cunningham

Tom.Cunningham@unthsc.edu

University of North Texas Health Science Center

Department of Physiology and Anatomy

3500 Camp Bowie Boulevard

Fort Worth, Texas 76107

Supplemental Methods

Microinjection Surgeries

Rats were anesthetized with 2% isoflurane and received stereotaxic microinjections of the retrograde AAV containing Cre (AAV9.CMV.HI.eGFP-Cre.WPRE.SV40; Penn State Vector Core) bilaterally into the PVN (-1.8 mm anterior, ± 0.4 mm lateral, 7.6 mm ventral from bregma) [1]. In the same surgery, caspase-3 (AAV5-flex-taCasp3-TEVp) or control (AAV5-hSyn-DIO-mCherry) virus (UNC VectorCore) was injected into the MnPO (microinjector angled at 8º from medial to lateral to avoid the septum, at coordinates 0.9 mm lateral, 6.7 mm ventral from bregma) [1]. A burr hole was then drilled at the measured site and a 30-gauge stainless steel injection needle was lowered to the MnPO, where 200-300 nL of AAV was delivered at a rate of 200 nL/min. The injector was connected to a Hamilton 5 µL syringe (#84851, Hamilton, Reno, NV) by calibrated polyethylene tubing that was used to determine the injection volume. The injector remained in place for 5 minutes to allow for absorption and then slowly withdrawn. Gel foam was packed in to the hole in the skull. Absorbable antibiotic suture was used to close the incision and minimize post-surgical infection. Each rat was given carprofen (Rimadyl, Bio-Serv, 1 mg) orally to minimize pain following surgery. Rats were allowed to recover for one week before radio telemetry surgery and for three weeks before beginning the CIH protocol.

Radio Telemetry Implantation

Rats were anesthetized as before with 2% isoflurane one week after microinjection surgeries. Rats were implanted with an abdominal aortic catheter attached to a HD-S10 radio telemetry transmitter (Data Sciences International, St. Paul, MN) to continuously record hemodynamic measurements (Dataquest IV, Data Sciences International, St.

Paul, MN). The transmitter was secured to the abdominal wall using prolene suture and remained in the abdominal cavity through the duration of the experiment. Two weeks were allowed for recovery from surgery. Blood pressure measurements obtained during a 10 s sampling period (500 Hz) were averaged and recorded every 5 min.

CIH Protocol

After 2 weeks of postsurgical recovery from microinjections and 1 week recovery from telemetry implantation, rats individually housed in their home cages were relocated to custom-built Plexiglass chambers for 2 days of acclimation and 5 days of baseline recording at normoxia (21% O_2). After this 7 day period, rats were exposed to CIH for 7 days from 0800 to 1600 h. The O_2 concentration in the chambers was regulated using custom-built user-controlled timers that separately switched the flow of room air and nitrogen into each chamber. The O_2 concentration was continuously monitored using O_2 sensors (KE-25, Kent Scientific Corporation, Torrington, CT) and recorded using Spike2 software (v. 5.07, Cambridge Electronic Design Limited, Cambridge, UK). Flow rates of room air and nitrogen to each chamber were controlled separately using individual flow meters, as previously described [2]. The CIH protocol consisted of 6 min cycles, with 3 minutes of hypoxia (10% O_2) using nitrogen infusion and 3 minutes of normoxia (21% O_2) using re-infusion of room air, as previously described [2-4]. These cycles repeated for 8 h per day for 7 days, resulting in 80 cycles of hypoxic exposure per day. During the remaining 16 h of the day, the chambers were open to normoxic room air (21% O_2). Controls were placed in identical chambers within the same room, but only exposed to normoxic room air (21% O_2). Following the 7-day CIH protocol, on the morning of the 8th day, all animals were euthanized.

Perfusions—Tissue and Body Fluid Collection

On the morning of day 8, after the 7-day CIH protocol terminated, animals were anesthetized using 100 mg/kg inactin ip (Sigma-Aldrich). Blood was collected from the left ventricle and transferred into an EDTA vacutainer containing heparin immediately preceding the perfusion, in order to measure plasma advanced oxidative protein products (AOPP). Blood was also transferred into a separate tube in order to measure hematocrit and plasma osmolality using a vapor pressure osmometer (Wescor, Logan, UT) as previously described [5]. Rats were transcardially flushed first with PBS (approximately 100 mL) and then perfused using 4% paraformaldehyde (PFA, 300 mL). Each brain was kept in 4% PFA overnight before being placed in 30% sucrose in PBS.

Tissue Processing

Methyl Green Staining: Methyl green staining was performed to detect microinjector tracks as an additional way to verify successful viral injections in the MnPO and PVN. The staining protocol was performed according to directions provided by the manufacturer (H-3402, Methyl Green Counterstain, Vector Laboratories, Inc.). Rats that did not have successful injections into the MnPO or PVN were excluded from anatomy studies. Those that received the caspase virus and exposed to CIH but had unsuccessful microinjections were used, however, in hemodynamic and blood component analyses (CASP CIH MISS) to serve as an additional control.

Immunohistochemistry (IHC): Forty µm coronal sections of each previously perfused brain were cut using a cryostat. Three sets of serial sections were collected in cryoprotectant and stored at -20^{o}C until they were processed for immunohistochemistry.

FosB: Separate sets of serial sections from brains injected with caspase-3 or control virus were stained for FosB (1:1000, goat polyclonal anti-Fos antibody, Santa Cruz Biotechnology). After 48 h, sections were washed using phosphate buffer solution (PBS) and transferred to a secondary antibody (BA-9500, biotinylated anti-goat, Vector Laboratories) for DAB reaction and labeling. After the DAB reaction, the sections were washed and placed in the primary antibody (DSHB-GFP3-1F5, GFP anti-mouse primary antibody, Developmental Studies Hybridoma Bank, University of Iowa) and incubated for an additional 48 h followed by incubation with a CY2 conjugated anti-mouse antibody (715-225-151, Jackson ImmunoResearch) for 4-5 h. The sections were then mounted on gelatin-coated slides, dried, and coverslipped with Permount for imaging.

NOS1 and GFAP: Other sections were stained separately for nitric oxide synthase 1, NOS1, (1:1000, sc5302, Santa Cruz Biotechnology) to determine MnPO-PVN projecting neuron phenotype or glial fibrillary acidic protein, GFAP, (1:500, G3893, Sigma-Aldrich) to ensure only neurons were affected caspase-3 induced apoptosis. For these anatomy studies, sections came from rats just injected into the PVN with the AAV9-GFP retrograde or rats injected into the PVN with the AAV9-GFP retrograde and caspase-3 into the MnPO. After 48 h, sections were washed using phosphate buffer solution (PBS) and transferred to a CY3 conjugated anti-mouse secondary antibody (711-165-152, Jackson ImmunoResearch). The sections were then mounted on gelatin-coated slides, dried, and coverslipped with Prolong Diamond mounting medium for imaging. All antibodies were diluted to working concentration in PBS diluent (0.25% Triton, 3% horse serum, and 96.75% PBS).

In situ hybridization (ISH): ISH experiments were performed in order to characterize the neuronal phenotype of PVN-projecting MnPO neurons transfected by the AAV. After the CIH protocol was terminated, separate groups of rats than those used for immunohistochemistry were anesthetized using 100 mg/kg inactin (Sigma-Aldrich) ip and transcardially flushed first with RNase-free PBS and then perfused using 4% paraformaldehyde (PFA). Brains were dehydrated in RNase-free 30% sucrose. Twenty µm coronal sections of each brain were cut using a cryostat (Leica). Four to six sets of serial MnPO sections were collected in RNase-free PBS, mounted on to Superfrost Plus Gold microscope slides (Thermo Fisher Scietific Inc., Waltham, MA, USA), and left at room temperature for ~2 h and then stored at -80ºC until used for ISH experiments. All reagents used for ISH experiments were purchased from Advanced Cell Diagnostics (Newark, CA, USA). Experiments were performed using a previously established protocol [6-9].

AT_1aR: ISH was performed for Agtr1a for AT_1aR detection (ref num: 422661) to study the role of AT_1aR in the MnPO during CIH using a chromogenic assay (ref num: 322310). Experimental protocols were performed according to the manufacturer described in RNAscope® 2.5 HD Detection Reagent – BROWN User Manual PART2 (Document Number 322310-USM, Advanced Cell Diagnostics).

vGLUT2: In a separate subset of sections, ISH was performed for vesicular glutamate transporter 2, or vGLUT2, (ref num: 317011) to study the phenotype of PVN-projecting MnPO neurons in rats only injected in the PVN with AAV9-GFP virus. ISH for vGLUT2

was performed using a fluorescent assay (ref num. 320293). Experimental protocls were performed according to the manufacturer described in RNAscope® Fluorescent Multiplex Kit User Manual PART 2 (Document Number 320293, Advanced Cell Diagnostics).

Imaging and Quantification: All tissue sections were imaged with microscope equipped for epifluorescence and (Olympus BX41, Olympus, Center Valley, PA, USA) with a digital camera (Olympus DP70). Cell counting and image analysis was performed using NIH ImageJ software (National Institutes of Health, v1.49).

For sections stained with methyl green or FosB, tissue was visualized using brightfield illumination. FosB counts were calculated in ImageJ. For sections stained for either vGLUT2 or NOS1, images were taken to identify AAV9-GFP expression at an emission/excitation frequency of 493/518 nm and vGLUT2 or NOS1 expression at an emission/excitation frequency of 550/568 nm. The separate images were merged in ImageJ in order to determine raw cell counts for colocalization. Sections used for AT_1aR detection were imaged using bright field illumination (AT_1aR detection) and for AAV9-GFP fluorescence. Brightfield images were inverted using ImageJ and merged with images of GFP fluorescence to determine colocalization.

Sections stained for GFAP were imaged for AAV9-GFP expression and GFAP expression. GFAP expression was then quantified in ImageJ using a densitometric approach. Sections from control rats that were not injected with virus (n=3) and stained only with CY3 anti-mouse secondary were processed according to the same IHC protocol. Images were taken of these sections using the same exposure settings that were converted to 8-bit grayscale in ImageJ. In ImageJ, the threshold was adjusted so

integrated density was as close to zero as possible in control sections to subtract out background. Once this threshold was set, sections stained for GFAP were analyzed using the same threshold to measure integrated density. Integrated density of GFAP fluorescence in the MnPO was then compared between rats only injected with the AAV9-GFP in the PVN and rats injected with the AAV9-GFP in the PVN and caspase-3 injected in the MnPO. This approach allowed us to determine if caspase-3 was significantly decreasing GFAP fluorescence density.

Advanced Oxidative Protein Products (AOPP) Assay

Plasma oxidative stress was measured using Cell Biolabs, Inc. OxiSelect Advanced Oxidative Protein Products assay kit (STA-318) and performed using a previously described protocol based on the manufacturer [10, 11]. The AOPP assay kit provides the ability to measure the concentration of total oxidized protein in a sample (uM) by reacting with Chloramine to initiate a color change. Samples are read at a wavelength of 340 nm and concentration is calculated by comparison with the predetermined Chloramine standard curve. Assay results are reported as a percent of control {individual value/(average of normoxic control values) x 100}, as previously described [10].

Supplement Results

GFAP: We used a CMV promotor in the Cre-expressing AAV9-GFP retrograde virus to increase transduction rate and viral spread to the MnPO neurons that project to the PVN [12]. In order to validate that we were specifically affecting neuronal populations, we did densitometric analysis of glial fibrillary acidic protein, or GFAP, and calculated the integrated density in the MnPO of rats injected with or without the caspase-3 virus (Figure S1). We found no changes in GFAP expression, indicating the AAV5-caspase-3 flex viral construct induced apoptosis specific to neurons ($t(7) = 0.303$, $p = 0.771$, Student's *t*-test).

Heart Rate: No significant differences were found overall among any of the groups for daily changes in HR (Figure S2A) during CIH ($F(4, 32) = 0.963$, $p = 0.441$, two-way RM ANOVA) or during the normoxic dark period ($F(4, 32) = 0.531$, $p = 0.714$, two-way RM ANOVA). However, there were significant differences in averages measuring overall changes in HR during the CIH period ($F(4, 32) = 19.026$, $p < 0.001$, one-way ANOVA) and normoxic dark period ($F(4, 32) = 11.723$, $p < 0.001$, one-way ANOVA). This was due to CIH exposure and was influenced by the caspase lesions (Figure S3A).

Body Temperature: No significant differences were found overall among any of the groups for daily changes in BT (Figure S2B) during CIH ($F(4, 32) = 0.398$, $p = 0.809$, two-way RM ANOVA) or during the normoxic dark period ($F(4, 32) = 0.757$, $p = 0.561$, two-way RM ANOVA). However, there were significant differences in averages measuring overall changes in BT during the normoxic dark period ($F(4, 32) = 22.392$, $p < 0.001$, one-way ANOVA). This was due to CIH exposure and was not dependent on whether groups were injected with the control or caspase virus (Figure S3B).

Figure S1. *Astrocytes were unaffected by caspase lesions in the MnPO.* Representative merged images of GFAP (red) and AAV9-GFP (green) in the MnPO injected without (left) or with caspase-3 (right) virus and integrated density for each group. Scale bar, 100 µm.

Figure S1.

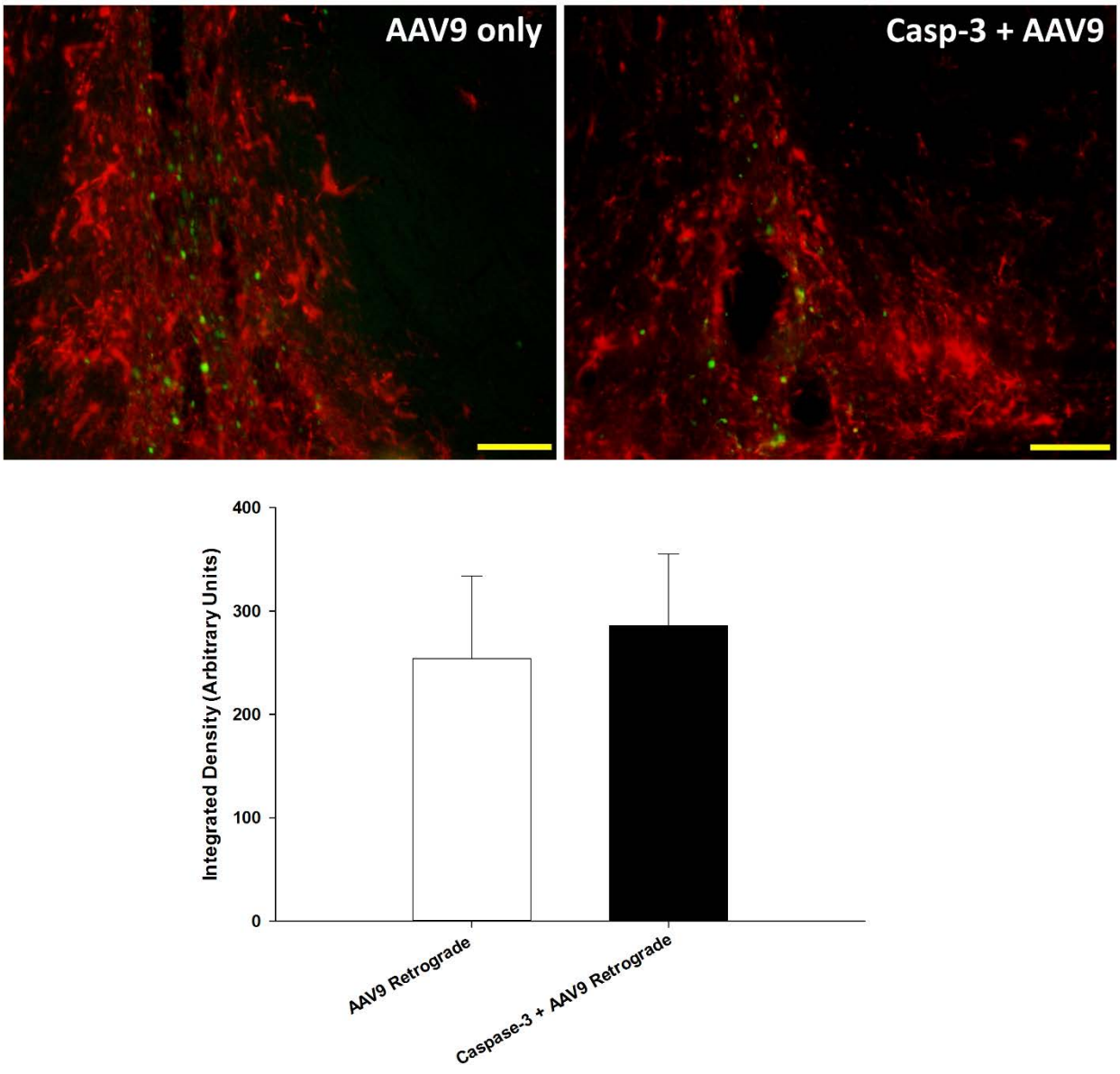
AAV9 only
Casp-3 + AAV9
Integrated Density (Arbitrary Units)
400
300
200
100
0
AAV9 Retrograde
Caspase-3 + AAV9 Retrograde

Figure S2. *CIH did not significantly affect daily changes in HR or BT.* A, Average daily changes in heart rate (HR) and B, body temperature (BT) during the CIH period (left column) and dark period (right column). Control-injected rats exposed to normoxia (CTRL NORM) or hypoxia (CTRL CIH); caspase-injected rats exposed to normoxia (CASP NORM), hypoxia (CASP CIH), or misses (CASP CIH MISS).

Figure S2.

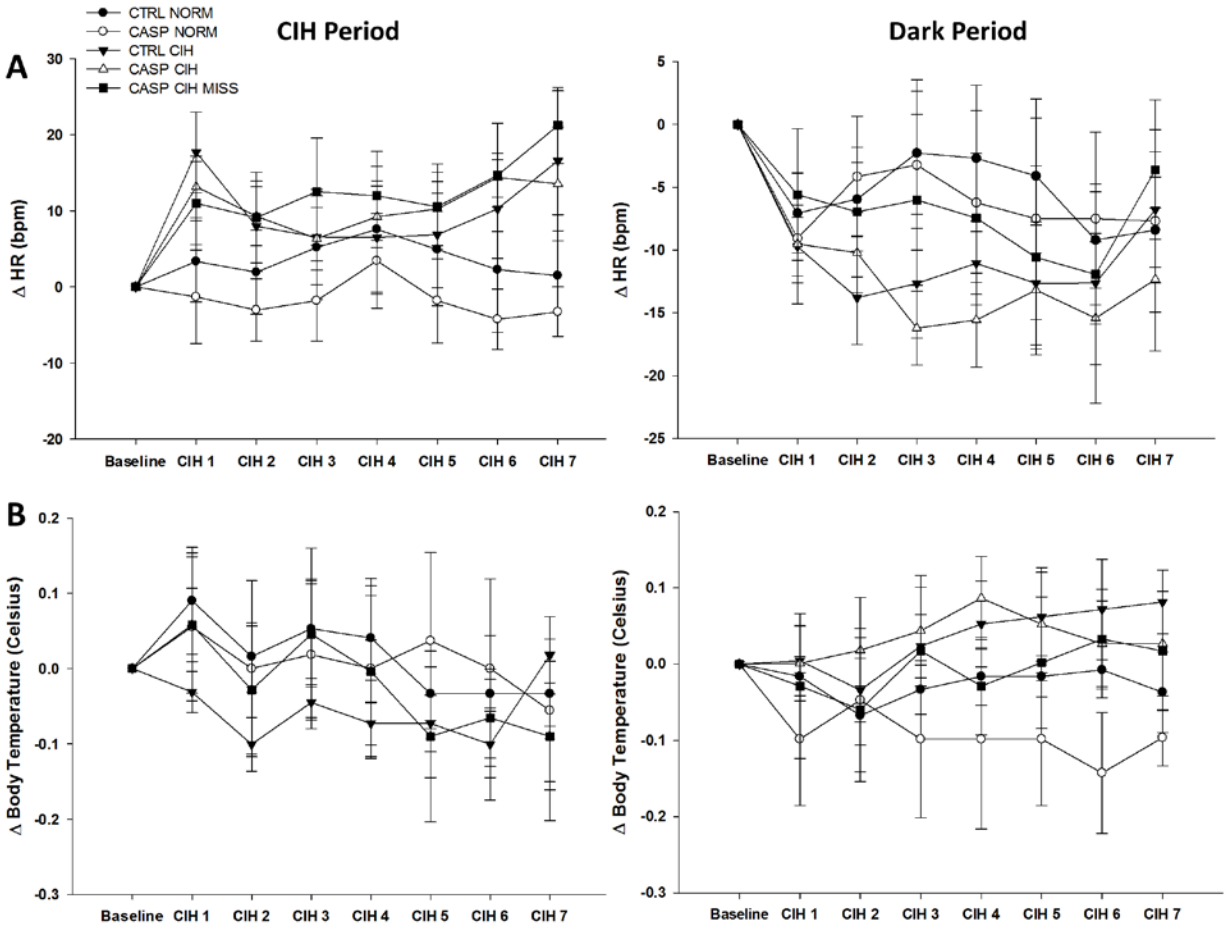
A
CTRL NORM
CASP NORM
CTRL CIH
CASP CIH
CASP CIH MISS
CIH Period
Dark Period
Δ HR (bpm)
Baseline
CIH 1
CIH 2
CIH 3
CIH 4
CIH 5
CIH 6
CIH 7
B
Δ Body Temperature (Celsius)

Figure S3. *Average 7-day changes in HR and BT were significantly different between CIH and normoxic control groups.* A, Heart rate (HR) during the light period was significantly increased to groups exposed CIH and significantly decreased during the dark period compared to normoxic controls. B, Body temperature (BT) decreased during the light period in groups exposed to CIH and significantly increased during the dark period compared to normoxic controls. Control-injected rats exposed to normoxia (CTRL NORM) or hypoxia (CTRL CIH); caspase-injected rats exposed to normoxia (CASP NORM), hypoxia (CASP CIH), or misses (CASP CIH MISS). **$p < 0.050$, compared to CTRL NORM and CASP NORM during CIH; ‡$p < 0.050$, compared to CTRL NORM and CASP NORM during the dark period.

Figure S3.

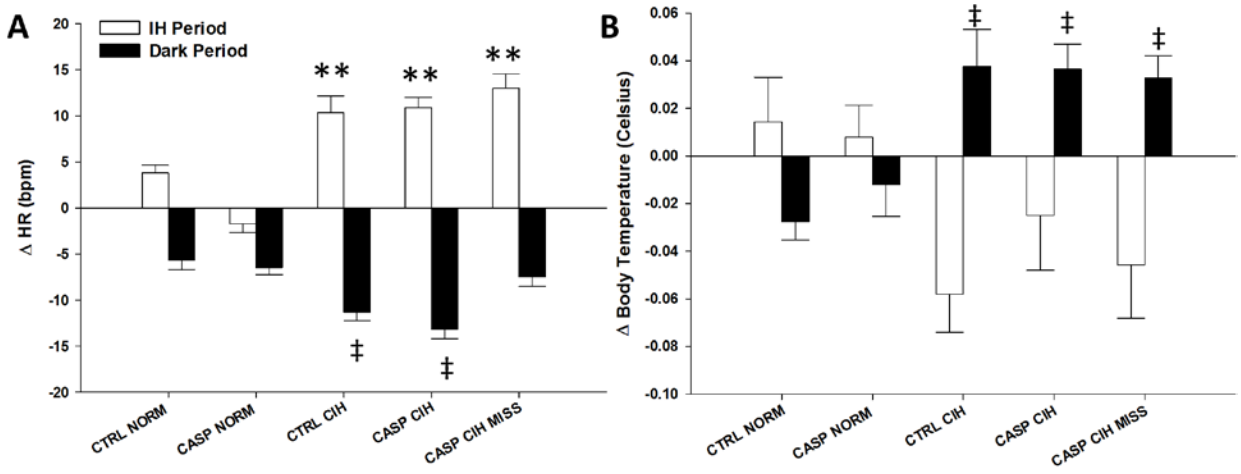
A
IH Period
Dark Period
Δ HR (bpm)
20
15
10
5
0
-5
-10
-15
-20
**
**
**
‡
‡
CTRL NORM
CASP NORM
CTRL CIH
CASP CIH
CASP CIH MISS
B
Δ Body Temperature (Celsius)
0.06
0.04
0.02
0.00
-0.02
-0.04
-0.06
-0.08
-0.10
‡
‡
‡
CTRL NORM
CASP NORM
CTRL CIH
CASP CIH
CASP CIH MISS

Figure S4. *FosB staining in the SFO, PVN, and RVLM*. Representative FosB staining in the subfornical organ (SFO, top row), paraventricular nucleus (PVN, middle row), and rostral ventral lateral medulla (RVLM, bottom row) in control-injected rats exposed to normoxia (CTRL NORM, first column), caspase-injected rats exposed to normoxia (CASP NORM), control-injected rats exposed to hypoxia (CTRL CIH), caspase-injected rats exposed to hypoxia (CASP CIH, right column). Scale bar, 100 µm.

Figure S4.

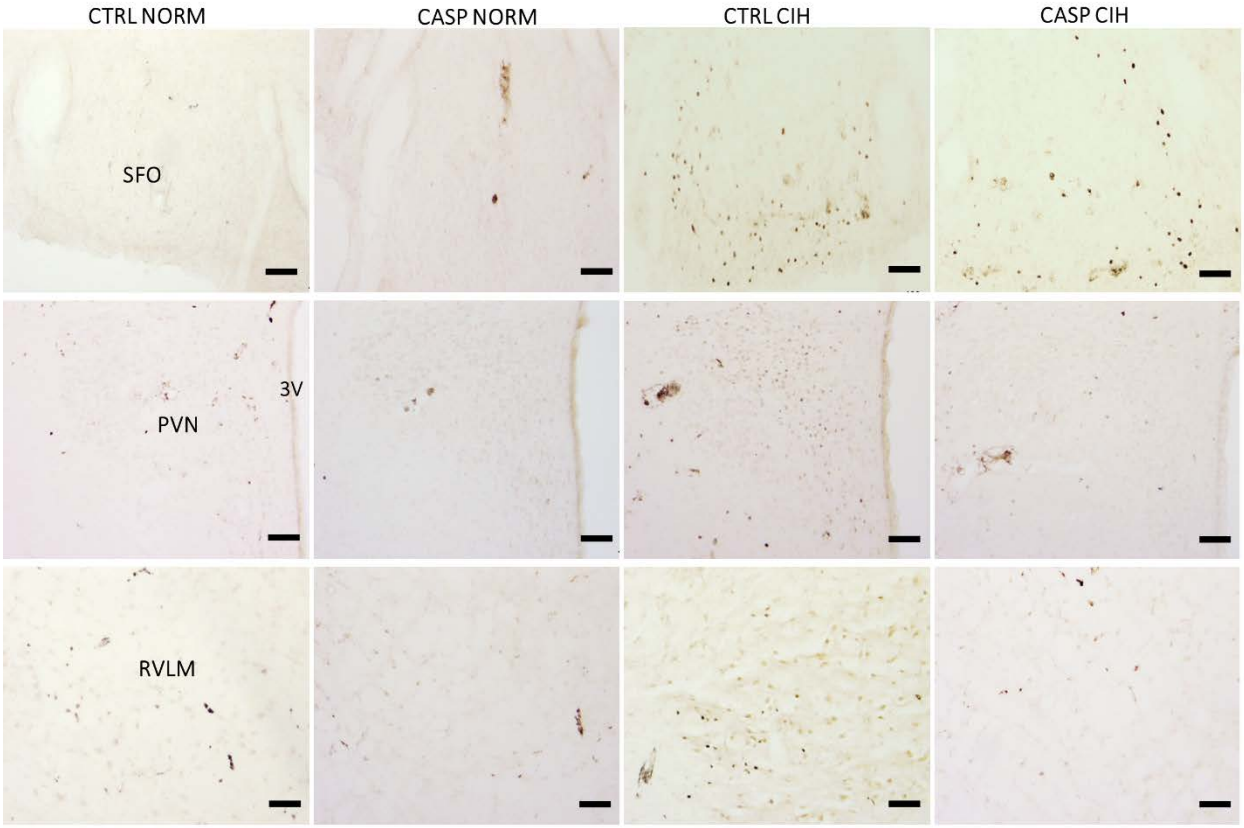

Table S1. Average mean, systolic, and diastolic arterial pressure (MAP, SAP, DAP, respectively), heart rates and body temperature during the light phase (0800-1600) and dark phase (1900-0700) during a 5-day baseline period prior to the 7-day CIH protocol. Control-injected rats exposed to normoxia (CTRL NORM) or hypoxia (CTRL CIH); caspase-injected rats exposed to normoxia (CASP NORM), hypoxia (CASP CIH), or misses (CASP CIH MISS).

Table S1.

		CTRL NORM n=8	CASP NORM n=6	CTRL CIH n=8	CASP CIH n=9	CASP CIH MISS n=6
MAP (mmHg)	Light Baseline	97.5±1.5	99.5±1.0	96.5±1.2	98.5±1.1	101.4±2.0
	Dark Baseline	103.8±2.0	104.1±1.8	102.5±1.4	104.2±1.5	103.1±2.4
SAP (mmHg)	Light Baseline	113.9±2.7	117.0±2.5	110.9±1.6	117.3±2.2	119.4±3.6
	Dark Baseline	120.3±3.2	121.3±3.2	117.0±1.4	123.4±2.6	122.4±4.1
DAP (mmHg)	Light Baseline	83.7±1.2	85.3±1.6	84.7±1.1	83.9±1.0	87.2±1.4
	Dark Baseline	90.0±1.7	90.2±2.0	91.0±1.6	89.8±1.3	89.2±1.4
Heart Rate (bpm)	Light Baseline	318.5±8.1	321.8±4.2	312.1±5.0	311.2±5.5	317.4±6.8
	Dark Baseline	372.0±10.0	375.2±8.0	367.4±9.2	364.7±8.0	357.3±11.9
Body Temperature (°C)	Light Baseline	37.1±0.0	37.2±0.1	37.1±0.0	37.2±0.1	37.4±0.1
	Dark Baseline	37.9±.01	37.9±0.1	37.9±0.1	38.0±0.1	37.8±0.1

References

1. Paxinos GaCW. The Rat Brain in Stereotaxic Coordinates, 4th Edition ed1998.

2. Knight WD, Little JT, Carreno FR, Toney GM, Mifflin SW, Cunningham JT. Chronic intermittent hypoxia increases blood pressure and expression of FosB/DeltaFosB in central autonomic regions. Am J Physiol Regul Integr Comp Physiol 2011;301:R131-139.

3. Cunningham JT, Knight WD, Mifflin SW, Nestler EJ. An essential role for ΔFosB in the median preoptic nucleus in the sustained hypertensive effects of chronic intermittent hypoxia. Hypertension 2012;60:179-187.

4. Faulk KE, Nedungadi TP, Cunningham JT. Angiotensin converting enzyme 1 in the median preoptic nucleus contributes to chronic intermittent hypoxia hypertension. Physiol Rep 2017;5.

5. Ji LL, Fleming T, Penny ML, Toney GM, Cunningham JT. Effects of water deprivation and rehydration on c-Fos and FosB staining in the rat supraoptic nucleus and lamina terminalis region. Am J Physiol Regul Integr Comp Physiol 2005;288:R311-321.

6. Smith JA, Wang L, Hiller H, Taylor CT, de Kloet AD, Krause EG. Acute hypernatremia promotes anxiolysis and attenuates stress-induced activation of the hypothalamic-pituitary-adrenal axis in male mice. Physiol Behav 2014;136:91-96.

7. de Kloet AD, Wang L, Pitra S, et al. A Unique "Angiotensin-Sensitive" Neuronal Population Coordinates Neuroendocrine, Cardiovascular, and Behavioral Responses to Stress. J Neurosci 2017;37:3478-3490.

8. Wang L, de Kloet AD, Pati D, et al. Increasing brain angiotensin converting enzyme 2 activity decreases anxiety-like behavior in male mice by activating central Mas receptors. Neuropharmacology 2016;105:114-123.

9. Wang L, Hiller H, Smith JA, de Kloet AD, Krause EG. Angiotensin type 1a receptors in the paraventricular nucleus of the hypothalamus control cardiovascular reactivity and anxiety-like behavior in male mice. Physiol Genomics 2016;48:667-676.

10. Snyder B, Duong P, Tenkorang M, Wilson EN, Cunningham RL. Rat Strain and Housing Conditions Alter Oxidative Stress and Hormone Responses to Chronic Intermittent Hypoxia. Front Physiol 2018;9:1554.

11. Snyder B, Shell B, Cunningham JT, Cunningham RL. Chronic intermittent hypoxia induces oxidative stress and inflammation in brain regions associated with early-stage neurodegeneration. Physiol Rep 2017;5.

12. Watakabe A, Ohtsuka M, Kinoshita M, et al. Comparative analyses of adeno-associated viral vector serotypes 1, 2, 5, 8 and 9 in marmoset, mouse and macaque cerebral cortex. Neurosci Res 2015;93:144-157.

CHAPTER IV: DISCUSSION

The Median Preoptic Nucleus

The median preoptic nucleus (MnPO) is an extremely important regulatory region and has been shown in many studies to be necessary for maintaining body fluid homeostasis and blood pressure regulation [1-4]. However, data on stimulus-dependence and pathway specificity signaling from the MnPO to afferent brain regions driving thirst and autonomic function are sparse. In these studies, we directly address how the MnPO differentially signals thirst during cellular versus extracellular dehydration. Additionally, we also provide evidence that the MnPO neurons that project to the paraventricular nucleus (PVN) of the hypothalamus are necessary in the development of chronic intermittent hypoxia (CIH)-induced diurnal hypertension.

The Role of the MnPO in Regulating Thirst

The MnPO plays an important and necessary role in regulating water intake associated with body fluid homeostasis in models of cellular (i.e. hypertonicity) and extracellular (i.e. hypovolemia associated with angiotensin II, ANG II) dehydration [2, 5-13]. It is well understood that the circumventricular organs (CVOs), the subfornical organ (SFO) and organum vasculosum of the lamina terminalis (OVLT), respond to fluctuations in plasma osmolality and circulating humoral factors, such as angtiotensin II (ANG II), and that the CVOs signal the MnPO [2]. However, studies have been limited in demonstrating whether the MnPO differentially responds to stimuli and if that effects how the MnPO signals to downstream thirst-driving brain regions.

In these experiments, the dipsogenic effects of ANG II and hypertonic saline challenges (3% NaCl) were used to increase water consumption [6, 10, 14, 15]. Using ANG II

and 3% NaCl, plasma arginine vasopressin (AVP) was significantly elevated compared to vehicle controls. Fos, a neuronal marker for acute activation part of the activator protein-1 (AP-1) complex, staining was also significantly increased by both ANG II and 3% NaCl in the MnPO, supraoptic nucleus (SON), paraventricular nucleus (PVN), lateral hypothalamus (LH), and paraventricular nucleus of the thalamus (PVT). However, upon CNO-induced inhibition of the MnPO, Fos staining was significantly attenuated in the MnPO, SON, posterior magnocellular (PM) and medial parvocellular (MP) subregions of the PVN and in the rostral ventral lateral medulla (RVLM) during ANG II exposure. However, Fos staining was significantly decreased in only the SON and LH during 3% NaCl exposure. Because of these differences in Fos staining, we show that thirst driven by ANG II as it relates to extracellular dehydration may favor MnPO signaling through the PVN, while thirst driven by 3% NaCl as it relates to cellular dehydration may favor MnPO signaling through the LH and that the PVT may be required mechanistically in response to both stimuli (Figure 1).

Previous studies have indicated that specific MnPO neuronal populations can have intrinsic osmosensitivity and can be sensitive to ANG II [16, 17]. Our results suggest that these may be different neuronal populations which could account for differing signaling mechanisms to downstream brain regions. Our results show that the MnPO has pathway-specific signaling and is dependent on stimulus.

The Role of the MnPO in CIH-Induced Hypertension

Obstructive sleep apnea (OSA) is a prevalent disease, characterized by repeated cessations in respiration during sleep that can lead to cardiovascular disease. Often this

disease goes unnoticed in patients until symptoms progress to end-organ damage, such as heart disease or stroke [18-20]. One early symptom that results from OSA is the development of diurnal hypertension, or a sustained increase in blood pressure that persists into the waking hours and is accompanied by increases in sympathetic nerve activity.

We use the 7-day CIH experimental model in these studies to successfully mimic the oxygen deprivation associated with apneic breathing patterns patients with mild to moderate forms of OSA. This model is most ideal for studying the initiation and dysregulation of hypertension and how it develops into sustained hypertension, because it allows us to observe the early development of pathologies that occur during CIH associated with OSA, without the confounding effects of end-organ damage [21, 22].

Our studies indicate that the MnPO contributes to the sustained component of CIH hypertension and our proposed mechanism is illustrated in Figure 2. Hypertension due to CIH initially develops during hypoxic conditions from signaling through the hindbrain and may be sustained through multiple mechanisms that include activity of the forebrain, specifically through modulation by the MnPO [23]. The MnPO is an integrating center in the hypothalamus that has projections to pre-sympathetic PVN neurons involved in blood pressure regulation, SNA, and the hypothalamic-pituitary-adrenal axis [23, 24]. Many studies have shown that the MnPO is necessary for CIH hypertension [25, 26]. However, the phenotypes of the MnPO neurons responsible for CIH hypertension had not yet been fully elucidated. Hypertension has been shown to be heavily associated with the dysregulation of the renin-angiotensin system (RAS), causing increases in ANG II concentration [27-30]. Based on the drinking study results and the importance of the PVN

in ANG II-induced thirst, we decided to focus on the MnPO neurons that project to the PVN in the development of CIH hypertension. In these studies, we identified the phenotypes of MnPO neurons involved in signaling to the PVN and selectively lesioned the neurons in the MnPO—PVN pathway. These lesions attenuated the sustained hypertension that develops during CIH.

CIH has been shown to significantly increase plasma advanced oxidative protein products (AOPPs), a marker for oxidative stress [31, 32]. Additionally, CIH significantly increases FosB staining, a neuronal marker of chronic activation of the activator protein-1 (AP-1) complex, in the MnPO, pre-sympathetic subregions of the PVN and RVLM, as well as upregulate AP-1 regulated genes including nitric oxide synthase 1 (NOS1) [31, 33, 34]. Angiotensin type 1a receptors (AT1aRs) has also been shown to be upregulated during CIH in the MnPO [31]. By blocking diurnal hypertension, we were also able to effectively block CIH-induced increases in circulating AOPPs and significantly attenuate FosB staining in the MnPO and in downstream pre-sympathetic subregions of the PVN and RVLM. Additionally, we were able to knockdown expression of AT1aRs and selectively lesion glutamatergic and NOS1-positive neurons, all of which have been shown to be significantly involved in CIH-hypertension [33, 35, 36].

Glutamatergic MnPO neurons have been shown to be involved in thermoregulatory processes [35]. We found that CIH had a significant effect on changes in diurnal thermoregulation compared to normoxic controls, suggesting that CIH may not only disrupt blood pressure regulation, but also thermoregulatory processes as well, and should be subject to address for future studies.

Sex as a Biological Variable

Only male rats were used in these projects due to protective effects induced by estrogen in females. In ***Specific Aim 1***, we induce thirst with ANG II, however, studies have shown estrogen attenuates the dipsogenic effects of centrally [37, 38] and peripherally [39] administered ANG II. Hormonally intact females drink significantly less to ANG II creating a possible floor effect in studies with the inhibiting G_i DREADDs. Sex differences in the responses to ANG II, however, would be interesting to address in future studies.

In ***Specific Aim 2***, we induce hypertension using CIH. Studies have shown that hormonally intact, non-pregnant female rats are protected against developing CIH hypertension [40]. Additionally, dysregulation of RAS and ANG II-driven increases in sympathetic outflow have been shown to play a major role in the development in hypertension [29, 30]; however, because hormonally intact females are less sensitive to the effects of ANG II than males [37, 39], this also provides an explanation for why intact females do not develop CIH hypertension. In this scenario, the females would not develop hypertension and could cause outcomes resulting from lesioning PVN-projecting MnPO neurons to be misinterpreted.

Perspectives

The studies in this project demonstrate how selective acute inhibition and chronic lesioning of excitatory neurons in the MnPO regulates activity at the protein, neuronal, behavioral, and physiological level. This study takes an important step in answering questions involving intercellular communication within the MnPO and how this produces

changes in projection terminals involved in regulating neuroendocrine and autonomic function. These studies also address how complex yet coordinated MnPO signaling must be in order to maintain body fluid homeostasis and regulation of blood pressure.

Additionally, mechanisms underlying the early development of sustained hypertension in CIH associated with OSA, a growing disease affecting the aging population, were conducted [18]. Performing these studies are pertinent to understanding how dysregulation of the MnPO—PVN pathway heavily contributes to the manifestation of CIH-induced hypertension, by providing a potential additional therapeutic target centrally for those suffering from OSA that may be resistant to the benefits of continuous positive airway pressure (CPAP) or other pharmacological treatments.

With the emergence of genetically-altered cell lines and transgenic models, these have become useful tools in learning how dysregulation can lead to the pathogenesis of diseases and important mechanistic processes that may be therapeutic. However, it is important to recognize that the genetically-based phenotypes are relative when considering environmental influence on function [41]. For example, activation of magnocellular neurons involves many different messengers other than oxytocin and vasopressin (i.e. peptides co-packaged with oxytocin and vasopressin, NO and prostaglandins produced *de novo*, and other neuromodulators) [42]. These implications also apply when considering neuronal phenotyping and the characterization of cells in regulatory regions part of a circuit. The results from the present studies begin to exemplify these stipulations by showing that neuronal characterization and functionality correlate in respect to the extra-, inter- and intra-cellular milieu (i.e. fluid osmolality, peptide and neurotransmitter release, etc.).

Future Directions

Preliminary electrophysiology studies conducted in this project using CNO-induced activation of CaMKIIa MnPO neurons expressing the G_q DREADD indicated potential recruitment activation of non G_q DREADD-expressing neurons (See Appendix). Although this is not ideal when attempting to study activity of only a specific phenotype of neurons, this has allowed us to begin studying how neuronal activation through G protein-coupled receptors can mediate the release of signaling molecules promoting inter- and intracellular crosstalk [43]. These studies are important to pursue, as they will continue to help us in understanding how the MnPO is able to integrate and signal in a discretionary manner to downstream brain regions that influence homeostatic physiological function.

Figure 1. *Schematic diagraming the proposed mechanism of how CNO-induced inhibition of MnPO CaMKIIa neurons attenuates thirst to peripherally administered ANG II and 3% NaCl.* Angiotensin II (ANG II) and 3% NaCl mimic the effects of extracellular and cellular dehydration, respectively, by inducing thirst. The median preoptic nucleus (MnPO) plays a key role in relaying signaling of ANG II and hypertonic challenges from the circumventricular organs, the subfornical organ (SFO) and organum vasculosum of the lamina terminalis (OVLT), to downstream thirst-driving brain regions. We show that the MnPO may be driving thirst from increased peripheral ANG II by signaling through the paraventricular nucleus (PVN), while increased peripheral hypertonic challenges (3% NaCl) may cause the MnPO to drive thirst through the lateral hypothalamus (LH). And that CNO-induced inhibition of MnPO can significantly attenuate drinking behavior and arginine vasopressin (AVP) release in response to either stimuli. SON, supraoptic nucleus; PVT, paraventricular nucleus of the thalamus (*adapted from Marciante, et al.* [44]).

Figure 1.

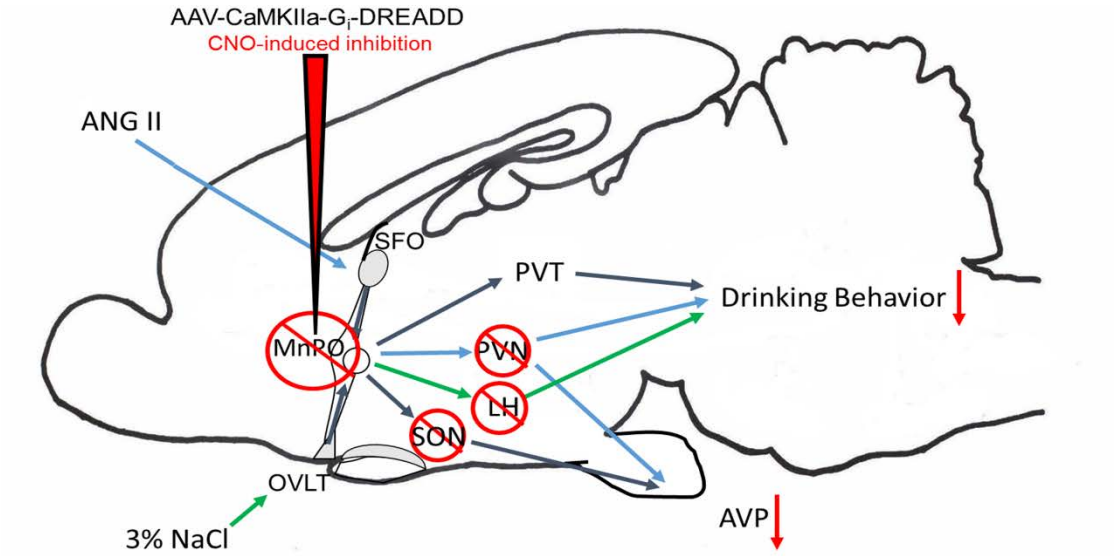
AAV-CaMKIIa-Gi-DREADD
CNO-induced inhibition
ANG II
SFO
PVT
Drinking Behavior
MnPO
PVN
LH
SON
OVLT
3% NaCl
AVP

Figure 2. *Schematic diagraming the proposed mechanism of how lesioning the MnPO—PVN pathway may block the sustained component of CIH-hypertension.* CIH causes upregulation through the hindbrain to increase sympathetic nerve activity (SNA). This can lead to upregulated plasma renin activity (PRA) and activation of the renin-angiotensin system, which results in a concomitant increase in angiotensin II and stimulates the sensory circumventricular organs—subfornical organ (SFO) and organum vasculosum of the lamina terminalis (OVLT)—that project to the median preoptic nucleus (MnPO) [23, 45, 46]. The MnPO has direct downstream effects that terminate in the paraventricular nucleus (PVN). Excitatory neurons in the PVN, particularly those in the parvocellular region, can excite neurons of the nucleus tract solitarius (NTS) and rostral ventrolateral medulla (RVLM), resulting in a vicious cycle from continuous elevated sympathetic outflow. By lesioning PVN-projecting MnPO neurons, persistent neural signaling is blocked, resulting in decreased excitation to the RVLM and NTS, thereby decreasing advanced oxidative protein products (AOPPs), SNA, PRA and therefore attenuated circulating angiotensin II. This is a proposed pathway for the initiation of hypertension and how lesioning MnPO neurons that project to the PVN can block the sustained component of CIH-hypertension. Abbreviation: AP, area postrema; CVLM, caudal ventrolateral medulla; IML, intermediolateral nucleus of the spinal cord; SON, supraoptic nucleus (adapted from Shell, et. al. [23]).

Figure 2.

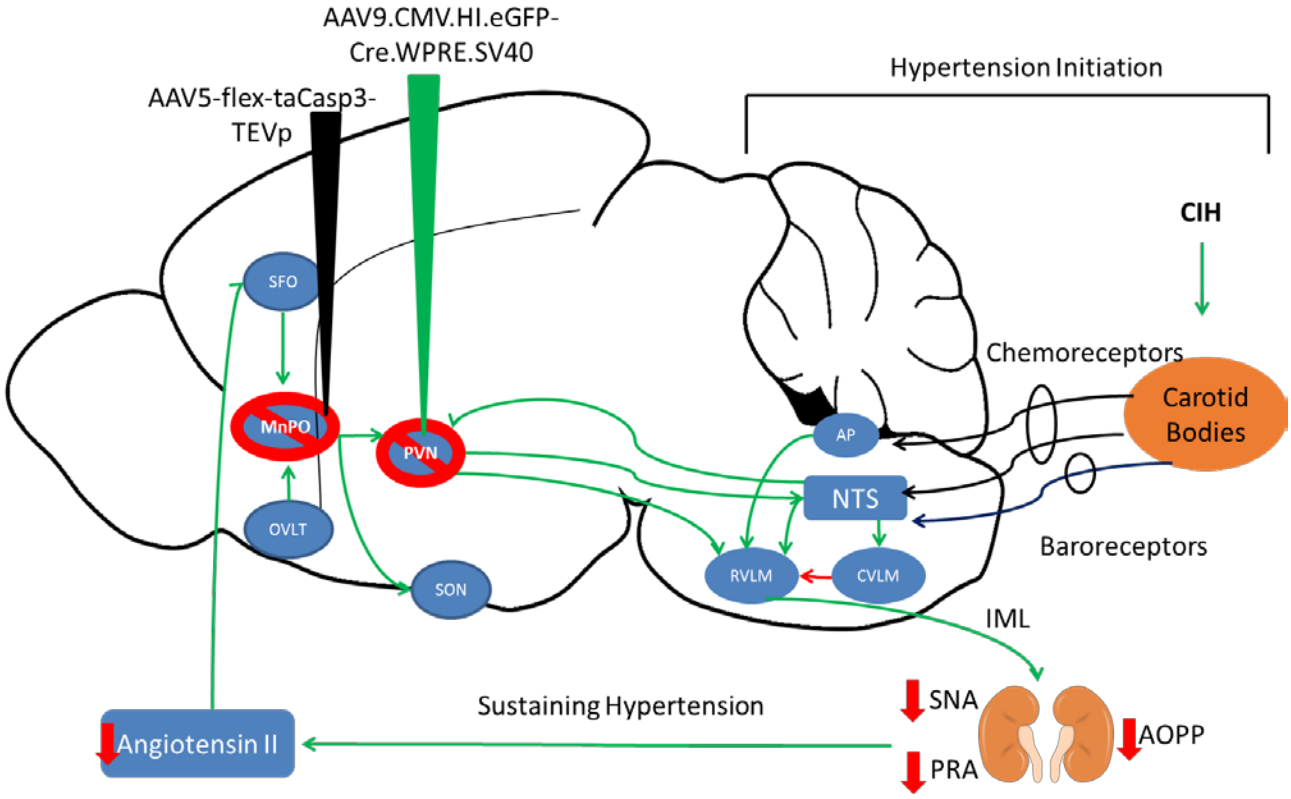
AAV9.CMV.HI.eGFP-Cre.WPRE.SV40
AAV5-flex-taCasp3-TEVp
Hypertension Initiation
CIH
SFO
MnPO
PVN
OVLT
SON
AP
NTS
RVLM
CVLM
Chemoreceptors
Carotid Bodies
Baroreceptors
IML
SNA
PRA
AOPP
Sustaining Hypertension
Angiotensin II

References

1. McKinley MJ, Denton DA, Ryan PJ, Yao ST, Stefanidis A, Oldfield BJ. From sensory circumventricular organs to cerebral cortex: neural pathways controlling thirst and hunger. J Neuroendocrinol 2019:e12689.

2. McKinley MJ, Yao ST, Uschakov A, McAllen RM, Rundgren M, Martelli D. The median preoptic nucleus: front and centre for the regulation of body fluid, sodium, temperature, sleep and cardiovascular homeostasis. Acta Physiol (Oxf) 2015;214:8-32. doi: 10.1111/apha.12487. Epub 12015 Apr 12481.

3. McKinley MJaAKJ. The Physiological Regulation of Thirst and Fluid Intake. News Physiol Sci 2004;19:1-6.

4. Menani JV, Vieira AA, Colombari DSA, De Paula PM, Colombari E, De Luca LA, Jr. Preoptic-Periventricular Integrative Mechanisms Involved in Behavior, Fluid-Electrolyte Balance, and Pressor Responses. In: De Luca LA, Jr., Menani JV, Johnson AK, eds. Neurobiology of Body Fluid Homeostasis: Transduction and Integration. Boca Raton (FL)2014.

5. Abbott SB, Machado NL, Geerling JC, Saper CB. Reciprocal Control of Drinking Behavior by Median Preoptic Neurons in Mice. J Neurosci 2016;36:8228-8237.

6. Allen WE, DeNardo LA, Chen MZ, et al. Thirst-associated preoptic neurons encode an aversive motivational drive. Science 2017;357:1149-1155.

7. Augustine V, Gokce SK, Lee S, et al. Hierarchical neural architecture underlying thirst regulation. Nature 2018;555:204-209.

8. Fitzsimons JT. Angiotensin, thirst, and sodium appetite. Physiol Rev 1998;78:583-686.

9. Fitzsimons JT. Angiotensin, thirst, and sodium appetite: retrospect and prospect. Fed Proc 1978;37:2669-2675.

10. Johnson AK, Cunningham JT. Brain mechanisms and drinking: the role of lamina terminalis-associated systems in extracellular thirst. Kidney Int Suppl 1987;21:S35-42.

11. Leib DE, Zimmerman CA, Poormoghaddam A, et al. The Forebrain Thirst Circuit Drives Drinking through Negative Reinforcement. Neuron 2017;96:1272-1281 e1274.

12. Mahon JM, Allen M, Herbert J, Fitzsimons JT. The association of thirst, sodium appetite and vasopressin release with c-fos expression in the forebrain of the rat after

intracerebroventricular injection of angiotensin II, angiotensin-(1-7) or carbachol. Neuroscience 1995;69:199-208.

13. Zimmerman CA, Lin YC, Leib DE, et al. Thirst neurons anticipate the homeostatic consequences of eating and drinking. Nature 2016;537:680-684.

14. Fitzsimons JT. The eighth J. A. F. Stevenson memorial lecture. Angiotensin II in the control of hypovolaemic thirst and sodium appetite. Can J Physiol Pharmacol 1980;58:441-444.

15. Oka Y, Ye M, Zuker CS. Thirst driving and suppressing signals encoded by distinct neural populations in the brain. Nature 2015;520:349-352.

16. Grob M, Drolet G, Mouginot D. Specific Na+ sensors are functionally expressed in a neuronal population of the median preoptic nucleus of the rat. J Neurosci 2004;24:3974-3984.

17. Stocker SD, Toney GM. Vagal afferent input alters the discharge of osmotic and ANG II-responsive median preoptic neurons projecting to the hypothalamic paraventricular nucleus. Brain Res 2007;1131:118-128.

18. Jean-Louis G, Zizi F, Clark LT, Brown CD, McFarlane SI. Obstructive sleep apnea and cardiovascular disease: role of the metabolic syndrome and its components. J Clin Sleep Med 2008;4:261-272.

19. Zhang W, Si LY. Obstructive sleep apnea syndrome (OSAS) and hypertension: pathogenic mechanisms and possible therapeutic approaches. Ups J Med Sci 2012;117:370-382.

20. Mozaffarian D BE, Go AS, Arnett DK, Blaha MJ, Cushman M, et al. Heart disease and stroke statistics—2015 update: a report from the American Heart Association. Circulation 2015;131.

21. Fletcher EC, Orolinova N, Bader M. Blood pressure response to chronic episodic hypoxia: the renin-angiotensin system. J Appl Physiol 2002;92:627-633.

22. Mifflin S, Cunningham JT, Toney GM. Neurogenic mechanisms underlying the rapid onset of sympathetic responses to intermittent hypoxia. J Appl Physiol (1985) 2015;119:1441-1448.

23. Shell B, Faulk K, Cunningham JT. Neural Control of Blood Pressure in Chronic Intermittent Hypoxia. Curr Hypertens Rep 2016;18:19.

24. Sharpe AL, Calderon AS, Andrade MA, Cunningham JT, Mifflin SW, Toney GM. Chronic intermittent hypoxia increases sympathetic control of blood pressure: role of neuronal activity in the hypothalamic paraventricular nucleus. Am J Physiol Heart Circ Physiol 2013;305:H1772-1780.

25. Cunningham JT, Knight WD, Mifflin SW, Nestler EJ. An Essential role for DeltaFosB in the median preoptic nucleus in the sustained hypertensive effects of chronic intermittent hypoxia. Hypertension 2012;60:179-187.

26. Knight WD, Saxena A, Shell B, Nedungadi TP, Mifflin SW, Cunningham JT. Central losartan attenuates increases in arterial pressure and expression of FosB/DeltaFosB along the autonomic axis associated with chronic intermittent hypoxia. Am J Physiol Regul Integr Comp Physiol 2013;305:R1051-1058.

27. Bader M, Ganten D. Update on tissue renin-angiotensin systems. J Mol Med (Berl) 2008;86:615-621.

28. Blaine EH, Cunningham JT, Hasser EM, Dale WE, Li Q, Sullivan M. Angiotensin hypertension. Clin Exp Pharmacol Physiol Suppl 1998;25:S16-20.

29. Deshotels MR, Xia H, Sriramula S, Lazartigues E, Filipeanu CM. Angiotensin II mediates angiotensin converting enzyme type 2 internalization and degradation through an angiotensin II type I receptor-dependent mechanism. Hypertension 2014;64:1368-1375.

30. Xu J, Sriramula S, Xia H, et al. Clinical Relevance and Role of Neuronal AT1 Receptors in ADAM17-Mediated ACE2 Shedding in Neurogenic Hypertension. Circ Res 2017;121:43-55.

31. Brent Shell GF, T. Nedungadi, Lei Wang, Alexandria Marciante, Brina Snyder, Rebecca Cunningham, and J. Cunningham. Angiotensin Type 1a Receptors in the Median Preoptic Nucleus Support Intermittent Hypoxia-Induced Hypertension. American Journal of Physiology - Regulatory, Integrative and Comparative Physiology 2019.

32. Snyder B, Shell B, Cunningham JT, Cunningham RL. Chronic intermittent hypoxia induces oxidative stress and inflammation in brain regions associated with early-stage neurodegeneration. Physiol Rep 2017;5.

33. Cunningham JT, Knight WD, Mifflin SW, Nestler EJ. An essential role for ΔFosB in the median preoptic nucleus in the sustained hypertensive effects of chronic intermittent hypoxia. Hypertension 2012;60:179-187.

34. Knight WD, Little JT, Carreno FR, Toney GM, Mifflin SW, Cunningham JT. Chronic intermittent hypoxia increases blood pressure and expression of FosB/DeltaFosB in central autonomic regions. Am J Physiol Regul Integr Comp Physiol 2011;301:R131-139.

35. Abbott SBG, Saper CB. Median preoptic glutamatergic neurons promote thermoregulatory heat loss and water consumption in mice. J Physiol 2017;595:6569-6583.

36. Llewellyn T, Zheng H, Liu X, Xu B, Patel KP. Median preoptic nucleus and subfornical organ drive renal sympathetic nerve activity via a glutamatergic mechanism within the paraventricular nucleus. Am J Physiol Regul Integr Comp Physiol 2012;302:R424-432.

37. Santollo J, Torregrossa AM, Daniels D. Sex differences in the drinking response to angiotensin II (AngII): Effect of body weight. Horm Behav 2017;93:128-136.

38. Tanaka J, Kariya K, Miyakubo H, Sakamaki K, Nomura M. Attenuated drinking response induced by angiotensinergic activation of subfornical organ projections to the paraventricular nucleus in estrogen-treated rats. Neurosci Lett 2002;324:242-246.

39. Fregly MJ. Effect of chronic treatment with estrogen on the dipsogenic response of rats to angiotensin. Pharmacol Biochem Behav 1980;12:131-136.

40. Hinojosa-Laborde C, Mifflin SW. Sex differences in blood pressure response to intermittent hypoxia in rats. Hypertension 2005;46:1016-1021.

41. Leng G, Russell JA. The osmoresponsiveness of oxytocin and vasopressin neurones: Mechanisms, allostasis and evolution. J Neuroendocrinol 2018:e12662.

42. Brown CH, Bains JS, Ludwig M, Stern JE. Physiological regulation of magnocellular neurosecretory cell activity: integration of intrinsic, local and afferent mechanisms. J Neuroendocrinol 2013;25:678-710.

43. Christopoulos A, El-Fakahany EE. The generation of nitric oxide by G protein-coupled receptors. Life Sci 1999;64:1-15.

44. Marciante A.B. WLA, Farmer G.E., Cunningham J.T. Selectively inhibiting the median preoptic nucleus attenuates angiotensin II and hyperosmotic-induced drinking behavior and vasopressin release in adult male rats. eNeuro 2019.

45. Foster GE, Hanly PJ, Ahmed SB, Beaudin AE, Pialoux V, Poulin MJ. Intermittent hypoxia increases arterial blood pressure in humans through a Renin-Angiotensin system-dependent mechanism. Hypertension 2010;56:369-377.

46. Zalucky AA, Nicholl DD, Hanly PJ, et al. Nocturnal hypoxemia severity and renin-angiotensin system activity in obstructive sleep apnea. Am J Respir Crit Care Med 2015;192:873-880.

CHAPTER V: APPENDIX

CNO-INDUCED ACTIVATION OF G_Q DREADD MNPO NEURONS CAUSES RECRUITMENT ACTIVATION OF NEIGHBORING, UNLABELED CELLS WITH NO

Alexandria B. Marciante, George E. Farmer and J. Thomas Cunningham

The University of North Texas

Health Science Center at Fort Worth

3500 Camp Bowie Blvd.

Fort Worth, TX 76107

to be submitted to Journal of Neuroscience, 2019.

Materials and Methods

Animals

Adult male Sprague-Dawley rats (250-300 g bw), Charles River Laboratories, Wilmington, MA) were used for all experiments. All rats were individually housed in a temperature-controlled (25 °C) room on a 12:12 light/dark cycle with light onset at 0700 h. Food and water was available *ad libitum* except on the day of perfusions. Rats were weighed daily and their food and water intake monitored. Experiments were performed according to the National Institute of Health *Guide for the Care and Use of Laboratory Animals* (8^{th} edition) using protocols approved by the University of North Texas Health Science Center Institutional Animal Care and Use Committee.

Microinjection Surgeries

Stereotaxic injections were performed as previously described (Cunningham et al. 2012). Stereotaxic coordinates for MnPO microinjections were based on the atlas of Paxinos and Watson (microinjector angled at 8º from medial to lateral to avoid the septum, 0.9 mm lateral, 6.7 mm ventral from bregma) (Paxinos 1986). Each rat was anesthetized with 2% isoflurane and placed in a Kopf stereotaxic head frame (David Kopf Instruments, Tujunga, CA). After the surface of the skull was exposed, it was leveled between bregma and lambda (Paxinos 1986). A burr hole was then drilled at the measured site and a 30-gauge stainless steel injection needle was lowered to the MnPO, where 200-300 nL of the excitatory DREADD (AAV5-CaMKIIa-hM3D(G_q)-mCherry) or control (AAV5-CaMKIIa-mCherry-Cre) virus (both from the UNC VectorCore) was delivered at a rate of 200 nL/min. The injector was connected to a Hamilton 5 µL syringe (#84851, Hamilton, Reno, NV) by calibrated polyethylene tubing

that was used to determine the injection volume. The injector remained in place for 5 minutes to allow for absorption and was then slowly withdrawn. Gel foam was packed in to the drilled hole in the cranium. An absorbable antibiotic suture was used to close the incision site and minimize post-surgical infection. Each rat was given carprofen (Rimadyl, Bio-Serv, 1 mg) orally to minimize pain following surgery. Rats were allowed two weeks for recovery and viral transduction.

Fos Studies

In order to determine how effective G_q DREADD-induced activation of MnPO neurons was, clozapine-*N*-oxide (CNO, Tocris Bioscience, Minneapolis, MN) was intraperitoneally (ip) injected to induce Fos expression. Rats were either treated with CNO (10 mg/kg bw) or vehicle (VEH). CNO was dissolved in DMSO and diluted in 0.9% saline (1:4) to a working concentration of 27 mM. After injections, rats were denied food and water access for 90 minutes.

Perfusions—Tissue and Body Fluid Collection

Animals were anesthetized using 100 mg/kg inactin (Sigma-Aldrich) ip. Blood was collected by cardiac puncture (3 mL) immediately preceding the perfusion in order to measure plasma osmolality and hematocrit. Rats were transcardially perfused first with phosphate buffer solution (PBS) and then 4% paraformaldehyde (PFA) in PBS. Brains were removed and fixed overnight in 4% PFA before being dehydrated in 30% sucrose in PBS.

Immunohistochemistry (IHC)

Forty µm coronal sections of each previously perfused brain were cut using a cryostat (Leica). Three sets of serial sections were separately collected in cryoprotectant and stored at -20 ^{o}C until they were processed for immunohistochemistry. All antibodies were diluted to working concentration in PBS diluent (0.25% Triton, 3% horse serum, and 96.75% PBS). One set of serial sections from brains injected with DREADD or control virus were stained for Fos (sc-253-G, goat polyclonal anti-c-Fos antibody, Santa Cruz Biotechnology, 1:1000). The sections were incubated in the solution containing the primary antibody for 48 hours at 4^{o}C. After 48 hours, sections were washed using PBS and transferred to a secondary antibody (BA-9500, biotinylated anti-goat, Vector Laboratories) for DAB reaction and labeling as previously described (Cunningham et al. 2012; Grindstaff et al. 2000). After the DAB reaction, the sections were washed and placed in the primary antibody diluted in PBS (ab167453, rabbit polyclonal anti-mCherry, Abcam 1:500) and incubated for an additional 48 hr followed by incubation with a CY3 conjugated anti-rabbit antibody (711-165-152, Jackson ImmunoResearch, West Grove, PA) for 4-5 hr. The sections were then mounted on gelatin-coated slides, dried, and coverslipped with Permount (Fisher Scientific) for imaging. Microinjections that missed the MnPO and were injected into the diagonal band of Broca (DBB), the region rostral to the MnPO, were used as an additional control for Fos studies.

A separate set of sections were stained for NOS1 (1:1000, sc5302, Santa Cruz Biotechnology) to determine MnPO-PVN projecting neuronal phenotype. After 48 hours, sections were washed using PBS and transferred to a CY2 conjugated anti-mouse

secondary antibody (711-165-151, Jackson ImmunoResearch). The sections were then mounted on gelatin-coated slides, dried, and coverslipped with Prolong Diamond Mounting Medium for imaging.

In Situ Hybridization (ISH)

ISH experiments detecting CaMKIIa mRNA were performed to determine transduction efficiency of the DREADD virus. A separate group of rats from those used for immunohistochemistry were anesthetized two weeks after microinjection surgery using 100 mg/kg inactin (Sigma-Aldrich) ip and transcardially perfused first with RNase-free PBS and then 4% paraformaldehyde (PFA). Brains were removed and dehydrated in RNase-free 30% sucrose. Twenty µm coronal sections of each brain were cut using a cryostat (Leica). Four to six sets of serial MnPO sections were collected in RNase-free PBS, mounted on to Superfrost Plus Gold microscope slides (Thermo Fisher Scietific Inc., Waltham, MA, USA), and left at room temperature for ~2 h and then stored at -80ºC until use in ISH experiments. All reagents used for ISH experiments were purchased from Advanced Cell Diagnostics (Newark, CA, USA). ISH was performed for CaMKIIa detection (reference number: 487559-C2) using a chromogenic assay (reference number: 322310). Experimental protocols were performed according to the manufacturer described in RNAscope® 2.5 HD Detection Reagent – BROWN User Manual PART2 (Document Number 322310-USM, Advanced Cell Diagnostics).

After ISH experiments, mCherry immunohistochemistry was performed due to quenching of the fluorescence by the chromogenic assay. Brain sections were rinsed 3 times in PBS, treated with a blocking solution at room temperature for 1 h, and then

incubated with rabbit anti-mCherry primary antibody (1:500 in 10% heat inactivated horse serum and 0.1% Triton X-100 in PBS, (Sigma Aldrich, St. Louis, MO, USA) at 4 °C for overnight. The next day, brain sections were rinsed with PBS and incubated with a CY3-conjugated donkey anti-rabbit secondary antibody (1:500 in blocking solution, Jackson ImmunoResearch, West Grove, PA, USA) at room temperature for 1 h. Slides were cover-slipped using ProLong® Diamond Antifade Mountant (Life technologies, Carlsbad, CA, USA).

Imaging and Analysis of Brain Tissue

Sections were examined using light microscopy to identify Fos-positive cells. Excitation wavelengths of 550-570 nm were used for emission of mCherry immunofluorescence. Images were captured using an epifluorescent microscope (Olympus BX41, Olympus, Center Valley, PA, USA) equipped with a digital camera (Olympus DP70) to image sections. Care was taken to ensure that sections included in this study were sampled from the same plane for each brain region. Co-localization was determined by quenching produced in cells with nuclear fos staining and cytosolic mCherry staining, as previously described (Grindstaff et al. 2000). Brightfield and fluorescent images were merged for analysis of the MnPO using ImageJ (NIH). Fos-positive neurons and their co-localization in the MnPO was determined blind to experimental conditions of the subjects.

Electrophysiology

Slice Preparation. Hypothalamic slices containing the MnPO were prepared as previously described (Farmer et al. 2018). Rats were anesthetized with 2% isoflurane and decapitated. Coronal slices (300 µm) containing the MnPO were cut using a Microslicer DTK Zero 1 (Ted Pella, Inc.) in ice cold (0-1° C), oxygenated (95% O_2, 5% CO_2) cutting solution consisting of (in mM): 3.0 KCl, 1.0 $MgCl_2$-$6H_2O$, 2.0 $CaCl_2$, 2.0 $MgSO_4$, 1.25 NaH_2PO_4, 26 $NaHCO_3$, 10 D-Glucose, 206 Sucrose (300 mOsm, pH 7.4). Slices were incubated at room temperature (22 °C) in oxygenated (95% O_2, 5% CO_2) artificial cerebrospinal fluid (aCSF) containing (in mM): 126 NaCl, 3.0 KCl, 2.0 $CaCl_2$, 2.0 $MgSO_4$, 1.25 NaH_2PO_4, 26 $NaHCO_3$, 10 and D-Glucose (300 mOsm, pH 7.4) for a minimum of 1 hour prior to recording.

Electrophysiology Protocols. These experiments were conducted to determine if CNO and DREADD-induced activation caused off-target effects that would influence the local circuitry. Slices containing the MnPO were transferred to a submersion recording chamber and superfused with aCSF (31 $\pm$ 1°C). Slices were visualized using an upright epifluorescent microscope (BX50WI, Olympus, Center Valley, PA) with differential interference contrast optics.

Whole cell (intracellular) recordings were performed using voltage clamp mode, for the first set of experiments, and current clamp mode. Recordings were obtained using borosilicate glass micropipettes (3-8 MΩ). The internal pipette solution consisted of (in mM): 145 K-gluconate, 10 HEPES, 1.0 EGTA, 2.0 Na_2ATP, and 0.4 NaGTP (300 mOsm, pH 7.2). A tight gigaohm seal on MnPO neurons were made and had an access resistance of less than 25 MΩ. Neurons were slightly depolarized with current injection to generate a regular spiking activity (range, -50 to -40 mV), as previously described

(Grob, Drolet, and Mouginot 2004). Loose patch voltage clamp (extracellular) recordings were obtained using borosilicate glass micropipettes (1-3 MΩ) containing aCSF as the internal solution. Voltage was clamped at 0 mV to measure changes in current.

Electrophysiological signals (voltage and current) were amplified and digitized using Multiclamp 200B and Digidata 1440A, respectively (Axon Instruments). Signals were filtered at 2 KHz and digitized at 10 KHz. Recordings from MnPO neurons were made by targeting both mCherry-expressing and non mCherry-expressing neurons in slices prepared from rats injected with the AAV. Electrophysiological signals were analyzed using 10s bins.

In the first set of experiments, intracellular or extracellular recordings were performed on MnPO neurons. Baseline membrane potential (for intracellular recordings) or action potential firing (for extracellular recordings) was recorded for 5 minutes. Then, CNO (10 µM) was focally applied for 10 s using a Pico spritzer (8 psi) and a patch pipette containing the drug placed 150-200 µm upstream of the recording electrode followed by an additional 10 minutes of recording. CNO was dissolved in DMSO, diluted in aCSF to final concentration of 10 µM (< 0.01% DMSO) and stored at -20°C until use in experiments.

In the second set of experiments, Nω-nitro-L-arginine (L-NNA, Cayman Chemical Company, Ann Arbor, MI) was used to determine if activating G_q DREADD-labeled neurons was causing release of nitric oxide (NO) and recruitment activation of neighboring, unlabeled neurons (G_q DREADDx). In these studies, brain slices were bath applied for 5 min with L-NNA (100 µM). Then, CNO (10 µM) was focally applied for 10 s using a Pico spritzer (8 psi) with a patch pipette containing the drug placed 150-200 µm

upstream of the recording electrode followed by an additional 10 min of recording. After each cell was exposed to CNO alone (5 min aCSF, 10 s CNO focal application, 10 min aCSF) the same protocol was repeated with the addition of 5 min L-NNA (100 µM). L-NNA was dissolved in aCSF and stored at a concentration of 5 mM at -20°C. L-NNA was diluted in aCSF its final working concentration of 100 µM immediately before it was used.

In the third set of experiments, bovine hemoglobin (Hb, Sigma-Aldrich, St. Louis, MO) dissolved in aCSF was bath-applied to confirm observed effects to be attributed to diffusible NO. In these studies, brain slices were bathed for 3 min in aCSF, 3 min in CNO (500 nM), 3 min in CNO (500 nM) + Hb (20 µM), 3 min in Hb (20 µM), and finally a 3 min recovery in aCSF. The Hb was prepared and stored in sterile water at a concentration 10 mM at -20°C until used for experiments, as previously described (Di et al. 2003).

Statistics

Immunohistochemical analysis of Fos staining used one-way ANOVA followed by Student-Newman-Keuls (SNK) post-hoc test. Electrophysiology data were analyzed for differences in baseline activity using either Student *t*-test or two-way repeated measures (RM) ANOVA with SNK post-hoc analysis. All other variables (changes in firing or instantaneous frequency, membrane potential, baseline current, etc.) were analyzed using two-way mixed effects ANOVA with SNK post-hoc analysis. Statistical significance was defined as an α level of 0.05 and exact p-values are reported. Values

are reported as mean ± SEM. All statistics were performed in SigmaPlot.v.12.0 (Systat Software, San Jose, CA).

Results

CNO-induced Activation of G_q DREADD and Fos Staining

Fos studies were conducted in order to determine effects of CNO and activation of G_q DREADD neurons at the injection site. We also wanted to identify if regions that receive afferent projections from the MnPO would be affected by activation of the transduced CaMKIIa MnPO neurons. Rats with microinjections that were located in the DBB were analyzed separately and had their own control groups. The treatment groups were rats injected with the control (CTRL) or G_q DREADD virus into the DBB or MnPO and treated with vehicle for CNO (VEH) or CNO. Injections sites were verified by identifying mCherry expression (Figure 1).

In rats injected in the DBB (Figure 1A, n = 5-6 rats each group, 2-3 tissue sections per rat per region), there was a significant effect of virus and treatment on Fos expression in the DBB ($F(3, 20) = 24.963$, $p < 0.001$, one-way ANOVA). Fos staining in the DBB of rats injected with Gq DREADD and treated with CNO was significantly increased as compared all of the other groups (Figure 2A & 2B; vs. G_q DREADD + VEH; vs. CTRL + VEH; vs. CTRL + CNO; all $p < 0.001$, SNK). The perinuclear zone (PNZ) of the supraoptic nucleus (SON) is a region downstream of the DBB and receives projections from the DBB. There was also a significant effect of virus and treatment on Fos in the PNZ of the SON ($F(3, 19) = 12.554$, $p < 0.001$, one-way ANOVA). Fos staining in the PNZ of the SON also was significantly increased in G_q DREADD injected

rats treated with CNO as compared to all other groups (Figure 2A & 2B; vs. CTRL + VEH; vs. CTRL + CNO; vs. G_q DREADD + VEH; all $p < 0.001$, SNK).

Based on DBB afferent projections, we would not expect to see Fos staining in the MnPO or paraventricular nucleus (PVN) during CNO-induced activation of the DBB. Additionally, the PNZ of the SON synapses onto the SON to inhibit its activity; therefore, we would not expect to see increased Fos staining in the SON either (Cunningham, Nissen, and Renaud 1994). CNO-induced activation did not cause a significant increase in Fos staining in the MnPO, SON or PVN (Figure 2B & 2C). In rats injected with the control vector, CNO treatments did not significantly influence Fos staining as compared to VEH treatments (Figure 2B & 2C).

In rats injected in the MnPO (Figure 1B, n = 6-7 rats each group, 2-3 tissue sections per rat per region), there was significant effect of virus and treatment on Fos expression in the MnPO ($F(3, 21) = 23.039$, $p < 0.001$, one-way ANOVA). Fos staining in the MnPO was significantly increased in G_q DREADD injected rats treated with CNO as compared to all other treatment groups (Figure 3A and 3B; vs. CTRL + VEH; vs. CTRL + CNO; vs. G_q DREADD + VEH; all $p < 0.001$, SNK). There were no significant differences between the CTRL + VEH or CNO, or G_q DREADD + VEH groups. Fos staining was also measured in downstream regions, including the SON, PVN and RVLM (Figure 3A and B). The effects of CNO on Fos expression in the SON was similar to what was observed in MnPO ($F(3, 21) = 23.976$, $p < 0.001$, one-way ANOVA. The SON of G_q DREADD rats treated with CNO had significantly elevated Fos staining compared to all other treatment groups (Figure 3A & 3B; vs. CTRL + VEH; vs. CTRL + CNO; vs.

G_q DREADD + VEH; all $p < 0.001$; SNK). ($F(3, 21) = 25.576$, $p < 0.001$, one-way ANOVA).

Analysis of the subregions within the PVN — posterior magnocellular (PM), dorsal parvocellular (DP), medial parvocellular (MP), and ventral lateral parvocellular (VLP) — showed G_q DREADD injected rats treated with CNO had significantly increased Fos expression in all subregions of the PVN as compared to all other treatment groups Figure 3A & 3C; all $P < 0.05$; one-way ANOVA and SNK). There were no significant differences between the CTRL + VEH or CNO, or G_q DREADD + VEH groups.

In the MnPO injected groups, there was no significant effect of virus and treatment on Fos staining in the PNZ between any of the treatment groups ($F(3, 21) = 2.114$, $p = 0.129$, one-way ANOVA). Additionally, Fos staining was analyzed in the rostral ventral lateral medulla (RVLM), a region containing sympathetic premotor neurons that are indirectly connected to the MnPO. There was a significant effect of virus and treatment on Fos staining in the RVLM ($F(3, 21) = 17.103$, $p < 0.001$, one-way ANOVA). In rats injected with Gq DREADD in the MnPO, CNO treatment significantly increased Fos staining in the RVLM as compared to all of the other treatment groups (Figure 3B; all $P < 0.001$, SNK). There were no significant differences between the CTRL + VEH or CNO, or G_q DREADD + VEH groups.

DREADDs have a high transduction efficiency of CaMKIIa neurons that also co-localize with NOS1 neurons

In order to determine transduction efficiency of DREADD virus containing a CaMKIIa promotor, co-localization of CaMKIIa RNA message detected using ISH and mCherry reporter from the DREADD virus was analyzed (Figure 4A). In the MnPO, 91.31 ± 1.39% (n = 5 rats, 2-3 MnPO sections) of neurons expressing CaMKIIa mRNA were also mCherry positive, while 98.27 ± 2.27% of mCherry positive neurons also expressed CaMKIIa mRNA. There was also a high degree of colocalization with NOS1. Of the MnPO neurons that were mCherry positive, 80.12 ± 6.94% (n = 5 rats, 2-3 MnPO sections) also expressed NOS1 (Figure 4B). In previous studies, we have also reported that 89.17 ± 1.32% of DREADD-transfected MnPO neurons co-localize with vesicular glutamatergic transporter 2 (vGLUT2) (Marciante A.B. 2019).

CNO-induced activation of G_q DREADD MnPO neurons increases firing frequency and depolarization events that also affect neighboring, unlabeled neurons

Firing Frequency

Loose-patch (extracellular) recordings were obtained from neurons in slices from rats injected in the MnPO with either the control vector (CTRL, n = 14 from 3 rats, 2 recording slices per rat) or G_q DREADD (G_q DREADD, n = 13 from 6 rats, 2 recording slices per rat). These cells were identified by the expression of mCherry (Figure 5A). In slices from rats injected in MnPO with the G_q DREADD virus, recordings were obtained from neurons that do not express mCherry (G_q DREADDx, n = 13, from 10 rats, 2 recording slices per rat) as an additional control for possible off target effects of CNO.

There were no significant differences in baseline activity ($F(2, 37) = 0.271$, $p = 0.764$, two-way RM ANOVA) among the three defined neuronal phenotypes (Figure 5B

& 5C; CTRL: 3.18 ± 0.69 Hz; G_q DREADD: 3.27 ± 0.47 Hz; G_q DREADDx: 3.69 ± 0.64 Hz). In neurons transfected with the control vector, CNO did not influence their activity (14/14 cells, Figure 5B & 5C). However, focal CNO application did significantly increase firing frequency of not only G_q DREADD MnPO neurons (13/14 cells), but also G_q DREADDx MnPO (13/24) neurons (Figure 5B and C, $F(2, 111) = 6.315$, $p < 0.003$, two-way mixed effects ANOVA). The time of peak response of G_q DREADD neurons was 121.4 ± 26.4 s with an effect duration of 312.9 ± 52.9 s before firing frequency returned to baseline. The time to peak response of G_q DREADDx neurons was 188.5 ± 56.5 s with an effect duration of 310.8 ± 40.3 s before firing frequency returned to baseline. G_q DREADD and G_q DREADDx MnPO neurons both exhibited significant increases in firing frequency following CNO focal application compared to CTRL neurons (Figure 5B & 5C; $p = 0.031$ and $p = 0.008$, respectively; SNK).

Membrane Potential

Based on the loose-patch data, whole cell current-clamp (intracellular) recordings were conducted to determine the membrane effects of G_q DREADD MnPO neurons influences unlabeled (G_q DREADDx) neurons. Using a similar protocol, current clamp recordings were obtained from mCherry-positive neurons in slices from rats injected in the MnPO with either the CTRL vector (n = 4 from 3 rats, 2 recording slices each rat) or G_q DREADD (n = 4 from 3 rats, 2 recording slices each rat). Current-clamp recordings were also made from cells not expressing mCherry in slices from rats injected with the Gq DREADD (G_q DREADDx; n = 5 from 5 rats, 2 recording slices each rat). Baseline membrane potential was not different among neurons from the different treatment

groups prior to CNO application (Figure 5D and E, F(18, 129) = 1.347, p = 0.179, two-way RM ANOVA; CTRL: -42.7 ± 5.1 mV; G_q DREADD: -43.6 ± 5.4 mV; G_q DREADDx: -43.0 ± 5.6 mV). Focal CNO did not influence the resting membrane potential of mCherry positive cells in slices from CTRL injected rats (Figure 5D & 5E; 4/4 cells). CNO was associated with membrane depolarization in mCherry-positive (Gq DREADD, 4/4 cells) and unlabeled cells (Gq DREADDX, 5/6 cells) neurons from in slices from rats injected in the MnPO with Gq DREADD (Figure 5D and 5E; F(2, 25) = 9.541, p = 0.001, two-way mixed effects ANOVA). Post-hoc analysis revealed that CNO-induced membrane potential depolarization was significant in G_q DREADD MnPO ($p < 0.001$, SNK) and G_q DREADDx MnPO neurons ($p = 0.006$, SNK) as compared to their own resting membrane potentials. There was no significant differences between baseline and post-CNO membrane potential in neurons from CTRL ($p = 0.681$, SNK).

L-NNA attenuates CNO-induced G_q DREADD activation of G_q DREADDx neurons

Because of these unexpected off-target effects of CNO-induced in G_q DREADDx neurons and the expression of NOS1 in mCherry-positive MnPO neurons, we hypothesized nitric oxide (NO) may be released from G_q DREADD neurons and stimulating the G_q DREADDx neurons. This hypothesis was tested using Nω-nitro-L-arginine (L-NNA), a specific competitive inhibitor of NOS.

Firing Frequency

The effects of focal CNO application were tested in the presence of aCSF bath solution or the same aCSF with L-NNA (50 µM). In some of the experiments, cells were

tested using both bath solutions but most of the data were obtained from cells that were exposed to either aCSF or L-NNA + aCSF. Loose-patch (extracellular) recordings were obtained from 6 cells from CTRL preparations (2 rats), 5 cells from G_q DREADD preparations (4 rats), and 11 G_q DREADDx cells (4 rats) where CNO was tested with aCSF. As reported previously, there were no differences in spontaneous firing frequency among the different groups and CNO (10 µM, 10 s) increased the activity of Gq DREADD and Gq DREADDX cells (Figure 6A). In experiments with 50 µM L-NNA added to the bath solution, the same dose of CNO increased the activity of Gq DREADD cells (n= 7 from 4 rats) but had no effect on the activity of CRTL cells (n = 6 from 2 rats) or Gq DREADDx cells (n = 18 from 4 rats; Figure 6A and B). The addition of L-NNA to the bath solution did not affect spontaneous firing frequency in any of the treatment groups (aCSF 4.8 $\pm$ 0.5 Hz; L-NNA 4.5 $\pm$ 0.7 Hz; $t(51) = 0.370$, $p = 0.713$, Student *t*-test). Overall, there was a significant effect of virus ($F(2, 47) = 18.852$, $p < 0.001$, two-way mixed effects ANOVA) and aCSF or L-NNA bath application ($F(1, 47) = 7.586$, $p = 0.008$, two-way mixed effects ANOVA) on change in firing frequency of MnPO neurons. During the aCSF protocol, CNO induced significant increases in G_q DREADD (12/12 cells) firing frequency compared to G_q DREADDx (11/21 cells; $p = 0.039$, SNK) and CTRL (12/12 cells; $p < 0.001$, SNK) neurons. G_q DREADDx neurons also had significantly increased change in firing frequency compared to CTRL ($p = 0.009$, SNK).

During the L-NNA protocol, however, the effects of CNO on G_q DREADDx neurons (18/24 cells) neurons were blunted and was not different from CTRL ($p = 0.0374$, SNK). Post-hoc analysis revealed that L-NNA had a significant effect on G_q

DREADDx neurons compared to aCSF bath application post-CNO focal application ($p < 0.001$, SNK), however, there was no effect of L-NNA compared to aCSF post-CNO focal application on CTRL ($p = 0.406$, SNK) or G_q DREADD ($p = 0.333$, SNK) neurons.

Membrane Potential

Whole cell current-clamp (intracellular) recordings were performed to measure changes in membrane potential using the same drug application protocols with either aCSF or 50 µM L-NNA (50 µM) + aCSF bath solutions. There was no significant difference in membrane potential of neurons exposed to baseline aCSF (-49.7 $\pm$ 2.0 mV) or baseline L-NNA (-46.9 $\pm$ 1.9 mV) bath application ($t(29) = -1.006$, $p = 0.323$, Student's *t*-test). In aCSF bath solution, CNO (10 µM, 10 s) depolarized Gq DREADD (n= 4 from 5 rats) and Gq DREADDx cells (n = 9 from 5 rats) but did not influence the membrane potential of control cells (n = 4 from 2 rats; Figure 6C). When L-NNA was added to the bath solution, the same dose of CNO produced membrane depolarization only in Gq DREADD cells (n= 4 from 5 rats) and not in GqDREADDx cells (n = 6 from 5 rats) or CTRL cells (n = 4 from 2 rats; Figure 6C and 6D).

When comparing changes in baseline membrane potential to the effects of CNO-induced G_q DREADD activation, there were significant effects dependent on virus (Figure 6C and D; $F(2, 27) = 6.602$, $p = 0.005$, two-way mixed effects ANOVA). As observed previously during aCSF bath application and focally applied CNO, G_q DREADD (7/8 cells) neuron membrane potential was significantly increased compared to CTRL (8/8 cells; $p = 0.039$, SNK) neurons. Additionally, G_q DREADDx (11/13 cells)

membrane potential was also significantly increased compared to CTRL neurons (p = 0.050, SNK), post-CNO application.

However, during the L-NNA protocol, the observed increase in G_q DREADDx (6/10 cells) membrane potential from CNO-induced activation of G_q DREADD neurons was blocked compared to changes induced during aCSF bath application (p = 0.034, SNK) and no longer differed from CTRL neurons (p = 0.695, SNK). G_q DREADD and CTRL neurons were unaffected by whether bath application was aCSF or L-NNA (p = 0.713 and p = 0.787, respectively; SNK).

Hemoglobin blocks CNO-induced G_q DREADD activation of G_q DREADDx neuronal activity

Based on data collected using L-NNA to block recruitment activation of G_q DREADDx neurons during CNO-induced activation of G_q DREADD neurons, NO is thought to be the most likely neurotransmitter involved, but we wanted to determine that NO was directly affecting activity of G_q DREADDx neurons. In order to verify the hypothesis that NO is directly affecting G_q DREADDx neurons and not an indirect NO-mediated mechanism, additional loose-cell voltage clamp (Figure 7) and whole cell current clamp (Figure 8) recordings were conducted using hemoglobin (Hb) to block the indirect CNO-induced activation of G_q DREADDx neurons. The protocol for these experiments consisted of bath application of 3 min aCSF, 3 min CNO (500 nM), 3 min CNO (500 nM) + Hb (20 µM), 3 min Hb (20 µM), 3 min aCSF recovery.

Firing Frequency

Recordings were made from CTRL (n = 9 from 2 rats, 2-3 recording slices each rat), G_q DREADD (n = 8 from 4 rats, 2 recording slices each rat) and G_q DREADDx (n = 15 from 4 rats, 2 recording slices each rat) MnPO neurons. There was no significant difference in aCSF baseline firing frequency between CTRL (9/9 cells; 3.1 $\pm$ 0.6 Hz), G_q DREADD (8/8 cells; 3.9 $\pm$ 0.6 Hz) or G_q DREADDx (15/16 cells; 3.2 $\pm$ 0.5 Hz) neurons ($F(2, 17) = 0.605$, $p = 0.553$, two-way RM ANOVA). There was a significant interaction detected, however, between neuronal phenotype and bath application applied ($F(8, 159) = 2.281$, $p < 0.025$, two-way mixed effects ANOVA). Bath application of CNO significantly increased firing frequency of G_q DREADD neurons compared to aCSF baseline ($p = 0.027$, SNK) and persisted throughout the remainder of the recording. Hb did not affect G_q DREADD firing frequency (aCSF vs CNO + Hb, $p = 0.043$; aCSF vs Hb, $p = 0.033$; aCSF vs aCSF Recovery, $p = 0.026$; SNK). Bath application did not affect firing frequency in CTRL neurons.

Post-hoc analysis of G_q DREADDx neurons revealed that CNO bath application indirectly caused a significant increase in firing frequency compared to aCSF baseline ($p = 0.006$, SNK) and began decreasing during CNO + Hb bath application. Firing frequency was consistent with that during aCSF baseline once CNO was absent during Hb ($p = 0.007$, SNK) and aCSF Recovery ($p = 0.002$) bath application.

Membrane Potential

Whole cell current clamp recordings were performed on CTRL (n = 2 from 1 rat, 2-3 recording slices each rat), G_q DREADD (n = 3 from 2 rats, 2 recording slices each rat), and G_q DREADDx (n = 4 from 2 rats, 2 recording slices each rat) MnPO neurons.

Because of the low number of recordings, statistics were not able to be effectively performed; however, absolute means and SEMs (for G_q DREADD and G_q DREADDx groups, only) are reported in Table 1. Changes in membrane potential from aCSF baseline are shown in Figure 9. CTRL neurons are trending to not be affected by CNO or aCSF bath application with or without Hb, consistent with results reported in this study. Also consistent with results from this study, the G_q DREADD are trending to have a sustained increase in membrane potential, indicating a characteristic depolarization event once CNO is bath applied. The G_q DREADDx neurons are trending to display this sustained increase in membrane potential throughout the recording—which may be due to the augmented G_q DREADD activation—however, more recordings are needed to verify these premature conclusions.

Table 1. *Changes in membrane potential of CTRL, G_q DREADD and G_q DREADDx MnPO neurons in response to CNO with or without Hemoglobin.*

	CTRL (mV)	**G_q DREADD (mV)**	**G_q DREADDX (mV)**
ACSF BASELINE	-42.7	-47.6 $\pm$ 0.9	-40.7 $\pm$ 1.8
CNO (500 NM)	-44.4	-40.4 $\pm$ 1.0	-38.5 $\pm$ 2.4
CNO (500 NM) + HB (20 µM)	-42.8	-33.5 $\pm$ 0.8	-33.4 $\pm$ 4.1
HB (20 µM)	-43.2	-29.3 $\pm$ 0.3	-33.0 $\pm$ 5.2
ACSF RECOVERY	-45.5	-29.2 $\pm$ 0.2	-36.3 $\pm$ 5.9

Future Directions

DREADDs are a very a useful tool in current *in vivo* and *in vitro* research models (Nation et al. 2016; Arico et al. 2017; Boender et al. 2014; Kyle S. Smith 2016; Zhu and Roth 2014). These data present new evidence suggesting CNO-induced activation of

G_q DREADDs may induce NO signaling, causing recruitment activation of neighboring neurons that do not express the G_q DREADD construct. Based on the presented data, we show that CNO does not alter activity of neurons expressing the CTRL virus. Additionally, CNO-induced activation is highly effective and consistent in augmenting neuronal activity in the G_q DREADD neurons. However, the specificity of chemogenetic activation may not be limited to only the G_q DREADD neurons because of recruitment activation of neurons not expressing the DREADD construct. We have shown that CNO-induced activation of G_q DREADD neurons can indirectly activate non DREADD-expressing neurons through NO mechanisms. Those that use the excitatory DREADD construct may need to consider the implications of this chemogenetic approach and control for it accordingly. More work is needed to understand the off-target effects involved in G_q DREADD activation.

Figure 1. *Diagram outlining the DBB and MnPO.* A, Coronal section of a rat brain outlining the diagonal band of Broca (DBB, left) and representative mCherry staining (right). B, Coronal section of a rat brain outlining the median preoptic nucleus (MnPO, left) and representative mCherry staining (right). Coronal rat brain illustrations adapted from (Paxinos 1986). Scale bar, 250 µm.

Figure 1.

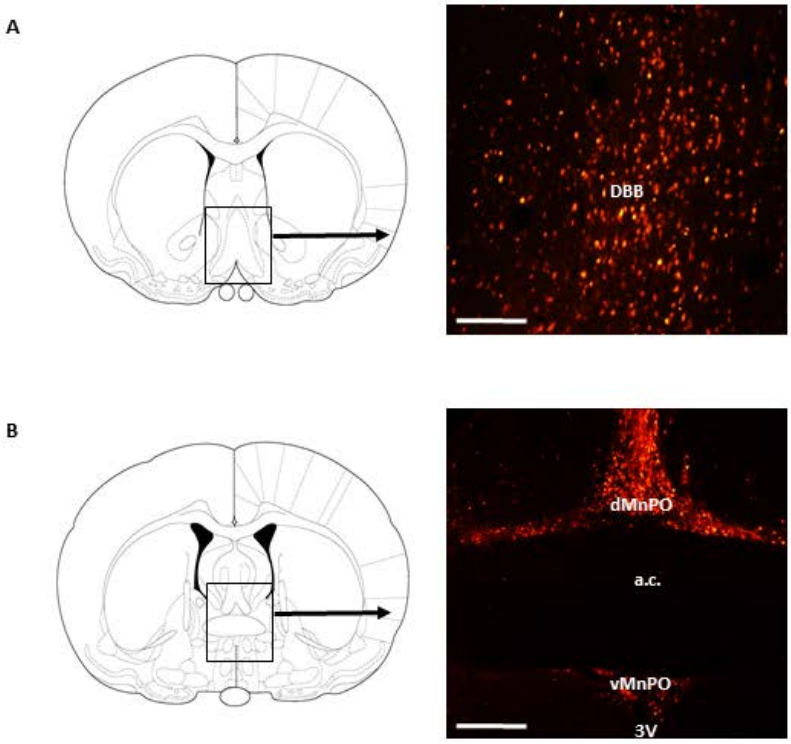

Figure 2. *CNO-induced activation of G_q DREADD DBB neurons significantly increased Fos staining in the DBB and downstream PNZ.* A, Representative Fos staining in the diagonal band of Broca (DBB, top row) and perinuclear zone (PNZ) of the supraoptic nucleus (SON, bottom row) of rats injected with the control virus and treated with vehicle (CTRL + VEH, left column) or CNO (CTRL + CNO) and rats injected with the G_q DREADD and treated with VEH (G_q DREADD + VEH) or CNO (G_q DREADD + CNO, right column). B, CNO-induced activation of G_q DREADD rats had significantly increased Fos staining in the DBB and PNZ of the SON. C, Fos staining was not different between any of the treatment groups in the subdivisions of the paraventricular nucleus (PVN). MnPO, median preoptic nucleus; PM, posterior magnocellular; DP, dorsal parvocellular; MP, medial parvocellular; vlp, ventral lateral parvocellular. *$p < 0.050$, compared to all treatment groups. Scale bar, 100 µm.

Figure 2.

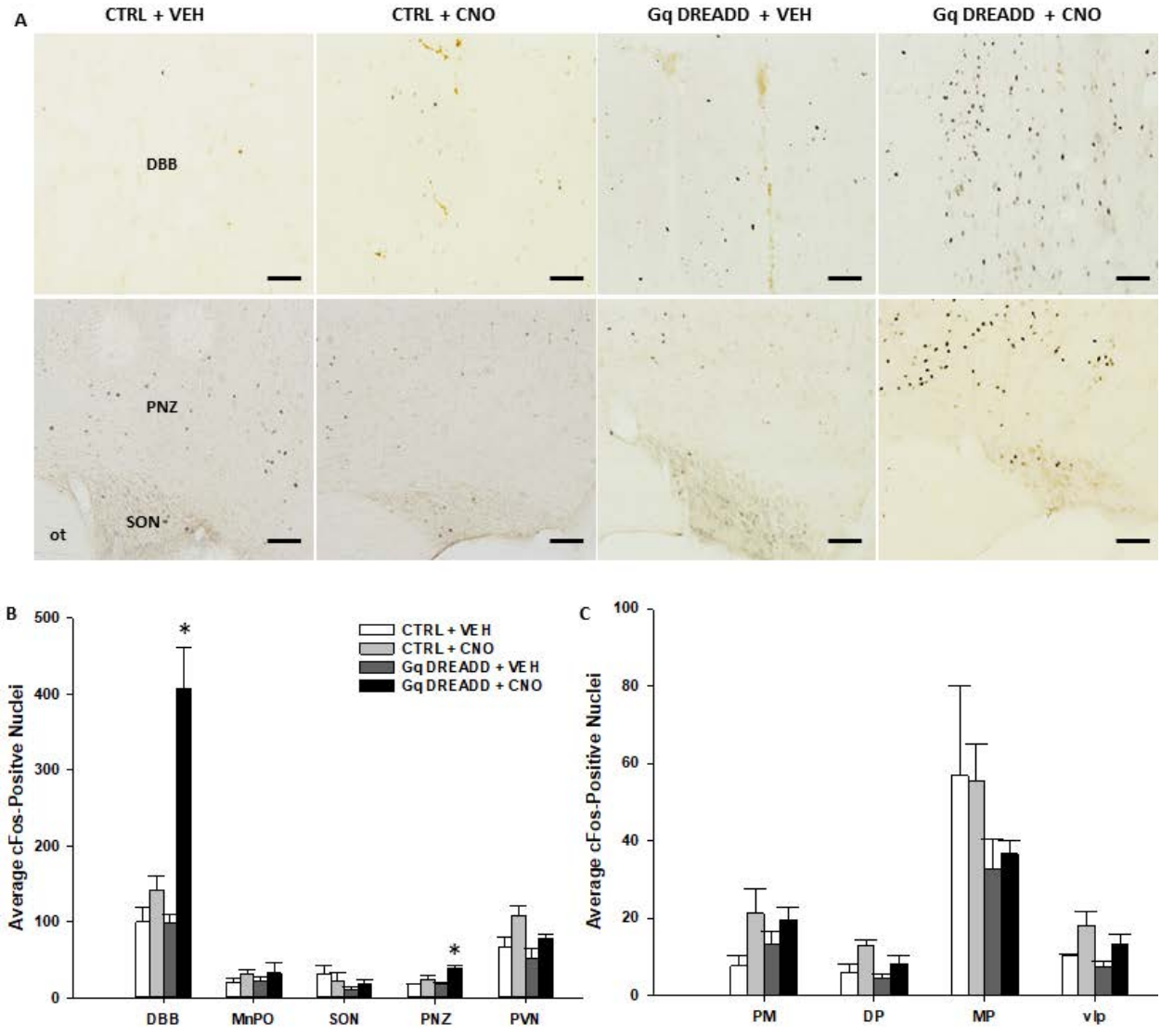
A
CTRL + VEH
CTRL + CNO
Gq DREADD + VEH
Gq DREADD + CNO
DBB
PNZ
SON
ot
B
Average cFos-Positive Nuclei
CTRL + VEH
CTRL + CNO
Gq DREADD + VEH
Gq DREADD + CNO
DBB
MnPO
SON
PNZ
PVN
C
Average cFos-Positive Nuclei
PM
DP
MP
vlp

Figure 3. *CNO-induced activation of G_q DREADD MnPO neurons significantly increased Fos staining in the MnPO and downstream SON, PVN and RVLM.* A, Representative Fos staining in the median preoptic nucleus (MnPO, top row), supraoptic nucleus (SON, middle row) and paraventricular nucleus (PVN, bottom row) of rats injected with the control virus and treated with vehicle (CTRL + VEH, left column) or CNO (CTRL + CNO) and rats injected with the G_q DREADD and treated with VEH (G_q DREADD + VEH) or CNO (G_q DREADD + CNO, right column). B, CNO-induced activation of G_q DREADD rats had significantly increased Fos staining in the MnPO, SON, PVN and rostral ventral lateral medulla (RVLM). C, Fos staining was significantly in the G_q DREADD + CNO group compared to all other treatment groups in the subdivisions of the paraventricular nucleus (PVN). PNZ, perinuclear zone of the SON; PM, posterior magnocellular; DP, dorsal parvocellular; MP, medial parvocellular; vlp, ventral lateral parvocellular. *$p < 0.050$, compared to all treatment groups. Scale bar, 100 µm.

Figure 3.

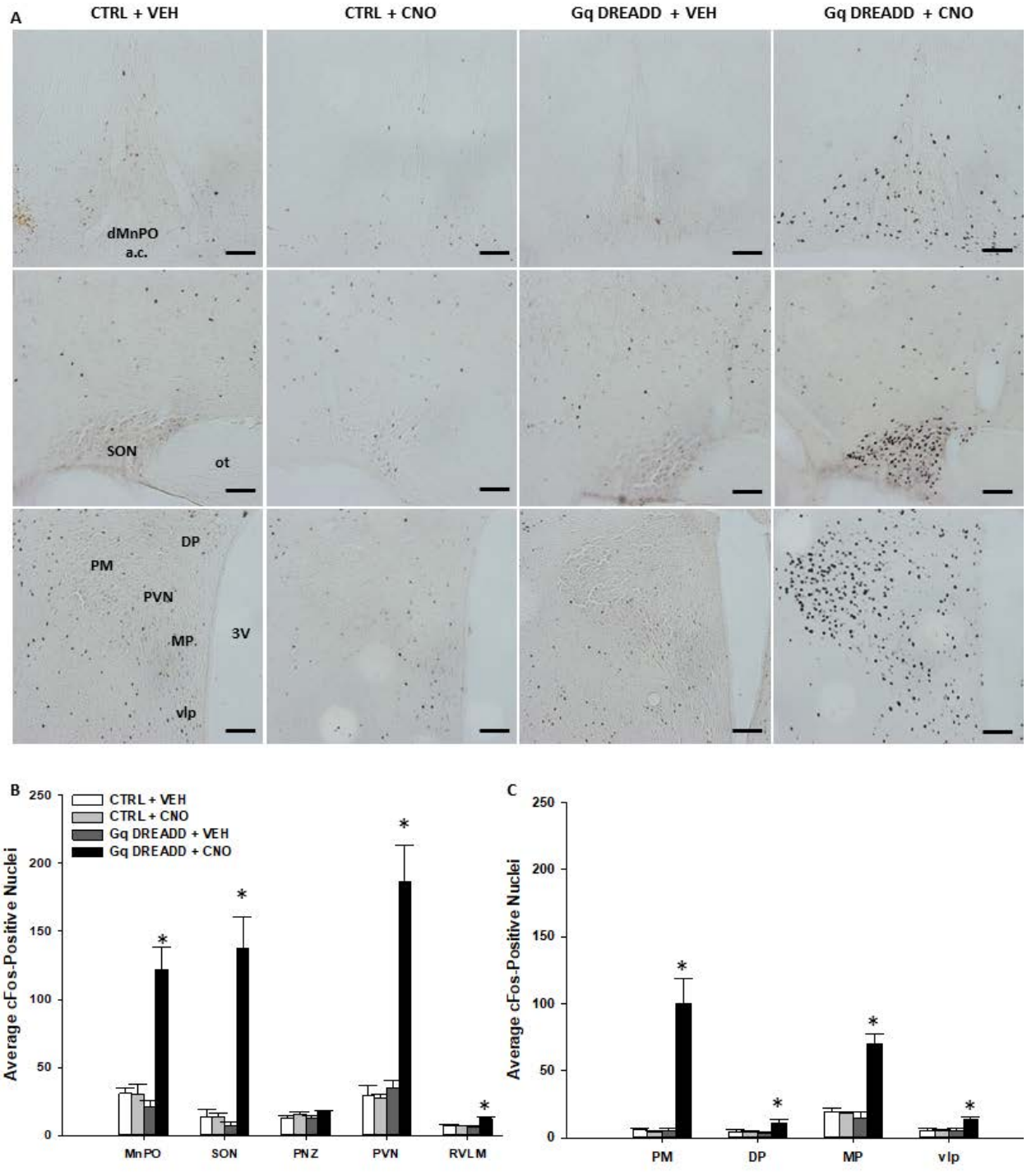
A
CTRL + VEH
CTRL + CNO
Gq DREADD + VEH
Gq DREADD + CNO
dMnPO
a.c.
SON
ot
DP
PM
PVN
MP
3V
vlp
B
CTRL + VEH
CTRL + CNO
Gq DREADD + VEH
Gq DREADD + CNO
Average cFos-Positive Nuclei
MnPO
SON
PNZ
PVN
RVLM
C
Average cFos-Positive Nuclei
PM
DP
MP
vlp

Figure 4. *DREADDs using a CaMKIIa promotor has a high transduction efficiency with CaMKIIa and NOS1-positive neurons.* A, Representative mCherry staining of the DREADD virus (left panel) and CaMKIIa mRNA (middle panel), separately and merged (right panel). B, Representative mCherry staining of the DREADD virus (left panel) and NOS1 (middle panel), separately and merged (right panel). Scale bar, 50 μm.

Figure 4.

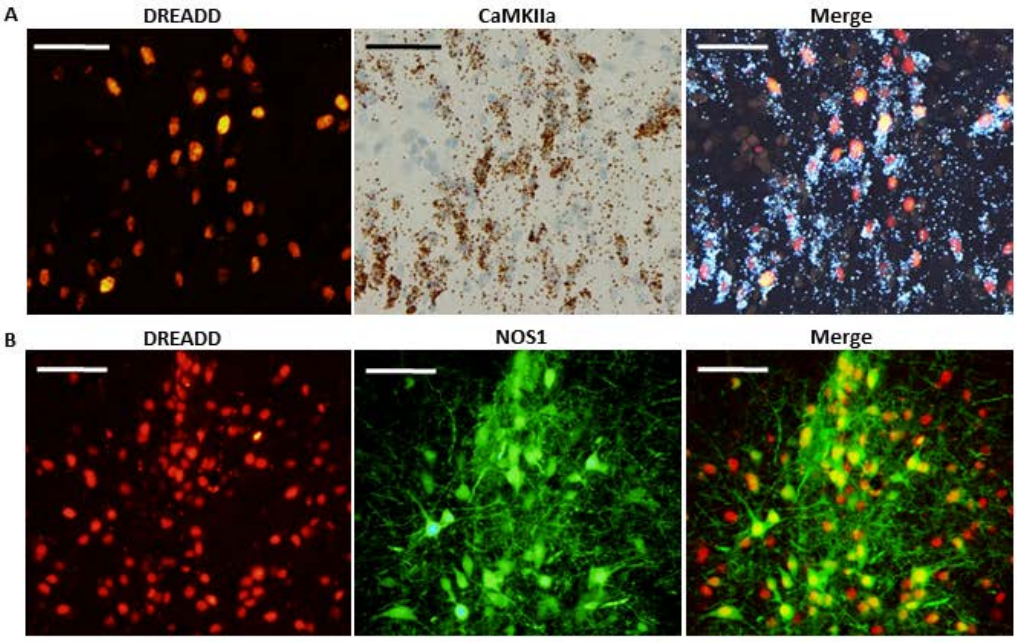

Figure 5. *CNO-induced activation significantly increased firing frequency and caused depolaization of G_q DREADD and G_q DREADDx MnPO neurons.* A, Representative image of brain tissue slice during electrophysiology recording with recording electrode of mCherry G_q DREADD (white arrow) and G_q DREADDx (yellow arrow) neurons in the dorsal median preoptic nucleus (dMnPO); scale bar, 20 µm. B, Representative loose-cell recordings of control (CTRL, top), G_q DREADD (middle), and G_q DREADDx (bottom) neurons before and after focal CNO (10 µM) application; scale bar, 10 s. C, Firing frequency was significantly increased in G_q DREADD and G_q DREADDx neurons post-CNO, compared to individual average aCSF baseline (AVG BL), CTRL neurons and recovery. D, Membrane potential was significantly increased in G_q DREADD and G_q DREADDx neurons post-CNO, compared to CTRL. E, Representative whole cell current-clamp tracing showing changes in membrane potential in CTRL (top), G_q DREADD (middle), and G_q DREADDx (bottom) neurons before and after focal CNO (10 µM) application. #$p < 0.050$, compared to individual BL and recovery; *$p < 0.050$, compared to CTRL; **$p < 0.050$, compared to BL and CTRL post-CNO; ***$p < 0.050$, compared to BL, CTRL and G_q DREADDx post-CNO.

Figure 5.

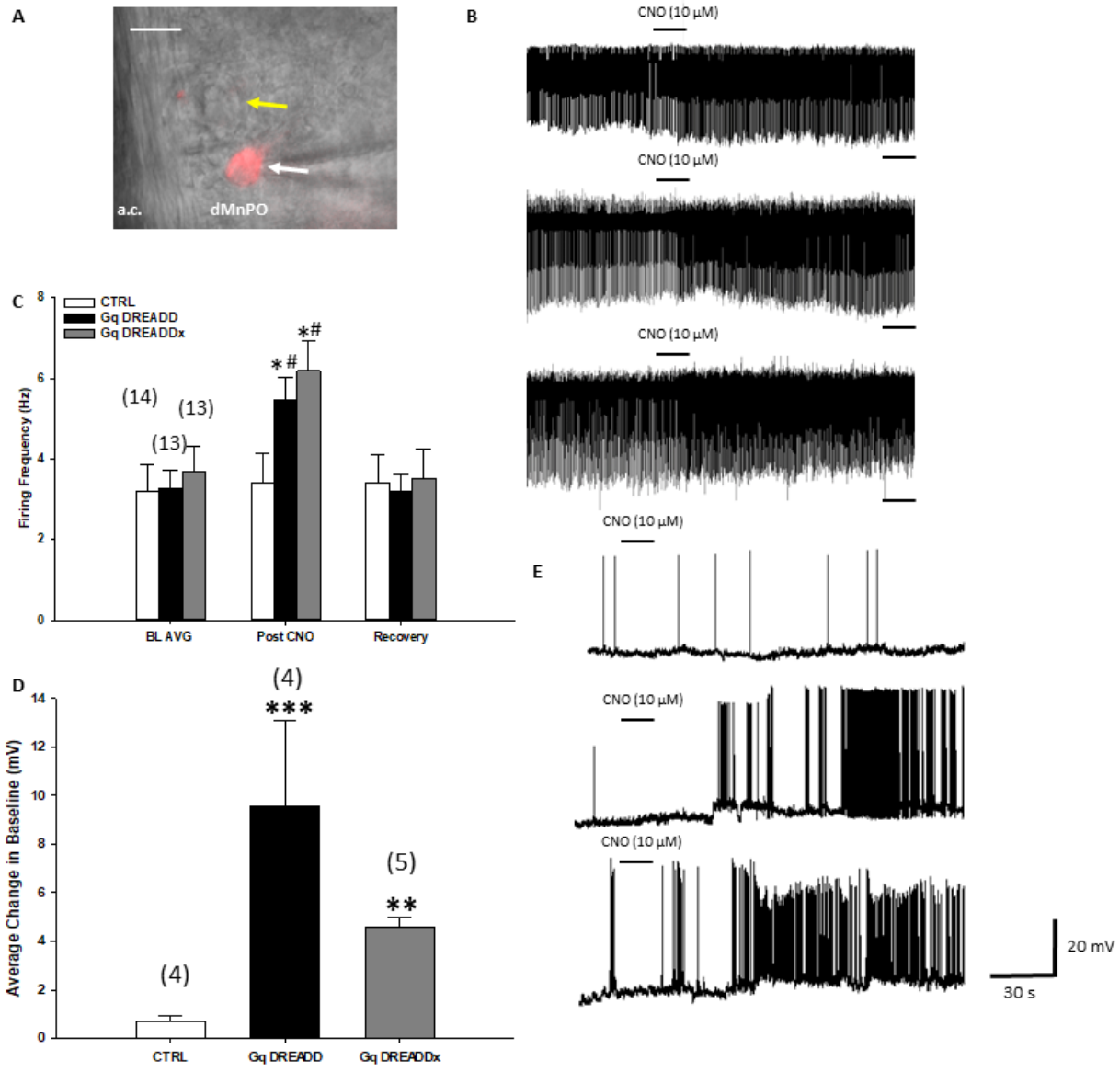
A
a.c.
dMnPO
B
CNO (10 μM)
CNO (10 μM)
CNO (10 μM)
CNO (10 μM)
C
CTRL
Gq DREADD
Gq DREADDx
Firing Frequency (Hz)
(14)
(13)
(13)
*#
*#
BL AVG
Post CNO
Recovery
D
Average Change in Baseline (mV)
(4)
***
(5)
**
(4)
CTRL
Gq DREADD
Gq DREADDx
E
CNO (10 μM)
CNO (10 μM)
CNO (10 μM)
20 mV
30 s

Figure 6. *L-NNA significantly inhibits CNO-induced increases in firing frequency and depolarization of G_q DREADDx, but not G_q DREADD MnPO neurons.* A, Firing frequency was significantly increased in G_q DREADD and G_q DREADDx neurons post-CNO during aCSF bath application, but these increases were blocked in G_q DREADDx neurons in L-NNA (50 µM) bath application. B, Representative loose-cell recordings of control (CTRL, top), G_q DREADD (middle), and G_q DREADDx (bottom) neurons before and after focal CNO (10 µM) application in L-NNA bath application; scale bar, 10 s. C, Membrane potential was significantly increased in G_q DREADD and G_q DREADDx neurons post-CNO, but these increases were blocked in G_q DREADDx neurons in L-NNA bath application. D, Representative whole cell current-clamp tracing showing changes in membrane potential in CTRL (top), G_q DREADD (middle), and G_q DREADDx (bottom) neurons before and after focal CNO (10 µM) application in L-NNA bath application. #$p < 0.050$, compared to individual aCSF bath application post-CNO; **$p < 0.050$, compared to BL and CTRL post-CNO; ***$p < 0.050$, compared to BL, CTRL and G_q DREADDx post-CNO.

Figure 6.

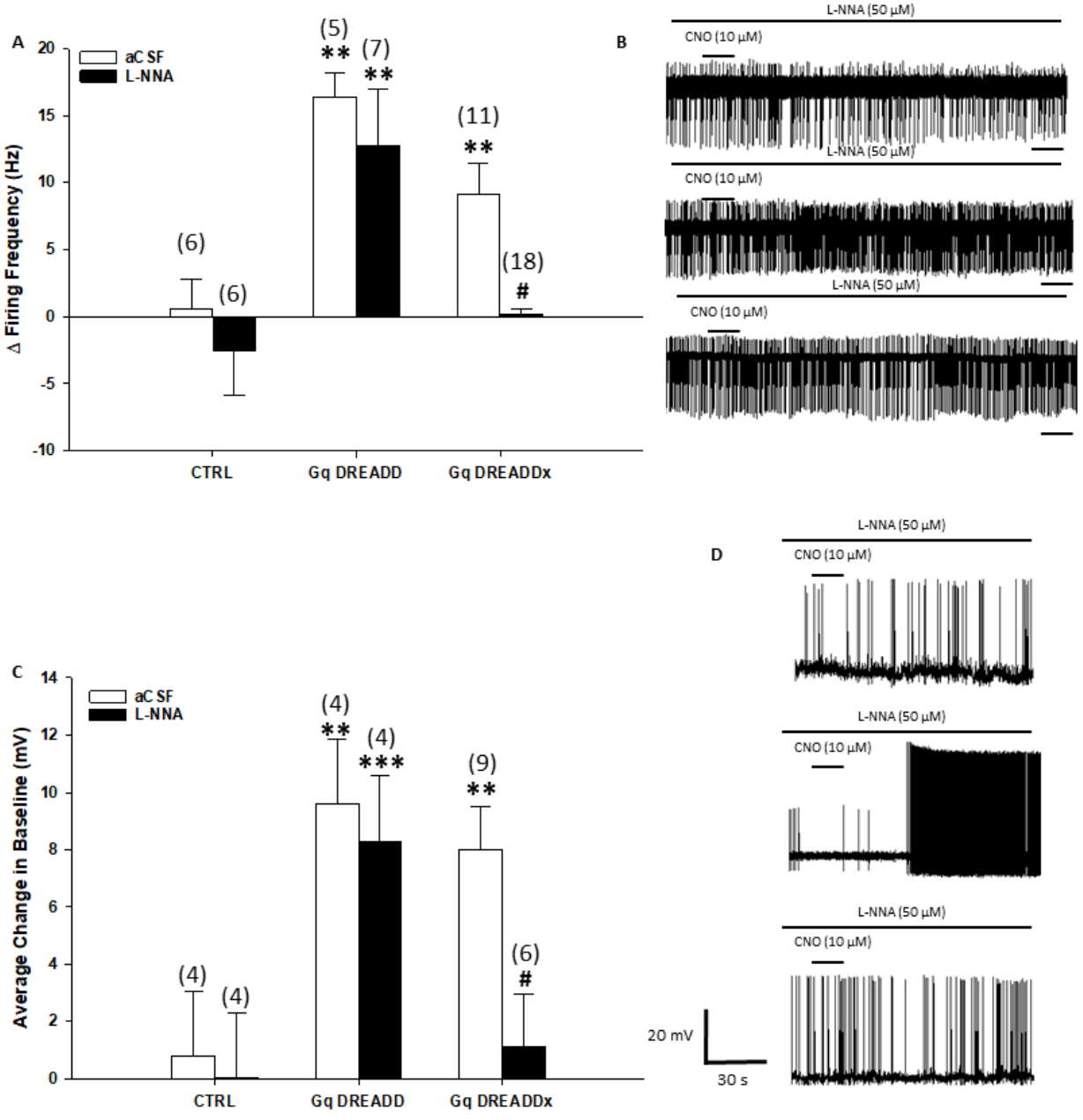
A
aC SF
L-NNA
Δ Firing Frequency (Hz)
20
15
10
5
0
-5
-10
(6)
(6)
(5)
**
(7)
**
(11)
**
(18)
#
CTRL
Gq DREADD
Gq DREADDx
B
L-NNA (50 μM)
CNO (10 μM)
L-NNA (50 μM)
CNO (10 μM)
L-NNA (50 μM)
CNO (10 μM)
C
aC SF
L-NNA
Average Change in Baseline (mV)
14
12
10
8
6
4
2
0
(4)
(4)
(4)
**
(4)
***
(9)
**
(6)
#
CTRL
Gq DREADD
Gq DREADDx
D
L-NNA (50 μM)
CNO (10 μM)
L-NNA (50 μM)
CNO (10 μM)
L-NNA (50 μM)
CNO (10 μM)
20 mV
30 s

Figure 7. *Hb significantly inhibits CNO-induced increases in firing frequency of G_q DREADDx, but not G_q DREADD MnPO neurons.* A, Firing frequency was significantly increased in G_q DREADD and G_q DREADDx neurons during CNO (500 nM) bath application, but these increases were attenuated during CNO (500 nM) + Hb (20 µM) bath application and blocked in G_q DREADDx neurons in Hb (20 µM) bath application. B, Representative loose-cell recordings of control (CTRL, top), G_q DREADD (middle), and G_q DREADDx (bottom) neurons during the recording protocol. #$p < 0.050$, compared to individual aCSF bath application; **$p < 0.050$, compared to CTRL; ***$p < 0.050$, compared to CTRL and G_q DREADDx.

Figure 7.

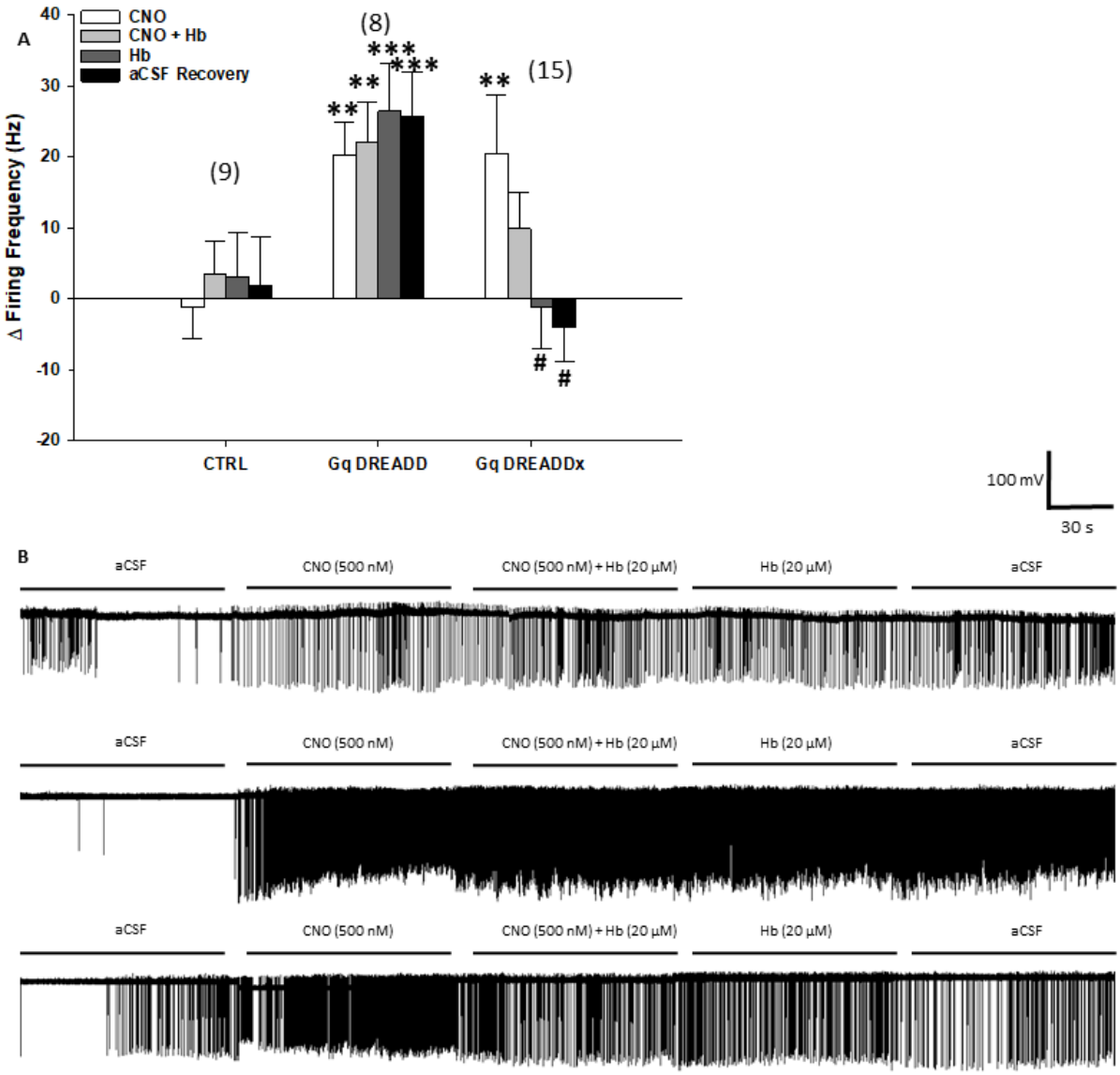
A
CNO
CNO + Hb
Hb
aCSF Recovery
Δ Firing Frequency (Hz)
40
30
20
10
0
-10
-20
(9)
(8)
(15)
**
***
#
CTRL
Gq DREADD
Gq DREADDx
100 mV
30 s
B
aCSF
CNO (500 nM)
CNO (500 nM) + Hb (20 μM)
Hb (20 μM)
aCSF

Figure 8. *Hb attenuates CNO-induced increases in membrane potential of G_q DREADDx, but not G_q DREADD MnPO neurons.* A, Membrane potential was increased in G_q DREADD and G_q DREADDx neurons during CNO (500 nM) bath application, but these increases were attenuated during CNO (500 nM) + Hb (20 µM) and in Hb (20 µM) bath application alone in G_q DREADDx neurons. B, Representative whole cell current-clamp recordings of control (CTRL, top), G_q DREADD (middle), and G_q DREADDx (bottom) neurons during the recording protocol.

Figure 8.

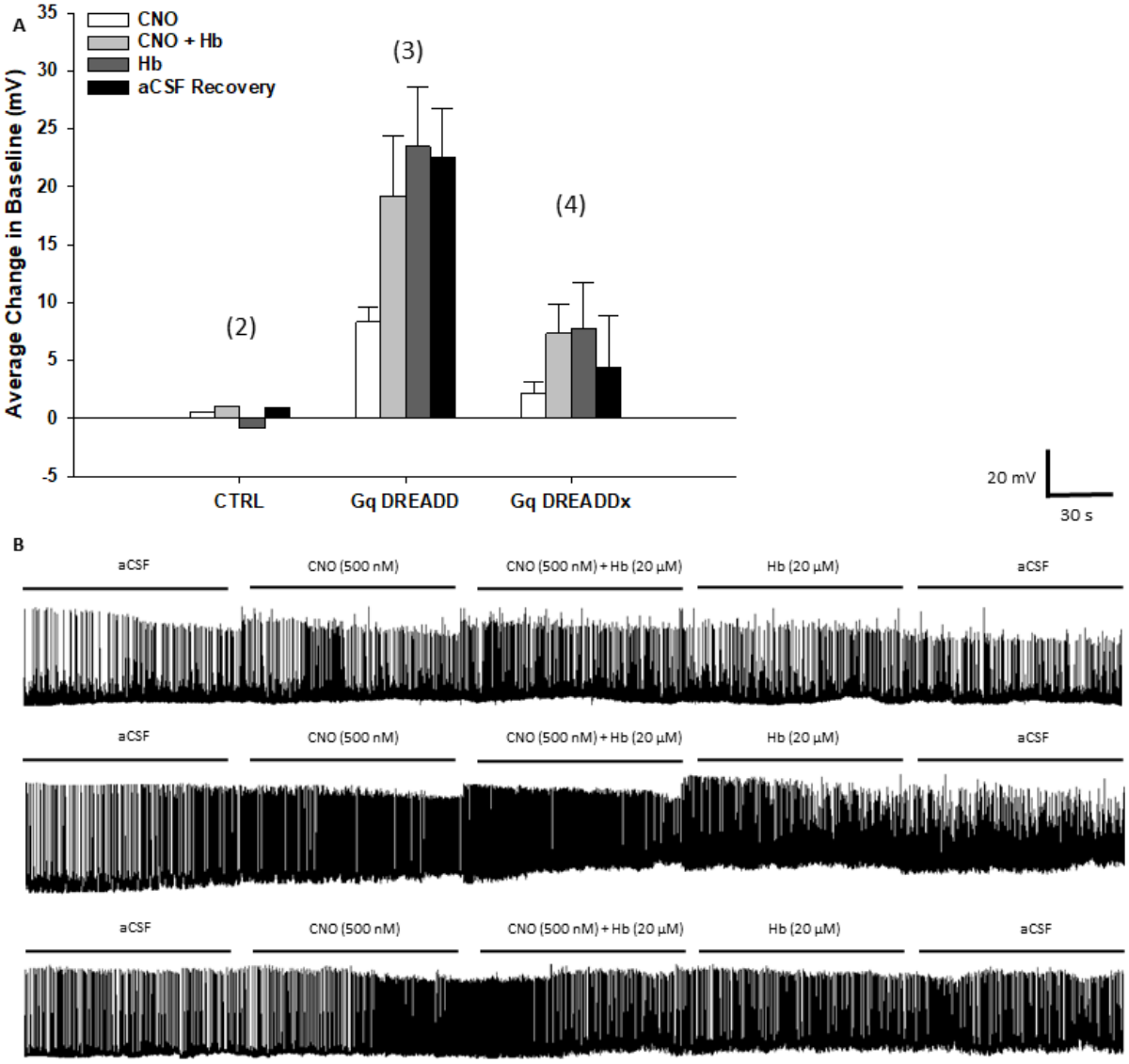
A
CNO
CNO + Hb
Hb
aCSF Recovery
Average Change in Baseline (mV)
35
30
25
20
15
10
5
0
-5
(2)
(3)
(4)
CTRL
Gq DREADD
Gq DREADDx
20 mV
30 s
B
aCSF
CNO (500 nM)
CNO (500 nM) + Hb (20 µM)
Hb (20 µM)
aCSF

References

Arico, C., E. E. Bagley, P. Carrive, N. Assareh, and G. P. McNally. 2017. 'Effects of chemogenetic excitation or inhibition of the ventrolateral periaqueductal gray on the acquisition and extinction of Pavlovian fear conditioning', *Neurobiol Learn Mem*, 144: 186-97.

Boender, A. J., J. W. de Jong, L. Boekhoudt, M. C. Luijendijk, G. van der Plasse, and R. A. Adan. 2014. 'Combined use of the canine adenovirus-2 and DREADD-technology to activate specific neural pathways in vivo', *PLoS One*, 9: e95392.

Cunningham, J. T., R. Nissen, and L. P. Renaud. 1994. 'Perinuclear zone and diagonal band lesions enhance angiotensin responses of rat supraoptic neurons', *Am J Physiol*, 267: R916-22.

Cunningham, J. Thomas, W. David Knight, Steven W. Mifflin, and Eric J. Nestler. 2012. 'An essential role for ΔFosB in the median preoptic nucleus in the sustained hypertensive effects of chronic intermittent hypoxia', *Hypertension*, 60: 179-87.

Di, S., R. Malcher-Lopes, K. C. Halmos, and J. G. Tasker. 2003. 'Nongenomic glucocorticoid inhibition via endocannabinoid release in the hypothalamus: a fast feedback mechanism', *J Neurosci*, 23: 4850-7.

Farmer, G. E., K. Balapattabi, M. E. Bachelor, J. T. Little, and J. T. Cunningham. 2018. 'AT1a influences GABAa mediated inhibition through the regulation of KCC2 expression', *Am J Physiol Regul Integr Comp Physiol*.

Grindstaff, R. J., R. R. Grindstaff, M. J. Sullivan, and J. T. Cunningham. 2000. 'Role of the locus ceruleus in baroreceptor regulation of supraoptic vasopressin neurons in the rat', *Am J Physiol Regul Integr Comp Physiol*, 279: R306-19.

Grob, M., G. Drolet, and D. Mouginot. 2004. 'Specific Na+ sensors are functionally expressed in a neuronal population of the median preoptic nucleus of the rat', *J Neurosci*, 24: 3974-84.

Kyle S. Smith, David J. Bucci, Bryan W. Luikart, Stephen V. Mahler. 2016. 'DREADDs: Use and Application in Behavioral Neuroscience', *Behavioral Neuroscience*: 1-19.

Marciante A.B., Wang L.A., Farmer G.E., Cunningham J.T. 2019. 'Selectively inhibiting the median preoptic nucleus attenuates angiotensin II and hyperosmotic-induced drinking behavior and vasopressin release in adult male rats', *eNeuro*.

Nation, H. L., M. Nicoleau, B. J. Kinsman, K. N. Browning, and S. D. Stocker. 2016. 'DREADD-induced activation of subfornical organ neurons stimulates thirst and salt appetite', *J Neurophysiol*, 115: 3123-9.

Paxinos, G, and Watson C. 1986. *The rat brain in stereotaxic coordinates* (Academic Press: New York, NY).

Zhu, H., and B. L. Roth. 2014. 'DREADD: a chemogenetic GPCR signaling platform', *Int J Neuropsychopharmacol*, 18.